ENERGY MARGIN CALCULATION BY THE RELEVANT FAULT-ON TRAJECTORY METHOD

By

Chi-keung Tang, B.A.Sc., M. Eng

A Thesis

Submitted to the School of Graduate Studies

in Partial Fulfilment of the Requirements

for the Degree of Doctor of Philosophy,

McMaster University

ENERGY MARGIN CALCULATION BY THE RELEVANT FAULT-ON TRAJECTORY METHOD

DOCTOR OF PHILOSOPHY (1995) McMaster University
(Electrical Engineering) Hamilton, Ontario, Canada

TITLE: Energy Margin Calculation by the Relevant Fault-on Trajectory Method

AUTHOR: Chi-keung Tang, B.A.Sc (University of Waterloo), M. Eng (University of Toronto)

SUPERVISORY COMMITTEE:

Robert T.H. Alden, B.A.Sc, M.A.Sc, Ph.D., P.Eng,
Professor of Electrical and Computer Engineering,
Director of Power Research Laboratory,
McMaster University,
Hamilton, Ontario, Canada

Raymond D. Findlay, B.A.Sc, M.A.Sc, Ph.D., P.Eng,
Professor of Electrical and Computer Engineering,
Power Research Laboratory,
McMaster University,
Hamilton, Ontario, Canada

Mohamed A. El-Kady, B.Sc, M.Sc, Ph.D., P.Eng,
Professor (Part-time) of Electrical and Computer Engineering,
Power Research Laboratory,
McMaster University,
Hamilton, Ontario, Canada

NUMBER OF PAGES: xiv, 158

ABSTRACT

The value of the time domain simulation technique for power system transient stability analysis can be greatly enhanced if it can indicate the degree of stability by producing a stability index. Often referred to as Energy Margin, the stability index offers additional insight into the transient stability problem being studied, and has the capability of speeding up transient stability limit derivations. Moreover, energy margins also have potential applications in dynamic contingency ranking and screening.

This thesis presents a new method, called the Relevant Fault-on Trajectory (RFT) method, for incorporating energy margin calculations into time domain simulations. The proposed method is based on the determination of the additional energy absorbing capability of the critical generator group, at the instant when the transient kinetic energy injected into this group by the disturbance is fully absorbed. The additional energy absorbing capability is obtained through the simulation of a relevant fault-on trajectory. The RFT method computes energy margins efficiently and reliably for systems exhibiting either plant mode or area mode stability problems.

The practicality of the proposed method has been successfully demonstrated on a 27-generator, an 89-generator, and a 144-generator system. The RFT method has the capability of speeding up transient stability limit derivation by reducing the number of stability runs.

ACKNOWLEDGEMENTS

I would like to take this opportunity to thank my supervisor at McMaster University, Dr. R.T.H. Alden, for his encouragement and guidance throughout the course of this research. Over the years he has given me confidence in carrying out and completing this work. Special thanks also go to Dr. R.D. Findlay and Dr. M.A. El-Kady, members of the Ph.D. supervisory committee, who have provided me with guidance and support at the various stages of this work.

I am very grateful to Dr. H.M. Zein El-din, one of my former supervisors at Ontario Hydro, who had helped me initiate my Ph.D. study at McMaster University. Under his supervision, I received basic training on the various aspects of dynamic security analysis.

My appreciation also goes to Dr. V.F. Carvalho and Mr. P.T. Chan, who offered me a career at Ontario Hydro starting in 1979. Dr. Carvalho also gave me the valuable opportunity to participate in the EPRI project RP2206-1, "Direct Analysis of Transient Stability for Large Power Systems", from which I have gained familiarity with direct methods.

I am deeply indebted to Dr. A.A. Fouad and Dr. V. Vittal of Iowa State University who, during the course of RP2206-1, provided me with precious training on the various aspects of direct methods and transient energy analysis. The many technical discussions we had held in the past have contributed directly or indirectly to the development of the RFT method proposed in this thesis.

Special thanks also go to Dr. P. Kundur, Mr. D. Wong, and Mr. G.J. Rogers, power system specialists and former employees of Ontario Hydro, who have provided me with a good understanding of the time domain simulation technique for power system stability analysis. Mr. Wong has been very helpful in explaining to me the programming details pertaining to the development of time domain simulation programs.

I would like to express my gratitude to Dr. G.A. Maria of Ontario Hydro, who has involved me in the development of the Hybrid transient stability analysis technique, of which the RFT method is an extension. In addition, Dr. Maria has also provided me with many practical ideas regarding on-line transient stability assessment.

Many of my colleagues have shared with me their valuable experience in power system security analysis, to whom I would like to express my appreciation. Special thanks should go to Mr. M. Radan, Mr. C.M. Louie, and Mr. K. Chan, who have significantly enriched my knowledge on power system transient stability limit derivation.

I am thankful to my company, Ontario Hydro, for providing me with the opportunity and financial assistance to perform this meaningful research at McMaster University. Special thanks should go to the management team of the Grid System Management Division, especially Mr. C.E. Graham and Mr. P.S. Li for their support.

Finally, I would like to express my deep appreciation to my wife, Sarina, for her support and encouragement without which this work would not have been possible.

TABLE OF CONTENTS

LIST OF SYMBOLS

A_{sat}	parameter of the generator saturation curve
B_{sat}	parameter of the generator saturation curve
e_d	d-axis component of the generator terminal voltage
e_q	q-axis component of the generator terminal voltage
E_R	R-axis component of the generator terminal voltage
E_I	I-axis component of the generator terminal voltage
e_t	generator terminal voltage
e_{fd}	generator field voltage
E_{FD}	exciter output
E''_d	d-axis component of the generator sub-transient voltage
E''_q	q-axis component of the generator sub-transient voltage
E''_R	R-axis component of the generator sub-transient voltage
E''_I	I-axis component of the generator sub-transient voltage
E'_d	d-axis component of the generator transient voltage
E'_q	q-axis component of the generator transient voltage
E_{fmax}	exciter limiter upper limit
E_{fmin}	exciter limiter lower limit
H	generator inertia constant
i_d	d-axis component of the generator current
i_q	q-axis component of the generator current
I_R	R-axis component of the generator current
I_I	I-axis component of the generator current
i_t	generator terminal current
I_{fd}	field current
I_G	current injection at a generator node
I_L	current injection at a load node
i_{kd1}	current of the amortisseur circuit on the d-axis
i_{kq1}	current of the first amortisseur circuit on the q-axis
i_{kq2}	current of the second amortisseur circuit on the q-axis
K	index group of the critical machines
K_D	generator damping factor
K_A	exciter gain

K_S power system stabilizer gain
k_{sat} generator saturation factor

M_a inertia of group a
M_b inertia of group b
M_{eq} inertia of the equivalent machine
M_i generator inertia (=2H) of machine i
M_T sum of generator inertia
M_{TK} total generator inertia of the critical generator group
M_{TS} total generator inertia of the stable generator group

P_m generator mechanical power input
P_e generator electrical power output
P_L real (MW) component of bus load
P_{COI} accelerating power of the centre of inertia

Q_L imaginary (MVAR) component of bus load

r_a armature resistance
r_{fd} field resistance
r_{kd1} resistance of the amortisseur circuit on the d-axis
r_{kq1} resistance of the first amortisseur circuit on the q-axis
r_{kq2} resistance of the second amortisseur circuit on the q-axis

S index group of the stable machines
S_p index group of the local potential energy peaks

T_e generator electrical torque output
T_m generator mechanical torque input
t_{kemin} time instant when V_{ke}^{grp} reaches a global minimum
T_R terminal voltage relay time constant
T_s time domain simulation period
T_W power system stabilizer washout time constant
T_1 power system stabilizer phase compensation time constant
T_2 power system stabilizer phase compensation time constant

x_{ad} d-axis saturated mutual reactance
x_{aq} q-axis saturated mutual reactance
x_{adu} d-axis unsaturated mutual reactance
x_{aqu} q-axis unsaturated mutual reactance
x_{al} armature leakage reactance
x_{kd1} leakage reactance of the amortisseur circuit on the d-axis
x_{kq1} leakage reactance of the first q-axis amortisseur circuit

x_{kq2} leakage reactance of the second q-axis amortisseur circuit
x_{fl} field leakage reactance

V_{cr} Critical energy
V_{cl} Transient energy at fault clearing
v_s power system stabilizer output
v_{smx} upper limit of PSS output limiter
v_{smn} lower limit of PSS output limiter
V_{ke} transient kinetic energy
V_{pe} transient potential energy
V transient energy function
V_{ke}^{c} corrected kinetic energy

δ rotor angle in synchronous frame of reference
δ^{cl} rotor angle at fault clearing
δ_o centre of angle in the COI frame
δ^{p} peak angle of the rotor during the first swing
δ^{s} SEP of the SMIB System
δ^{u} UEP of the SMIB System
ΔG change in plant output
ΔPE potential energy due to inter-machine oscillation
ΔT integration step size
ΔV energy margin

Ψ_a generator air gap flux
Ψ_{ao} air gap flux assuming no saturation
Ψ_{ad} d-axis mutual flux linkage
Ψ_{aq} q-axis mutual flux linkage
Ψ_I difference with Ψ_{ao} and Ψ_a
Ψ_{kd1} d-axis amortisseur circuit leakage flux linkage
Ψ_{kq1} q-axis amortisseur circuit leakage flux linkage
Ψ_{kq2} q-axis amortisseur circuit leakage flux linkage
Ψ_{fd} field flux linkage

θ rotor angle in the COI frame

ω generator speed in the synchronous frame
ϖ generator speed in the COI frame
ω_o centre of speed
ϖ_{eq} equivalent generator speed in the COI frame
ϖ_a equivalent generator speed of group a
ϖ_b equivalent generator speed of group b

LIST OF ACRONYMS

AC	Alternating Current
AGEF	Approximate Group Energy Function
BCU	Boundary of Stability Region for the Controlling UEP
CCT	Critical Clearing Time
COI	Center of Inertia
COA	Center of Angle
CPU	Central Processing Unit
CTDS	Conventional Time Domain Simulation
CUEP	Controlling Unstable Equilibrium Point
DC	Direct Current
EMS	Energy Management System
FACTS	Flexible AC Transmission
GEF	Group Energy Function
HVDC	High Voltage DC
IMEF	Individual Machine Energy Functions
LU	Lower and Upper
MOI	Mode of Instability
PEBS	Principal Energy Boundary Surface
PEF	Partial Energy Function
PEPP	Potential Energy Peak Point
PSS	Power System Stabilizer
RFT	Relevant Fault-on Trajectory
SEP	Stable Equilibrium Point
TEF	Transient energy function
UEP	Unstable Equilibrium Point

LIST OF FIGURES

CHAPTER 1
INTRODUCTION

1.1 INDUSTRY PERSPECTIVE

Secure electricity supply at the lowest possible cost is fundamental to the economy of a nation and to the quality of lives of its citizens. Hence system security analysis becomes a major aspect of power system planning and operation. Insecure system operation may result in catastrophic system wide blackouts and/or equipment damage, while overly secure system operation often leads to higher operating costs.

In North America, where the utility networks are interconnected to form one large power pool, stringent operating security criteria have been established in order to achieve an acceptable level of system security by all utilities. Specifically, a system should be designed and operated in such a way that it can withstand a set of recognized contingencies while achieving satisfactory steady state and dynamic system performance.

Recognizing the importance of power system security, utility companies and research institutes have been devoting a significant amount of resources and effort to improve their security assessment capability. Modern control centers are now equipped with highly sophisticated energy management system (EMS) software with superb security analysis and monitoring capability. These control centers monitor system security on a minute-to-minute basis, allowing system operators to undertake appropriate preventive as well as corrective actions in a

timely and cost effective manner whenever system security is threatened.

Power system security analysis is generally divided into two main areas: static and dynamic security analysis. Static security assessment is primarily concerned with the steady state performance aspects of a power system, such as equipment thermal overloading and post-contingency voltage decline. Dynamic security assessment mainly deals with the stability problems the system can encounter, such as large signal transient stability, small signal dynamic stability, and voltage stability. Static security analysis is accomplished by employing DC and AC load flow solution techniques, which are usually implemented on-line. Dynamic security analysis is usually performed off-line, since it requires advanced analytical tools and is computationally intensive. This thesis is primarily concerned with the transient stability aspect of dynamic security assessment.

Transient stability analysis is a complicated task due to the complexity of the problem being analyzed. Despite the incorporation of effective control aids and special system protection schemes, power transfers in many utility systems today are still severely restricted due to transient stability concerns. This trend is expected to continue as utilities strive to utilize their transmission systems to the maximum capability. Advanced analytical techniques are therefore much needed for fast and accurate transient stability analysis.

To ensure power system transient stability, the present approach is to first identify those transient stability interfaces that may limit system operation, and then conduct off-line studies to derive their maximum transfer capabilities in the form of transient stability limits. System operators have to make sure that power flows over these interfaces do not exceed their pre-determined limits. A

significant number of transient stability simulations are required to derive transient stability limits, due to the large number of system outage conditions and contingencies that need to be considered. The conventional time domain simulation technique is the principal analytical tool for this task.

Off-line transient stability limit derivation has some short-comings. First, because of the relatively long study lead time, transient stability limits can only be provided for a limited set of system conditions. The common practice is to provide stability limit coverage for the normal system and for the system with a single critical transmission element out of service. For forced outage conditions that are beyond the scope of coverage, system operators often have to make their own judgement as to what limits are appropriate. This may result in either insecure or overly secure system operation. Secondly, because the worst scenarios are usually assumed in deriving transient stability limits off-line, these limits are usually conservative and result in higher system operating costs.

Recognizing the short-comings of the existing transient stability limit derivation methodology, power system engineers and researchers have been constantly seeking advanced analytical methods to speed up power system transient stability assessment. The ultimate goal is to provide on-line dynamic security assessment capability to assist system operators in making timely decisions concerning power system security.

1.2 OVERVIEW OF POWER SYSTEM STABILITY

Power system stability can be classified into three types: large signal transient stability, small signal dynamic stability, and voltage stability. The first two types deal primarily with rotor angle stability. Thus, when the system is

unstable, one or more machines lose synchronism. Large signal transient stability deals with the system's capability to withstand large disturbances such as short circuits on the system. Small signal dynamic stability deals with the system's capability to withstand small disturbances such as incremental load changes. Voltage stability deals with the system's capability to maintain pre- and post-contingency voltages within acceptable levels.

A power system consists of synchronous generators connected to numerous loads through a transmission network. Transient instability will occur when there is a lack of synchronizing torque on the system. The time frame of interest is usually less than 10 seconds. Analysis of power system transient stability is accomplished by modelling network devices to any desired level of detail, by a set of non-linear algebraic and differential equations. Power system transient stability can be improved by a number of ways including the following:

- reinforcement of the transmission system
- installation of fast and high gain excitation systems equipped with power system stabilizers
- installation of static var compensators
- installation of series compensators
- application of generation rejection
- application of fast valving techniques
- application of braking resistors
- application of fast breakers

Dynamic instability manifests itself in the form of growing or undamped system oscillations. It will occur when there is a lack of damping torque on the system. For small signal disturbances, the power system model can

be linearized and analyzed by eigenvalue techniques. Small signal stability can be enhanced by reinforcement of the transmission system, installation of properly tuned power system stabilizers, as well as installation of static var compensators.

Power system stability can also be categorized into plant mode and area mode stability, based on the mode of system separation. Plant mode stability is primarily concerned with the ability of one generating plant to remain in synchronism with the rest of the system. Area mode stability deals with the ability of many generating plants to remain transiently stable following a given disturbance.

1.3 OBJECTIVE OF THE THESIS

In the planning and operation of power systems, one of the major tasks performed by power engineers is to ensure satisfactory transient stability performance for a set of recognized contingencies. Power system transient stability analysis is accomplished using the conventional time domain simulation technique, which is a highly accurate tool because of its superb and unlimited modelling capability. This analytical tool, however, can only indicate whether the system is stable or unstable, with no information on the degree of stability. Therefore, transient stability limit derivation has to be done by a trial-and-error approach which requires a large number of stability runs. Each transient stability run is computationally time consuming.

Direct methods based on the formulation of an energy function provide an alternative tool for power system transient stability assessment. Still in a developmental stage, they have the much desired capability of producing a

transient stability index which measures the degree of stability. The stability index produced by direct methods is often referred to as Transient Energy Margin or simply Energy Margin. Energy margins provide additional insight into the stability problem being studied. They also have potential applications in fast transient stability limit derivation and dynamic contingency ranking. However, the accuracy, speed, and reliability of direct methods need to be much improved before they can become a practical tool for transient stability limit derivation.

The main objective of this thesis is to develop an effective and efficient analytical method to incorporate energy margin calculation into the conventional time domain simulation technique. The method will be called the Relevant Fault-on Trajectory (RFT) method. This method is a powerful tool since it determines transient stability as accurately as the conventional time domain method, and at the same time provides energy margins which can be used to speed up transient stability limit derivation. Furthermore, the method also has potential applications in dynamic contingency ranking.

To accomplish this objective, various approaches to calculating energy margins by direct methods have been reviewed. Essentially, direct methods compute energy margins through either unstable equilibrium point (UEP) based techniques or fault-on trajectory based techniques. Terms will be explained in Chapter 2. In incorporating energy margin calculation into the conventional time domain simulation technique, the author has decided to explore the fault-on trajectory based techniques since system trajectories are computed in time domain simulations. The proposed method must be reliable, computationally efficient, and reasonably accurate, while retaining the superb modelling capability of the time domain simulation method.

1.4 ORGANIZATION OF THE THESIS

This section presents the organization of the thesis which contains seven chapters. A brief description of the each chapter is provided below:

Chapter 1: Introduction - This chapter first presents an industry perspective on analytical tools for power system transient stability assessment. This is followed by an overview of different types of stability problems, and a brief description of the main objective of this thesis. Finally, the organization of the thesis is presented.

Chapter 2: Review of Analytical Techniques for Transient Stability Assessment - This chapter first describes the conventional time domain simulation technique, highlighting its accuracy and superb dynamic modelling capability. Then it presents an overview of direct methods. Two approaches to calculating energy margins by direct methods are described: the unstable equilibrium point based and fault-on trajectory based approaches. The chapter ends with a summary of the advantages and disadvantages of the two classes of analytical techniques.

Chapter 3: Energy Margins by the RFT Method - This chapter first presents an overview of the Hybrid method, followed by a general description of the proposed RFT method for incorporating energy margin calculation into conventional time domain simulations. The power system model for transient energy analysis is then given, followed by a description of energy margin calculation. Benchmark energy margins are then defined to assess the accuracy of the RFT method. The algorithm for the proposed method is presented next. Finally, test results are provided based on three test systems: the 27-, the 89-, and

the 144-generator system.

Chapter 4: Approximate Group Energy Functions - This chapter investigates an alternative way of calculating the transient energy of the critical generator group, based on approximate group energy functions. The mathematical formulation of approximate group energy functions is described first, followed by a presentation of the modified RFT algorithm. Finally, test results are based on the three test systems.

Chapter 5: Energy Margin Sensitivity and Transient Stability Limit Derivation - This chapter presents the application of first order sensitivity techniques to fast transient stability limit derivation. Derivation of numerical sensitivities of energy margins is described first, followed by a presentation of test results based on the simulation of the 27-generator and the 89-generator systems.

Chapter 6: Dynamic Contingency Ranking - This chapter presents the application of energy margin to dynamic contingency ranking. Based on the 27-generator system, the effectiveness of energy margins on dynamic contingency ranking is demonstrated, using energy margins obtained from the RFT method.

Chapter 7: Conclusions - This chapter first provides a brief summary of the main contributions of the thesis, followed by a presentation of the recommendations for future research work.

CHAPTER 2
REVIEW OF ANALYTICAL TECHNIQUES FOR TRANSIENT STABILITY ANALYSIS

2.1 INTRODUCTION

Transient stability analysis is a major task in power system planning and operation. Power utilities around the world devote significant amounts of resources to transient stability analysis in order to ensure system dynamic security. The task is becoming increasingly difficult because of the following factors:

(i) Modelling Complexities - To enhance both the steady state and dynamic system performance, modern power systems are equipped with sophisticated devices such as HVDC (High Voltage DC), advanced excitation controls, and FACTS (Flexible AC Transmission System) devices. Accurate modelling of these devices is essential to accurate transient stability simulations.

(ii) Complex Mode of Instability - Because of the interconnected mode of operation, the effects of a major disturbance on one part of an interconnected system can propagate to some other parts of the system, causing system wide power interruptions. Hence the mode of instability can vary from the simple plant mode to the more complex area mode.

(iii) Increasing Network Size - Also as a result of the interconnected mode of operation, a utility often finds it necessary to have a good representation

of its own network as well as that of the external system. This is especially true for those contingencies that have area wide implications. A typical study system may contain hundreds of machines and thousands of buses.

Two classes of analytical methods are currently available for power system transient stability analysis. These are the so-called direct methods and the conventional time domain simulation technique. Both have their strengths and weaknesses. The purpose of this chapter is to present a brief overview of these analytical techniques, and to summarize their capabilities in terms of computational speed, accuracy, and reliability.

2.2 CONVENTIONAL TIME DOMAIN SIMULATION TECHNIQUE

2.2.1 BACKGROUND

The conventional time domain simulation technique for power system transient stability analysis has been extensively developed over the last several decades [28, 36, 62]. With its superb modelling capability, this technique is highly accurate, flexible, and reliable in simulating transient stability problems. Today, all commercial software packages for transient stability analysis are invariably based on this technique.

The time domain simulation technique models the power system by a set of differential and algebraic equations. These equations are solved step by step in the time domain by using appropriate numerical integration and network solution algorithms. Transient stability is determined by monitoring the time trajectories of rotor angles. If one or more rotor angles increase out of bound within the simulation period, then the system is declared transiently unstable. Otherwise, it is declared stable. The time frame for transient stability analysis usually varies from 5 to 10 seconds.

In addition to rotor angles, time domain simulations also provide time trajectories of other system quantities such as bus voltages and line flows. Some of these quantities are necessary for checking other dynamic performance criteria, including those on transient voltage dips and protective relay margins.

2.2.2 POWER SYSTEM MODEL

A power system consists of synchronous generators connected to their loads through a transmission network, as shown in figure 2.1. Transient stability is largely determined by the dynamic performance of the synchronous machines and their auxiliary controls, and the strength of the transmission network. Accurate modelling of these power system elements is essential to transient stability analysis.

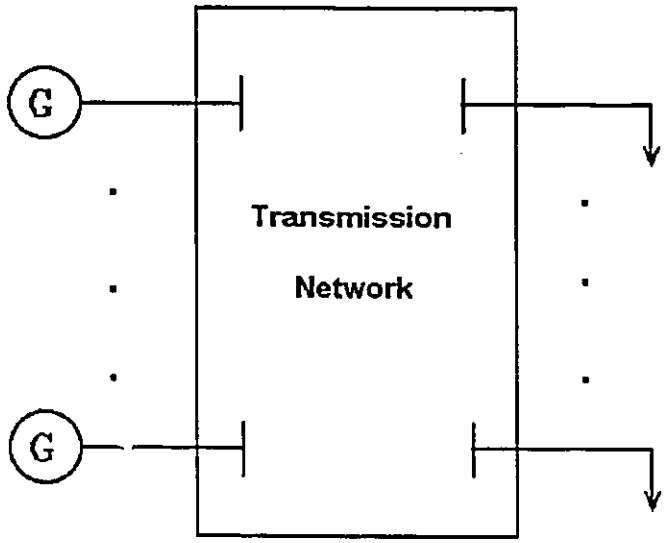

Figure 2.1: Multi-Machine Power System

2.2.2(a) Synchronous Generator

A synchronous machine is represented by Park's equations [48] in which the stator quantities are transformed into the d- and q- axis of the rotor. Depending on the number of rotor circuits represented, the generator can be modelled to any level of detail. Given below are Park's equations for a typical round rotor generator with two windings on each axis (figure 2.2). Equations for any number of rotor circuits can be defined similarly. All symbols are defined in pages xi to xiii, and expressed in per unit. The per unit system for generator modelling is provided in Appendix I.

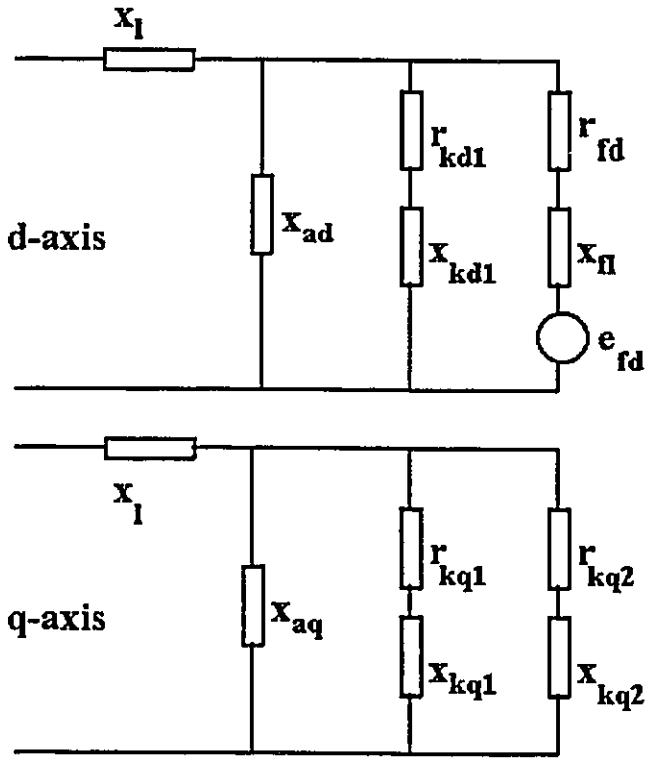

Figure 2.2: Two-Axis Generator Model

(i) Stator equations

Ignoring stator transients and assuming $\omega/\omega_o = 1.0$, the following equations can be obtained by choosing rotor flux linkages as state variables and by eliminating stator fluxes and rotor currents:

$$e_d = -r_a i_d + [i_q(x''_{aq} + x_{al}) - x''_{aq}(\frac{\psi_{kq1}}{x_{kq1}} + \frac{\psi_{kq2}}{x_{kq2}})] \quad (2.1)$$

$$e_q = -r_a i_q - [i_d(x''_{ad} + x_{al}) - x''_{ad}(\frac{\psi_{fd}}{x_{fl}} + \frac{\psi_{kd1}}{x_{kd1}})] \quad (2.2)$$

After further simplification,

$$e_d = -r_a i_d + x''_q i_q + E''_d \quad (2.3)$$

$$e_q = -r_a i_q - x''_d i_d + E''_q \quad (2.4)$$

where:

$$E''_d = -x''_{aq}(\frac{\psi_{kq1}}{x_{kq1}} + \frac{\psi_{kq2}}{x_{kq2}}) \quad (2.5)$$

$$E''_q = x''_{ad}(\frac{\psi_{fd}}{x_{fl}} + \frac{\psi_{kd1}}{x_{kd1}}) \quad (2.6)$$

Usually sub-transient saliency is ignored ($x"_d = x"_q$), then the complex quantity ($E"_d + jE"_q$) is the voltage behind the sub-transient impedance. Equations 2.3 and 2.4 provide an interface between the network equations with the generator differential equations.

(ii) Rotor equations

The rotor flux linkage equations are given below, with "p" standing for the time derivative operator:

$$p\psi_{fd} = \omega_o[e_{fd} + \frac{r_{fd}}{x_{fl}}(\psi_{ad} - \psi_{fd})] \tag{2.7}$$

$$p\psi_{kd1} = \omega_o\frac{r_{kd1}}{x_{kd1}}(\psi_{ad} - \psi_{kd1}) \tag{2.8}$$

$$p\psi_{kq1} = \omega_o\frac{r_{kq1}}{x_{kq1}}(\psi_{aq} - \psi_{kq1}) \tag{2.9}$$

$$p\psi_{kq2} = \omega_o\frac{r_{kq2}}{x_{kq2}}(\psi_{aq} - \psi_{kq2}) \tag{2.10}$$

where:

$$\psi_{ad} = x''_{ad}(-i_d + \frac{\psi_{fd}}{x_{fl}} + \frac{\psi_{kd1}}{x_{kd1}}) \tag{2.11}$$

$$\psi_{aq} = x''_{aq}(-i_q + \frac{\psi_{kq1}}{x_{kq1}} + \frac{\psi_{kq2}}{x_{kq2}}) \tag{2.12}$$

$$\frac{1}{x''_{ad}} = \frac{1}{x_{ad}} + \frac{1}{x_{fl}} + \frac{1}{x_{kd1}} \tag{2.13}$$

$$\frac{1}{x''_{aq}} = \frac{1}{x_{aq}} + \frac{1}{x_{kq1}} + \frac{1}{x_{kq2}} \tag{2.14}$$

For modelling salient pole generators, one rotor circuit on the q-axis is sufficient.

(iii) Mechanical equations

Generator acceleration is described by the following equations:

$$\dot{\omega} = \frac{\omega_o}{M}[T_m - T_e - K_D\frac{\omega}{\omega_o}] \tag{2.15}$$

$$\dot{\delta} = \omega \tag{2.16}$$

where

$$T_e = \psi_{ad}i_q - \psi_{aq}i_d \tag{2.17}$$

Equation 2.15 is referred to as the swing equation. The rotor speed (ω) is given in radians/second.

(iv) Generator Saturation

Generator saturation can be represented by modifying the mutual reactances x_{ad} and x_{aq} which are greatly affected by iron saturation. One saturation factor, k_{sat}, is usually applied to both axes:

$$x_{ad} = k_{sat}\, x_{adu} \tag{2.18}$$

$$x_{aq} = k_{sat}\, x_{aqu} \tag{2.19}$$

where:

$$k_{sat} = \frac{\psi_a}{\psi_a + \psi_I} \tag{2.20}$$

$$\psi_I = A_{sat} e^{B_{sat}(\psi_a - \psi_t)} \tag{2.21}$$

In per unit values, the air gap flux Ψ_a is equal to the air gap voltage E_a:

$$\bar{E}_a = \bar{E}_t + (r_a + jx_{al})\bar{I}_t \tag{2.22}$$

The quantities A_{sat} and B_{sat} are obtained by equation (2.21) given any two points on the generator saturation curve as shown in figure 2.3. For salient pole generators, the q-axis saturation is generally neglected.

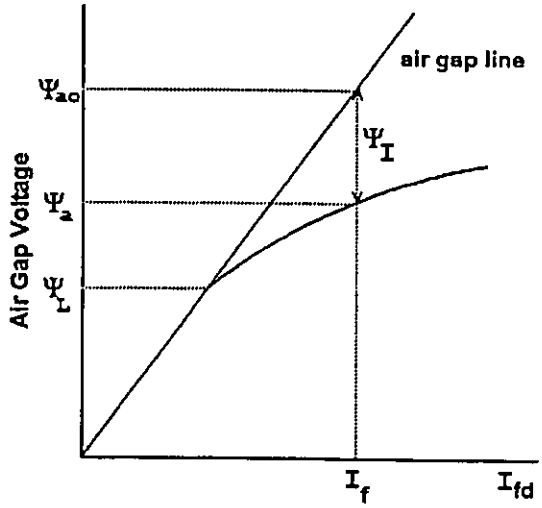

Figure 2.3: Generator Saturation Characteristics

2.2.2(b) Excitation Systems

Many different types of excitation systems [78] exist on today's power systems, for which differential-algebraic equations can be derived. To illustrate the modelling of excitation systems in transient stability analysis, let us consider a simple static exciter equipped with a $\Delta\omega$ power system stabilizer (PSS) as shown in figure 2.4.

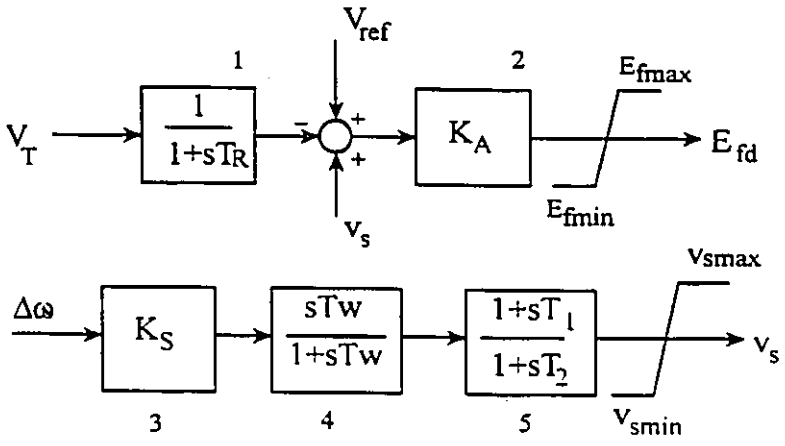

Figure 2.4: Static Exciter With $\Delta\omega$ PSS

By assigning state variables x_1, x_2, x_3 to the blocks 1,4, and 5, this simple excitation system can be represented by the following equations:

$$E_{fd} = K_A[V_{ref} - x_1 + v_s] \tag{2.23}$$

where $E_{fdmin} \leq E_{fd} \leq E_{fdmax}$

$$\dot{x}_1 = [E_t - x_1] / T_R \tag{2.24}$$

$$\dot{x}_2 = K_s \Delta\dot{\omega} - x_2 / T_w \tag{2.25}$$

$$\dot{x}_3 = [T_1\dot{x}_2 + x_2 - x_3] / T_2 \tag{2.26}$$

where $x_3 = v_s$ and $v_{smin} \leq v_s \leq v_{smax}$

The relationship between the generator field voltage e_{fd} and the exciter output E_{fd} is:

$$e_{fd} = \frac{r_{fd}}{L_{adu}} E_{fd} \tag{2.27}$$

2.2.2(c) Axis Transformation

The stator quantities in equations 2.1 to 2.6 are expressed in the individual machine dq frame of reference, which rotates with the rotor. In solving the network equations, the stator quantities are expressed in the common RI (real and imaginary) frame of reference, which rotates at the synchronous speed. In interfacing between the differential equations and the network

equations, it is required to transform these quantities from one frame to the other. The relationship between the two frames of reference is illustrated in figure 2.5, where δ is the angle between the generator q-axis and the reference axis which is taken as the R-axis of the common RI frame.

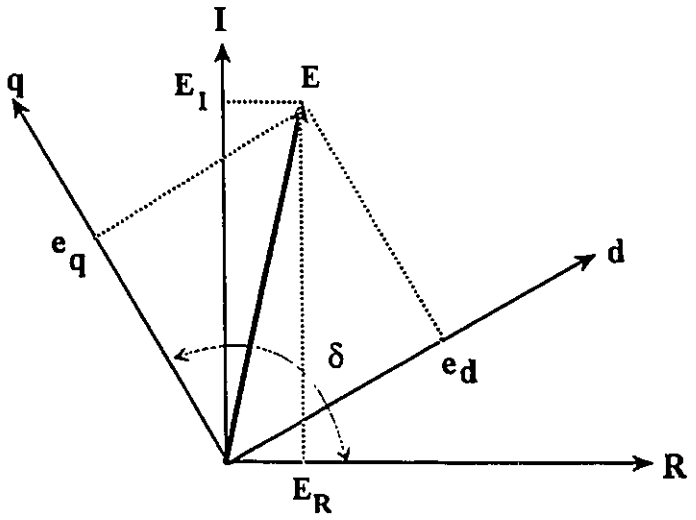

Figure 2.5: Axis Transformation

Let us assume $(e_d + je_q)$ and $(E_R + jE_I)$ are the stator voltages in the machine dq frame and the common RI frame respectively. Their relationships are given below:

$$
\begin{aligned}
e_d &= E_R \sin\delta - E_I \cos\delta \\
e_q &= E_I \sin\delta + E_R \cos\delta \\
E_R &= e_d \sin\delta + e_q \cos\delta \\
E_I &= e_q \sin\delta - e_d \cos\delta
\end{aligned}
\tag{2.28}
$$

Similarly, the internal voltage components E"d and E"q can be transformed into the common RI frame as follows:

$$
\begin{aligned}
E''_R &= E''_d \sin\delta + E''_q \cos\delta \\
E''_I &= E''_q \sin\delta - E''_d \cos\delta
\end{aligned}
\tag{2.29}
$$

Ignoring sub-transient saliency, i.e., $x''_d = x''_q = x''$, it can be shown that the internal voltage $(E''_R + jE''_I)$ is the voltage behind the sub-transient impedance $(r_a + jx'')$.

$$
(E_R + jE_I) = (E''_R + jE''_I) - (I_R + jI_I)(r_a + jx'') \tag{2.30}
$$

Equation (2.30) indicates that the generator can be represented either by Thevenin's or Norton's equivalent circuit when solving the network equations.

2.2.2(d) Load Representation

In transient stability analysis, loads are usually represented by static load models based on their voltage dependent characteristics. A widely used static load model is the ZIP (constant impedance, constant current, and constant power) model as given below:

$$P_L = P_o[\ a_1V^2 + a_2V + a_3\ ]$$
$$Q_L = Q_o[\ b_1V^2 + b_2V + b_3\ ] \qquad (2.31)$$

The three components in equation (2.31) represent the constant impedance, constant current, and constant power components respectively. The coefficients (a_i, b_i) represent the proportion of each component.

When modelling parameters are available, bus loads can also be represented as induction motors or synchronous motors. In this case, differential-algebraic equations need to be derived, similar to those developed for synchronous machines (equations 2.1 to 2.17).

2.2.2(e) Network Equations

Synchronous generators in a power system interact with each other through a transmission network. The network equations are formulated by defining the boundary conditions at the generator and load buses at each time step. In forming the network equations, the generators are usually represented by their Norton's equivalent circuits, while the loads are represented by current injections at the load buses (figure 2.6).

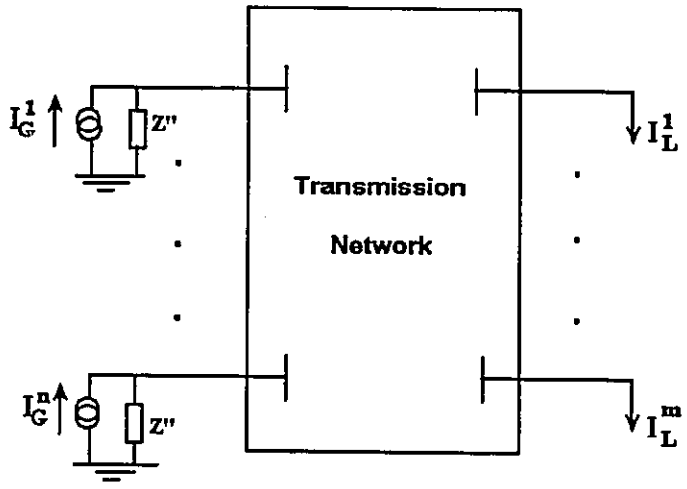

Figure 2.6: Generator and Load Representation

The generator and load current injections in figure 2.6 are given as follows:

$$\bar{I}_g = \frac{(E''_R + jE''_I)}{(r_a + jx'')} \tag{2.32}$$

$$\bar{I}_L = -\frac{P_L - jQ_L}{\bar{V}^*} \tag{2.33}$$

The network equation in matrix form is defined as:

$$[I] = [Y][V] \tag{2.34}$$

where:

[Y] = nodal admittance matrix

[V] = vector of bus voltages

[I] = vector of bus current injections

Note that the current vector [I] is a function of the state variables [x] and the bus voltages [V].

2.2.3 SOLUTION TECHNIQUES

The power system is now represented by a set of differential and algebraic equations in the following form:

$$\dot{x} = f(x,V) \tag{2.35}$$

$$I(x,V) = YV \tag{2.36}$$

This set of equations can be solved either by an explicit or implicit integration method in conjunction with a network solution algorithm. Given below are two integration algorithms commonly used.

2.2.3(a) Explicit Integration - Modified Euler Method

The modified Euler method is one of the simplest integration methods that performs well in power system transient stability analysis. The method is basically a predictor-corrector type as described below:

Predictor step:

$$x_p^{t+1} = x^t + f(x^t, V^t)\Delta t \tag{2.37}$$

$$YV_p^{t+1} = I(x_p^{t+1}, V^t) \tag{2.38}$$

Corrector step:

$$x^{t+1} = x^t + [f(x^t, V^t) + f(x_p^{t+1}, V_p^{t+1})]\ \Delta t / 2 \tag{2.39}$$

$$YV^{t+1} = I(x^{t+1}, V_p^{t+1}) \tag{2.40}$$

Note that equation (2.40) can be solved by LU factorization. In order to ensure numerical stability, the Modified Euler method requires relatively small time steps to be used. Commonly used step sizes vary from 0.004 to 0.008 seconds. Because of the small integration step sizes, the Modified Euler method usually requires more CPU time than other higher order integration methods which permit larger step sizes.

2.2.3(b) Implicit Integration - Trapezoidal Method

Implicit integration techniques have gradually found their way into transient stability programs. Given below is a typical algorithm based on the trapezoidal rule.

After converting the differential equations into algebraic equations using the trapezoidal rule, one can obtain the following:

$$F(x^{t+1},V^{t+1}) = x^{t+1} - x^{t} - [f(x^{t},V^{t}) + f(x^{t+1},V^{t+1})]\ \Delta t/2 \tag{2.41}$$

$$G(x^{t+1},V^{t+1}) = Y\ V^{t+1} - I(x^{t+1},V^{t+1}) \tag{2.42}$$

Equations 2.41 and 2.42 can be solved by applying the iterative Newton-Raphson method:

$$\begin{bmatrix} J_1 & J_2 \\ J_3 & J_4 \end{bmatrix} \begin{bmatrix} \Delta x \\ \Delta V \end{bmatrix} = \begin{bmatrix} -F \\ -G \end{bmatrix} \tag{2.43}$$

where J_1, J_2, J_3, and J_4 are the Jacobian matrices:

$$\begin{aligned} J_1 &= \frac{\partial F}{\partial x} \\ J_2 &= \frac{\partial F}{\partial V} \\ J_3 &= \frac{\partial G}{\partial x} \\ J_4 &= \frac{\partial G}{\partial V} \end{aligned} \tag{2.44}$$

To start the iterative solution process, the starting values of x_o are usually based on the Euler method, while the starting values of V_o are based on the geometry prediction [36]:

$$x_o^{t+1} = x^t + f(x^t, V^t)\ \Delta t \tag{2.45}$$

$$V_o^{t+1} = \frac{V^t\ V^t}{V^{t-1}} \tag{2.46}$$

Implicit integration techniques are numerically stable and allow larger time steps to be used. Typical step sizes vary from 0.01 to 0.02 seconds. Hence time domain simulations based on implicit integration techniques can be several times faster than those using explicit integration methods.

2.2.4 MAJOR STEPS OF TRANSIENT STABILITY SIMULATION

The time domain simulation technique solves the transient stability problem by determining the dynamic response of the power system to a disturbance such as a three-phase fault. It involves simulating the fault-on and the post-fault system trajectory in the time domain. Figure 2.7 illustrates the major steps of a typical transient stability simulation [37].

Block 1 reads in four types of input data, i.e, load flow data, generator data, switching data, and program control parameters. The load flow data provides the transmission network as well as generator initial conditions. The generator data includes machine modelling parameters such as reactances and time constants, inertia constants, and generator saturation curves. The switching data specifies where the fault is applied and how it is cleared, along with other switching operations. The program control parameters specify integration step size, length of the simulation period, monitored quantities, etc.

Block 2 represents the initialization step, in which all the state variables

and control signal reference quantities are initialized. Alarm messages will be given if some of the state variables have initial values outside their normal ranges.

Block 3 identifies if there are any changes to the network due to switching operations, such as the application or removal of fault. If such changes are identified, the nodal admittance matrix needs to be updated, which is done in block 4.

Blocks 5, 6, and 7 perform the numerical integration and network solution. These blocks are repeated more than once, depending on the order of the numerical integration method. For example, they will be looped through twice for each time step if the second order Modified Euler method is chosen.

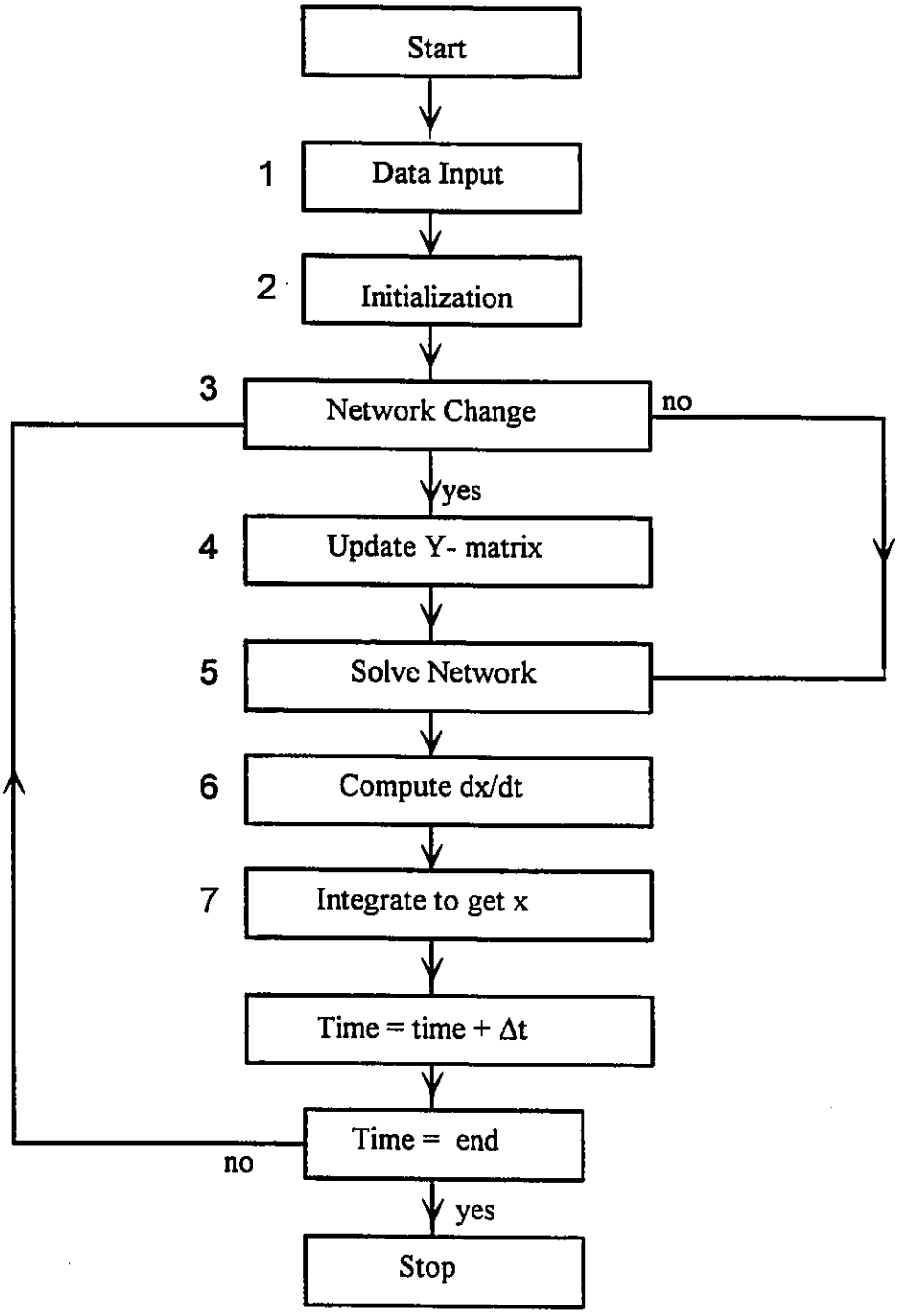

Figure 2.7: Major Steps of Transient Stability Simulation

2.2.5 CONCLUDING REMARKS

The conventional time domain simulation technique solves transient stability problems by simulating system trajectories step by step in the time domain. The method is highly accurate, due to its superb modelling capability. Its major shortcoming is that it only yields a stable-or-unstable answer, with no information provided on the degree of stability. Consequently, transient stability limit derivation based on this technique is essentially a trial-and-error approach requiring a large number of stability runs. If a stability index can also be derived from a time domain simulation, it will not only help engineers to gain additional insight into the stability analysis, but also enable them to speed up the transient stability limit derivation process by applying sensitivity techniques.

Since time domain simulations were considered expensive in the past, they were usually submitted as overnight runs. During that time, the maximum system size was often restricted to less than 1000 buses, and the typical turnaround time was several hours. With the recent advances in computer technology, transient stability simulations can now be performed rapidly during the day time on dedicated workstations for systems containing up to 12,000 buses. Recently, the time domain simulation technique has been considered capable of performing real time transient stability analysis.

2.3 DIRECT METHODS

2.3.1 BACKGROUND

Direct methods, also referred to as energy methods in the literature, provide an alternative approach to power system transient stability analysis. This class of analytical techniques is appealing for two reasons. First, they are potentially fast by avoiding the time domain simulation of post-fault system trajectories. More importantly, they have the ability to provide a transient stability index, called energy margin, for measuring the degree of stability.

Direct methods are based on Lyapunov's second method for stability analysis of non-linear systems. The power system is represented by a vector of state variables x. For a classically represented system, the state variables consist of the rotor angles and speeds. The general procedure of direct methods is to compute the system state at the instant of fault clearing (x_{cl}), which is the initial state of the system in the post-fault period. If x_{cl} lies inside the domain of attraction of the post-fault stable equilibrium point, the system is said to be stable. Otherwise, it is declared unstable. The domain of attraction is also called the region of stability, and is approximated by the surface $\{ x \mid V(x) \leq V_{cr} \}$, where V(x) is an energy function and V_{cr} represents the critical energy of the post-fault system. The stability region for a SMIB system is illustrated in figure 2.8. The most critical step in direct transient stability assessment is the determination of the region of stability. Energy margin (ΔV) is defined as $V_{cr} - V(x_{cl})$. A positive energy margin indicates the system is stable, while a negative energy margin indicates an unstable system.

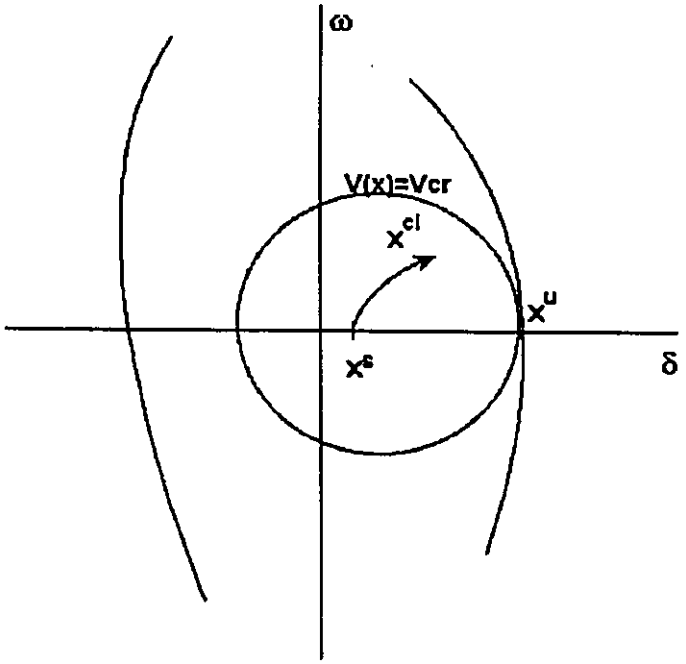

Figure 2.8: Region of Stability

When first introduced [14,41,73], direct methods were considered too conservative for any practical use. The conservativeness was due to two main reasons. First, the stability region computed was too pessimistic as will be explained later. Secondly, the use of the primitive classical generator model also contributed to conservativeness of the earlier attempts.

Over the last two decades, direct methods have drawn much attention of the power industry again. Significant advances have been made to improve their practicality for power system transient stability analysis. Some of the recent developments include:

- the development of the PEBS concept and its application in estimating the stability region [4,29],

- the development of the controlling or relevant UEP concept which takes into account the fault location [4],

- the appropriate accounting of transient kinetic energy that contributes to system separation [17],

- the development and application of Individual Machine Energy Functions and Group Energy Functions [68],

- the use of structure preserving network models for large scale system applications [1,2],

- the enhancement of the modelling capability of direct methods [23,47,58],

- the theoretical characterization of the boundary of the stability region [9], which subsequently led to the development of advanced solution algorithms for UEP computations [10],

- the rigorous testing and evaluation of direct methods using practical utility systems [7,44].

2.3.2 MATHEMATICAL FORMULATION

Given an n-generator system, the dynamic equations for machine i in the synchronous frame of reference are given as follows:

$$\dot{\delta}_i = \omega_i \tag{2.47}$$

$$M_i\dot{\omega}_i = P_{mi} - P_{ei} \tag{2.48}$$

In transient energy function analysis, the centre of inertia (COI) frame of reference is usually used, which has the advantage of removing the change in energy associated with the motion of the system center of inertia. The COI frame of reference is defined as:

$$\delta_o = \frac{1}{M_T}\sum_{i=1}^{n} M_i\delta_i \tag{2.49}$$

$$\omega_o = \frac{1}{M_T}\sum_{i=1}^{n} M_i\omega_i \tag{2.50}$$

where:

$$M_T = \sum_{i=1}^{n} M_i$$

After transforming the rotor angles and speeds from the synchronous frame into the COI frame, the swing equations become:

$$\theta_i = \delta_i - \delta_o$$

$$\tilde{\omega}_i = \omega_i - \omega_o$$

$$M_i\dot{\tilde{\omega}} = P_{mi} - P_{ei} - \frac{M_i}{M_T} P_{COI} \tag{2.51}$$

where:

$$P_{COI} = \sum_{i=1}^{n} (P_{mi} - P_{ei}) \tag{2.52}$$

For the n-generator system, the transient energy function (TEF) is defined for the post-fault system as the sum of n integrals over the path from θ^s to θ, where θ^s is the post-fault stable equilibrium point (SEP):

$$\begin{aligned} V &= \sum_{i=1}^{n} \int_{\theta_i^s}^{\theta_i} [M_i\dot{\tilde{\omega}}_i - (P_{mi} - P_{ei} - \frac{M_i}{M_T}P_{COI})] \, d\theta_i \\ &= \frac{1}{2}\sum_{i=1}^{n} M_i\tilde{\omega}_i^2 - \sum_{i=1}^{n} \int_{\theta_i^s}^{\theta_i} (P_{mi} - P_{ei} - \frac{M_i}{M_T}P_{COI}) \, d\theta_i \end{aligned} \tag{2.53}$$

The TEF (V) has two components, namely the transient kinetic energy (V_{ke}) and potential energy (V_{pe}). The former is a function of rotor speeds, while the latter is a function of rotor angles.

$$V = V_{ke} + V_{pe} \tag{2.54}$$

$$V_{ke} = \sum_{i=1}^{n} \frac{1}{2} M_i\tilde{\omega}_i^2 \tag{2.55}$$

$$V_{pe} = -\sum_{i=1}^{n} \int_{\theta_i^s}^{\theta_i} (P_{mi} - P_{ei} - \frac{M_i}{M_T}P_{COI}) \, d\theta_i \tag{2.56}$$

where θ^s is the post-fault SEP. Note that equation 2.56 applies to all power system models. The transient kinetic energy in equation (2.55) represents the total kinetic energy of the system. The units are given as follows:

Angle	[radians]
Speed	[radians/sec]
Power	[per unit]
Energy	[per unit power x radians]

The portion of V_{ke} that contributes to system separation is identified as the corrected kinetic energy V_{ke}^c [17]. When the system goes unstable, its generators separate into two groups: the group of the critical machines whose rotor angles increase indefinitely, and the rest of the system. Let N_a represent the index group of the critical machines and N_b the rest of the system. Given by equation (2.57), the corrected kinetic energy is represented by the transient kinetic energy of an equivalent SMIB system, with the equivalent machine representing the group of the critical machines.

$$V_{ke}^c = \frac{1}{2} M_{eq} \varpi_{eq}^2 \tag{2.57}$$

where:

$$M_{eq} = \frac{M_a M_b}{M_a + M_b}$$

$$M_a = \sum_{i \in N_a} M_i, \quad M_b = \sum_{i \in N_b} M_i$$

$$\varpi_{eq} = \varpi_a - \varpi_b$$

$$\varpi_a = \sum_{i \in N_a} \frac{M_i \varpi_i}{M_a}$$

$$\varpi_b = \sum_{i \in N_b} \frac{M_i \varpi_i}{M_b}$$

A disturbance such as a three-phase fault injects transient energy into the system causing it to depart from its stable equilibrium point. After fault removal, the post-fault system possess a certain amount of energy absorbing capability referred to as the critical energy V_{cr}. The system will be stable if the post-fault system can completely absorb the transient energy injected by the disturbance. The energy margin, which defines the degree of stability, is the difference between the critical energy of the post-fault system and the transient energy at fault clearing:

$$\Delta V = V_{cr} - V_{cl}(\underline{\omega}^{cl}, \underline{\theta}^{cl}) \qquad (2.58)$$

2.3.3 REGION OF STABILITY

Direct methods of transient stability analysis seek to characterize the initial conditions of post-fault system trajectories, i.e., system conditions at fault clearing, that converge back to the post-fault SEP. The set of such initial conditions comprises the region of stability. Hence direct methods solve the transient stability problem by checking whether the state of the system at fault clearing lies inside the stability region, which is approximated by the set $\{x \mid V(x)$

$\leq V_{cr}$ }. Correct evaluation of V_{cr} is most important in direct transient stability analysis. There are two general approaches to computing V_{cr}, the controlling UEP and the PEBS approach.

2.3.3(a) Controlling UEP Approach

Let us consider an n-generator system represented by classical models and constant impedance loads. The swing equations with rotor angles and speeds in the COI frame are represented by equation (2.51). The equilibrium points of the system are obtained by setting the derivatives to zero:

$$\dot{\theta}_i = \varpi_i = 0 \tag{2.59}$$

$$M_i\dot{\varpi}_i = P_{mi} - P_{ei} - \frac{M_i}{M_t} P_{COI} = f_i = 0 \tag{2.60}$$

Each solution to this set of equations represents an equilibrium point $(\theta^{ep},\varpi^{ep})$. At these equilibrium points, the rotor speeds are zero ($\varpi^{ep}=0$), and therefore only the rotor angles θ^{ep} need be considered. The equilibrium point at which the transient potential energy V_{pe} is at a global minimum is called the stable equilibrium point θ^s. All other equilibrium points are unstable equilibrium points (θ^u), at which V_{pe} is at a local maximum along a certain direction. Some of the unstable equilibrium points (θ^u) lie on the boundary of the PEBS.

For a given disturbance, the critically stable system trajectory, when projected onto the potential energy surface in the angle space, approaches one of the UEP's on the PEBS. This UEP is called the controlling or relevant UEP (θ^{cuep}). A good approximation of the region of stability is given by { (θ,ϖ)|

$V(\theta,\varpi) \leq V(\theta^{cuep},0)=V_{cr}$ } as shown in figure 2.8. Note that $V(\theta^{cuep},0) = V_{pe}(\theta^{cuep})$. The controlling UEP is usually obtained by solving the following optimization problem:

$$\min F = \sum_{i=1}^{n} f_i^2(\theta) \tag{2.61}$$

Numerical techniques for solving equation (2.61) include the Corrected Gauss-Newton method, and the second order Newton method. These methods require a good starting point in order to converge to the correct UEP. Under stressed system conditions or when the mode of instability is complex, the controlling UEP becomes very time consuming and difficult to obtain [7,44].

The controlling UEP is closely related to the mode of instability (MOI) which describes the pattern of system separation. If a generator tends to separate from the rest of the system for a given disturbance, its angle at the controlling UEP solution will have a large value usually greater than 90°. This machine is also referred to as an advanced or critical machine in the literature.

In the early days [14], the region of stability was estimated using the UEP that gives the smallest V_{cr}, i.e, the so-called closest UEP method. The closest UEP does not reflect the correct mode of instability, hence resulting in very pessimistic transient stability assessment.

2.3.3(b) The PEBS Approach

It has been mentioned that at an unstable equilibrium point, the potential energy V_{pe} is at a local maximum.. This observation motivated Kakimoto et al

[29] to develop the PEBS method for estimating V_{cr}.

Consider a 3-generator system whose potential energy as a function of the rotor angles is given in figure 2.9. Again, the potential energy is at a local maximum at each UEP on the potential energy surface along a certain direction. Kakimoto et al proposed to construct a Potential Energy Boundary Surface by connecting all the V_{pe} maxima through the ridge of the potential energy surface as shown in figure 2.9. Note that along the direction orthogonal to the PEBS, V_{pe} reaches a local maximum at the PEBS crossing.

An algorithm for the PEBS method of determining V_{cr} is summarized below:

Step 1: For a given disturbance, simulate the fault-on trajectory (θ(t), ϖ(t)).

Step 2: Along the fault-on trajectory θ(t) projected onto the potential energy surface in the angle space, identify the point θ^{pcp} at which V_{pe} reaches its first peak.

Step 3: The region of stability is approximated locally by the surface: $\{ (\theta,\varpi) \mid V(\theta,\varpi) \leq V_{pe}(\theta^{pcp}) \}$.

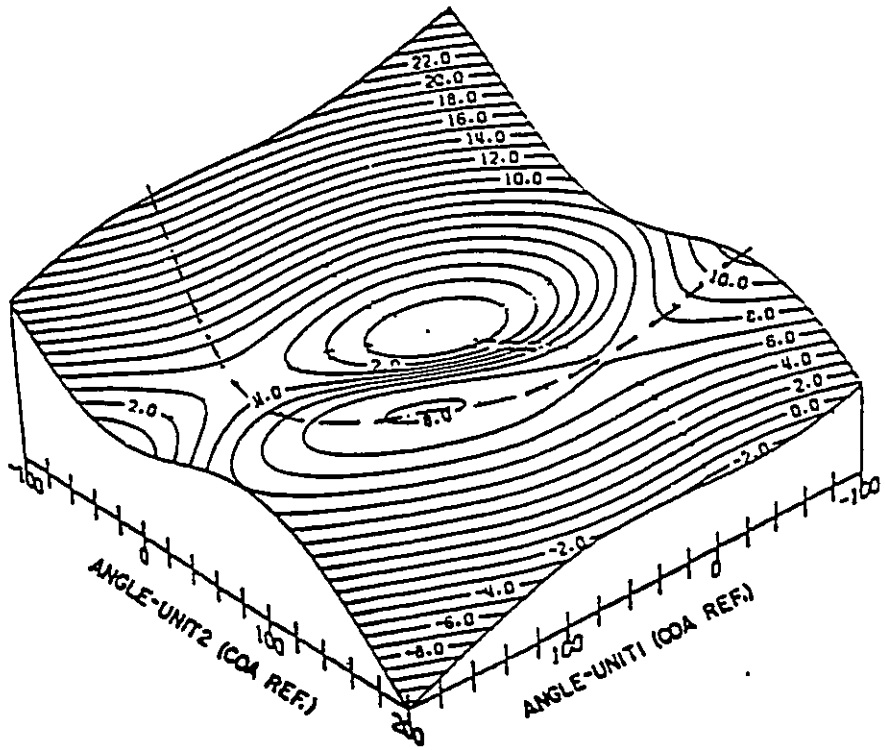

Figure 2.9: PEBS for a 3-Generator System [4]

2.3.3(c) The Exit Point Method

The Exit Point method is also called the Boundary of Stability Region Based Controlling Unstable Equilibrium Point (BCU) method. It is essentially a combination of the PEBS and the controlling UEP method. Chiang et al [9] characterizes the PEBS as the stability region boundary of an associated gradient system in the angle space:

$$\dot{\theta}_i = -\frac{\partial V_{pe}}{\partial \theta_i}, \quad i=1,n \tag{2.62}$$

Note that if (θ^{uep}) is an equilibrium point of the gradient system, then

$(\theta^{ucp},0)$ is an equilibrium point of the original power system. The stability region boundary of the gradient system is the union of all the stable manifolds of the equilibrium points on the stability region boundary. The stable manifold of an equilibrium point x^{cp} is defined as follows:

$$W^s(x^{cp}) = \{x \mid x(t) \to x^{cp} \text{ as } t \to \infty\}$$

Based on this, Chiang et al [10] proposed the BCU method to compute the controlling UEP of the original power system, via the computation of the controlling UEP of the associated gradient system. The algorithm for the BCU method is briefly summarized below:

Step 1: Simulate the fault-on trajectory and, along the projected fault-on trajectory, determine the point θ^{pcp} at which V_{pe} reaches its first maximum, i.e., the PEBS crossing point.

Step 2: With θ^{pcp} as the initial conditions, simulate the associated gradient system described by equation 2.62, until the point $\underline{\theta}^{Fmin}$ is reached at which the following quantity reaches its first minimum:

$$\sum_{i=1}^{n} \|f_i(\theta)\|$$

Step 3: Use θ^{Fmin} as the starting point to solve for the controlling UEP (equation 2.61), using any optimization technique.

After extensive testing by Ontario Hydro [44], the BCU method is

considered the best method for computing controlling UEP's.

2.3.4 INCORPORATION OF EXCITER EFFECTS

Significant efforts [23,44,47,58] have been made to extend direct methods to include the effects of excitation control systems, which are vital to transient stability assessment. Earlier approaches [59] attempted to formulate energy functions based on a full set of state variables. These approaches were considered impractical for multi-machine system applications, since such energy functions are difficult to obtain and calculation of their UEP's is computationally inhibitive. A practical approach was proposed by Sasaki [56] who incorporated the flux decay model into the transient energy function analysis. Instead of adding more state variables into the energy function, Sasaki retained the form of the energy function for the classical generator model, but treated generator internal voltages as varying parameters. This approach has been adopted by other researchers [4,23].

Another approach is to completely avoid the derivation of a closed form energy function, and to rely on a numerical energy function whose evaluation involves path integration. This approach involves time domain simulation, and is adopted by the RFT method.

2.3.4(a) Extension of the PEBS Approach

Athay et al [4] first attempted to incorporate excitation systems into the PEBS method. They proposed to compute the potential energy along the fault-on trajectory through numerical integration. Let us consider an n-generator system, with each generator represented by a two-axis transient model. Its field voltage

varies according to the dynamics of the excitation system. The power system is described by the following equations:

$$\dot{\delta} = \omega \tag{2.63}$$

$$M\ \dot{\omega} = f(\delta,x,y) \tag{2.64}$$

$$\dot{x} = g(\delta,x,y) \tag{2.65}$$

$$0 = h(\delta,x,y) \tag{2.66}$$

where:

x = vector of state variables other than ω and δ

y = vector of algebraic variables (i_d, i_q, e_d, e_q)

For a given disturbance, simulating equations 2.63 to 2.66 in the time domain produces the fault-on trajectory. The potential energy along the fault-on trajectory can be evaluated by integrating the following equation:

$$\dot{V}_{pe} = -\sum_{i=1}^{n} (\omega-\omega_{COI})\ f_i(\delta,x,y^*) \tag{2.67}$$

where y^* is computed based on the post-fault Y-matrix:

$$0 = h(\delta,x,y^*) \tag{2.68}$$

The first V_{pe} peak along the fault-on trajectory is taken as the critical energy V_{cr}. This approach does not yield satisfactory results, due to the effects of fast dynamics [58]. Sauer et al proposed to separate the state variables x into two groups, x_1 and x_2. The first group contains the state variables associated with

fast dynamics, which should be computed using the post-fault Y-matrix. The potential energy along the fault-on trajectory is then evaluated by integrating the following equation:

$$\dot{V}_{pe} = -\sum_{i=1}^{n} (\omega_i - \omega_{COI})\, f_i(\delta, x_1^*, x_2, y^*) \tag{2.69}$$

where x_1^* is computed based on y^*:

$$\dot{x}_1^* = g_1(\delta, x_1^*, x_2, y^*) \tag{2.70}$$

2.3.4(b) Extension of the Exit Point Method

Using the parameter variation approach, Fouad et al [23,44] extended the controlling UEP approach to include the effects of excitation controls in transient energy function analysis. A two-axis transient generator model and a simplified exciter model with one gain and one time constant were tested. In the transient generator model, the internal voltage is represented by two components, E'_d and E'_q, which are state variables. One significant observation reported was that when the post-fault system trajectory approaches the boundary of the stability region, the time derivatives of the state variables associated with the generator fluxes and exciter controls do not vanish. Hence, they proposed to replace the controlling UEP with the peak point (x^{pp}) of the critically stable trajectory. The peak point is defined as the point at which the critically stable trajectory is closest to the stability region boundary. The biggest task is then to compute x^{pp}, which is similar to the calculation of the controlling UEP. In estimating the peak point x^{pp}, not only the rotor angles, but also the E'_d and E'_q components of the internal voltages of the detailed machines need to be obtained.

$$x^{pp} = \begin{bmatrix} E'^{pp}_{d} \\ E'^{pp}_{q} \\ \theta^{pp} \end{bmatrix}$$

In [44], the BCU method described earlier was modified to compute the peak point. Given the system state at fault clearing x^{cl}, and the peak point x^{pp} of the critically stable trajectory, the energy margin is defined as:

$$\Delta V = V_{pe} \Big|_{x^{cl}}^{x^{pp}} - \frac{1}{2} M_{eq} \varpi_{eq}^{2} \tag{2.71}$$

where V_{pe} is obtained by:

$$V_{pe} = -\sum_{i=1}^{n} \int_{\theta_i^{cl}}^{\theta_i^{pp}} [P_{mi} - P_{ei} - \frac{M_i}{M_T} P_{COI}] d\theta_i \tag{2.72}$$

A closed form expression for V_{pe} is given in [23], by making linear angle trajectory approximation and treating E'_d and E'_q as constants:

$$E'_{d_i} = (E'^{cl}_{d_i} + E'^{pp}_{d_i})/2 \tag{2.73}$$

$$E'_{q_i} = E'^{pp}_{q_i} \tag{2.74}$$

2.3.5 CONCLUDING REMARKS

Direct methods based on the controlling UEP approach and the sustained fault approach have been presented in this section. The most appealing feature of direct methods is its capability to produce energy margins which indicate the degree of stability. Furthermore, direct methods are potentially faster than the conventional time domain simulation technique in evaluating power system transient stability. Despite significant advances made in the last two decades to improve the practicality of direct methods, further enhancements are required to improve their accuracy and reliability, before they can find more general use in the industry. Their main application so far has been limited to dynamic contingency screening.

Between the two classes of direct methods, the sustained fault approach is computationally faster but produces less accurate results than the controlling UEP approach. Test results to date [63] indicate that transient stability limits derived by the sustained fault approach, even for plant mode systems classically represented, can have an error as large as 15%, when compared to those derived based on conventional time domain simulations. Transient stability limits derived by the controlling UEP approach are usually within 5% of those based on time domain simulations [7,44,63]. However, the controlling UEP approach occasionally encounters solution divergence problems, especially when analysing stressed systems or systems of complex modes of instability. In summary, direct methods have potential applications in both on-line and off-line transient stability limit derivation, once their speed, accuracy, and reliability have been improved and successfully demonstrated.

2.4 CONCLUSIONS

Two classes of analytical tools for power system transient stability analysis have been presented in this chapter: the conventional time domain simulation technique and the so-called direct methods. Direct methods are considered as emerging tools, having the advantage of producing energy margins which indicate the degree of stability. Further enhancements are needed in order to improve their accuracy, speed, and reliability, before they can become a production tool for power system transient stability analysis.

The conventional time domain simulation technique is the principal tool for transient stability analysis in the power industry. This technique is flexible, reliable, and highly accurate due to its superb power system modelling capability. In addition to indicating whether a given system is stable or unstable, it also provides time responses of the system quantities which are requried for checking other dynamic performance criteria such as relay margins and transient voltage dips. Its major shortcoming, however, is the lack of information on the degree of stability. Transient stability limit derivation based on this technique has to be accomplished through a trial and error approach, which requires many stability runs. Each run is computationally expensive. Furthermore, the lack of energy margin information makes this tool inefficient for dynamic contingency ranking.

The main objective of this thesis is to combine the strengths of the time domain simulation technique and direct methods in one tool, by incorporating energy margin calculation into the former. Energy margin provides additional insight into the stability analysis. Its main application is to speed up the overall transient stability limit derivation process by reducing the number of stability runs. Direct methods offer two general approaches to energy margin calculation:

the controlling UEP approach and the sustained fault approach. Although the controlling UEP approach is more accurate, it requires significantly more CPU time and occasionally encounters solution divergence problems.

In incorporating energy margin calculation into the conventional time domain simulation technique, the author's judgement is that only approximate energy margins are required. Unlike direct methods in which energy margins are used to determine whether the system is stable or unstable, the conventional time domain simulation technique can accurately determine the transient stability of the system, even without any energy margin information. When the time domain simulation method is used, energy margins are additional output quantities which serve as trend indicators and can be used to speed up transient stability limit derivation by reducing the number of stability runs. Therefore, the sustained fault approach has been adopted for incorporating energy margin calculation into the conventional time domain simulation technique, which already has the capability of simulating sustained faults. Other advantages of the sustained fault approach are that it is relatively fast, and does not encounter solution divergence problems.

CHAPTER 3
ENERGY MARGINS BY THE RFT METHOD

3.1 INTRODUCTION

Both the conventional time domain simulation technique and direct methods for power system transient stability analysis have been reviewed in the previous chapter. Because of its accuracy, flexibility, and reliability, the time domain simulation method is the principal tool for transient stability assessment in the power industry. Recently, its computational speed has been much improved by the incorporation of implicit integration techniques such as the trapezoidal method [36,38].

The main disadvantage of the conventional time domain simulation method is its inability to provide any information on the degree of stability. As a result, transient stability limit derivation can only be accomplished via a trial and error approach, which is not only tedious but also requires a large number of stability runs. In addition, the lack of information on the degree of stability also makes the conventional time domain method inefficient for dynamic contingency ranking and screening.

Direct methods based on transient energy analysis, on the other hand, have the appealing feature of providing energy margins which indicate the degree of stability. These methods, however, are still at a developmental stage. Additional research efforts are needed to improve their accuracy and reliability before they receive widespread use in the industry. At the present time, their

main application is primarily restricted to fast contingency screening.

Since both the conventional time domain technique and direct methods have their strengths and weaknesses, it is highly desirable to combine their strengths in one tool, which is the main objective of this thesis. This chapter presents a new analytical technique, named as the Relevant Fault-on Trajectory (RFT) method, for incorporating energy margin calculation into conventional time domain simulations. The development of the RFT method is based on a combination of the Hybrid method [43], the PEBS method, and the analysis of the transient energy associated with the critical generator group. Energy margins not only provide additional insight into the stability analysis, but also have the capability of speeding up transient stability limit derivation by reducing the number of stability runs. By indicating the degree of stability, they also have potential applications in dynamic contingency ranking. Fast transient stability limit derivation is essential to on-line dynamic security assessment, which is the main objective of many current research and development activities in the power industry [12, 27, 33, 42].

3.2 REVIEW OF THE HYBRID METHOD

Recognizing the shortcomings of direct methods, Maria, Tang, and Kim proposed the Hybrid method to derive energy margins by combining conventional time domain simulation with transient energy analysis. Since its publication, the Hybrid method has received favourable comments from research and utility engineers [42, 52]. Its algorithm is briefly reviewed in this section.

For a classically represented system, the Hybrid method first simulates the trajectories of rotor angles and speeds for the first swing period by performing a conventional time domain simulation. Projecting the rotor angle trajectories onto a potential energy surface in the angle space provides a system trajectory on this potential energy surface. A system trajectory for a stable 3-generator system is given in figure 3.1, which shows three local potential energy peaks along the first swing trajectory. Figure 3.1 also shows the PEBS which represents the boundary of the region of stability of the post-fault SEP. Let ΔV^{i}_{pe} represent the potential energy difference (equation 2.56) between the i^{th} local PE peak and the PEBS along a linear ray passing through the fault clearing state (θ^{cl}) and the i^{th} PE peak (θ^{pepp}). The Hybrid method defines the energy margin (ΔV) for a stable case as follows:

$$\Delta V = \min \{ \Delta V^{i}_{pe}, i \in S_p \}$$

where S_p represents the index set of the local PE peaks along the post-fault system trajectory. The local PE peak which yields the minimum ΔV^{i}_{pe} is called the dominant PE peak. Energy margin defined in this manner represents the proximity of the dominant PE peak to the PEBS along a specific linear ray.

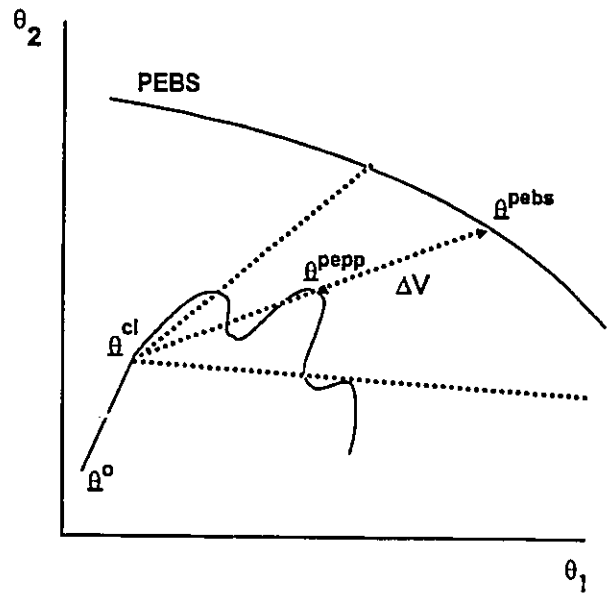

Figure 3.1: Hybrid Method: ΔV for a Stable Case

If the system is unstable as indicated by extremely large rotor angles, the system trajectory on the potential energy surface will cross the PEBS. The Hybrid method defines the energy margin for an unstable case as the minimum corrected kinetic energy (equation 2.57) along the post-fault trajectory (figure 3.2). The minimum corrected kinetic energy (min V_{ke}^{c}) represents the portion of the transient kinetic energy, injected into the critical machines by the disturbance, that the post-fault system fails to absorb.

When detailed generator models are represented, the Hybrid method simulates the system trajectory based on the detailed models. Along this trajectory, the local PE peaks are identified in the usual manner. However, before line searches are performed to detect the PEBS, the detailed generators are

converted into their equivalent classical representations using the generator conditions at the local PE peaks. In so doing, the TEF developed for the classical generator model (equation 2.56) is still applicable for potential energy calculation.

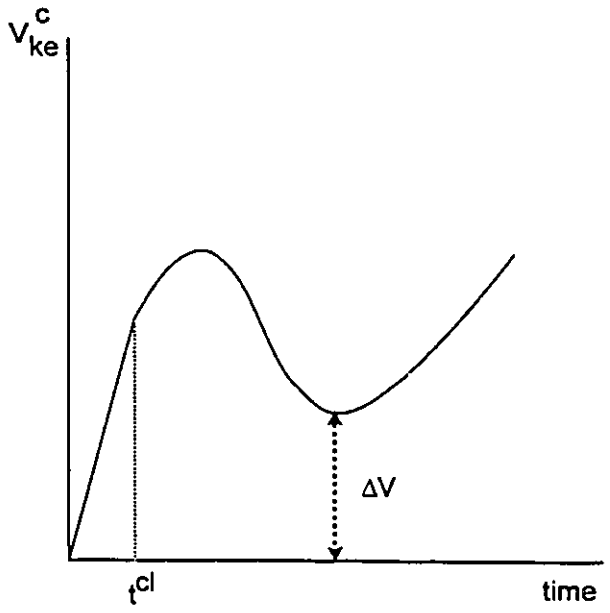

Figure 3.2: Hybrid Method: ΔV for an Unstable Case

The Hybrid method has one major shortcoming [44] in that the energy margins so produced may not be monotonically decreasing as system conditions are increasingly stressed. This is due to the fact that as system conditions are varied, usually through some changes in the generation dispatch, some local PE peaks that existed previously may disappear while new PE peaks may arise. Consequently, different dominant PE peaks may be chosen to define energy margins in different cases, resulting in discontinuities in the energy margins vs interface flow relationship. Such discontinuities make it difficult if not impossible to apply sensitivity techniques to speed up transient stability limit derivation.

The RFT method remedies the shortcoming of the Hybrid method. By using the corrected kinetic energy to identify the dominant PE peak, the RFT method eliminates the energy margin discontinuity problem, since the local PE peaks due to inter-machine oscillations among the critical generators are eliminated. The RFT method retains the Hybrid approach in computing energy margins for unstable cases, which simply involves corrected kinetic energy calculation for a given mode of instability. For stable cases, the RFT method computes energy margins by determining the additional energy absorbing capability of the critical generators, after they have fully absorbed the transient kinetic energy injected into them by the disturbance. The determination of the additional energy absorbing capability of the critical generators is accomplished through the simulation of a sustained fault, as described in the next section.

3.3 GENERAL DESCRIPTION OF THE RFT METHOD

Let us first review the basic mechanism of power system transient instability. The occurrence of a fault on a power system injects transient energy into the machines, causing them to deviate from their equilibrium positions. When the fault is cleared just beyond the critical clearing time, the group of unstable machines forms a critical generator group. In [17], Fouad et al identified that the transient kinetic energy associated with the critical generator group (V_{ke}^{grp}) is directly responsible for system separation. In the literature, the transient kinetic energy is also referred to as the corrected kinetic energy (V_{ke}^{c}). This is represented by the transient kinetic energy associated with an equivalent SMIB system as described by equation (2.57). In [68], Vittal identified that the critical generator group in the post-fault period has a finite amount of energy absorbing capability, which can be estimated by simulating a sustained or long duration fault in the time domain. Transient stability is maintained if the transient kinetic energy injected into the critical generator group by the disturbance is less than the post-fault energy absorbing capability of this group.

The RFT method computes energy margins by analysing the transient energy of the critical generator group and adopts the two-stage approach of the Hybrid method. For a given contingency, the first stage is to perform a conventional time domain simulation from which the transient stability of the system is accurately determined. If the system is unstable, V_{ke}^{grp} will not reach zero in the post-fault period during the simulation of the first swing transient. The unabsorbed portion of V_{ke}^{grp} provides a good measure of how unstable the system is. The Hybrid method uses it to define energy margins for unstable cases, so does the RFT method.

If the system is stable, V_{ke}^{grp} will reach zero some time after fault removal. A second stage will be initiated to determine the energy margin for a stable case. While simulating the first swing transient in stage 1, the RFT method identifies the time instant, t^{kemin}, when the transient kinetic energy of the critical generator group reaches a minimum of zero. Note that the potential energy of the critical generator group reaches a maximum at the same time. The energy margin for a stable case is determined by the amount of additional energy absorbing capability that the critical generator group has at the time of t^{kemin}.

In order to determine the additional energy absorbing capability of the critical group at time t^{kemin}, a sustained fault approach similar to the PEBS method is adopted for stage 2 of the RFT method. After restoring the system conditions at t^{kemin}, a sustained fault is applied which causes the critical machines to advance further and eventually separate from the rest of the system. The maximum potential energy gained by the critical generator group along the fault-on trajectory represents the additional energy absorbing capability of the critical group at time t^{kemin}.

Figure 3.3 shows the potential energy of the critical generator group during the first swing transient (stage 1), and along the fault-on trajectory (stage 2). At time t^{kemin}, the transient kinetic energy injected into the critical generator group is completely converted so that its potential energy reaches a peak. This is the PE peak along the post-fault system trajectory as simulated in stage 1. Starting with the system conditions at time t^{kemin}, a fault-on trajectory is simulated in stage 2, along which the critical generator group reaches another PE peak (at time t^{P}). The maximum potential energy gained by the critical generator group along the fault-on trajectory represents the energy margin, as shown in figure 3.3.

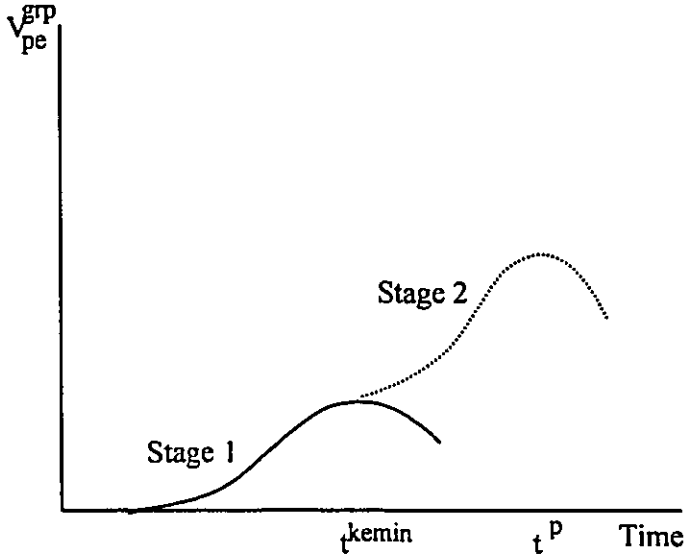

Figure 3.3: PE of the Critical Group in Stages 1 and 2

Two factors are critical to energy margin calculation by the RFT method. First, the identification of the critical machines must be accurate, based on the mode of instability associated with the disturbance. The RFT method relies on the user to supply the MOI, assuming that he or she is familiar with the test system. Secondly, the fault-on trajectory must be a relevant one, implying that the system separation pattern at time t^p along the fault-on trajectory must agree with that of the critically unstable system trajectory. For most systems, a relevant fault-on trajectory can be obtained easily by applying a sustained three-phase fault at the original fault location. For complex area mode systems where many machines within a large geographical area lose synchronism, it is recommended to apply simultaneous faults at two or more locations in order to severely disturb the whole set of critical machines to produce a relevant fault-on trajectory with the desired system separation pattern.

The computing requirements of the RFT method largely depend on the time domain simulation periods of the two stages. The simulation of stage 1 depends on the duration of the first swing period of the test system, which usually varies from two to five seconds. The stage 2 simulation period is short relative to that of stage 1, and depends on when the potential energy of the critical generator group reaches a peak along the fault-on trajectory - typically less than half a second.

3.4 MATHEMATICAL FORMULATION

3.4.1 Power System Model

For an n-generator system, the swing equations are repeated below:

$$\dot{\delta}_i = \omega_i \tag{3.1}$$

$$M_i \dot{\omega}_i = P_{mi} - P_{ei} \tag{3.2}$$

where:

δ_i = rotor angle of machine i in the synchronous frame of reference

ω_i = rotor speed of machine i

P_{mi} = mechanical input of machine i

P_{ei} = electrical output of machine i

M_i = inertia of machine i (2H)

Note that equation (3.2) applies to any generator model. Equations (3.1) and (3.2) together with other differential and algebraic equations can be put into the general form:

$$\dot{\underline{x}} = \underline{g}(\underline{x}, \underline{y}) \tag{3.3}$$

$$\underline{0} = \underline{h}(\underline{x}, \underline{y}) \tag{3.4}$$

where:

$\underline{x}$ = vector of state variables

$\underline{y}$ = vector algebraic variables

Equation (3.3) describes the dynamic models while equation (3.4) describes the network and generator interface equations. A conventional time domain simulation program solves these two sets of equations through step-by-step integration in the time domain as described in section 2.1. The network equations for the fault-on and post-fault periods depend on the fault-on and post-fault admittance matrices respectively.

3.4.2 Transient Energy of the Critical Generator Group

The transient energy associated with the critical generator group can be represented by the transient energy of an equivalent SMIB system [19, 51, 74]. An alternative way of computing this energy based on Individual Machine Energy Functions will be presented in the next chapter. Let us divide the n machines of the system into two groups. Group K consists of the critical machines that tend to go unstable, while Group S contains the rest of the machines. The swing equations for each group of machines are:

$$M_k\ddot{\omega}_k = P_{m_k} - P_{e_k}, \quad k \in K \tag{3.5}$$

$$M_l\ddot{\omega}_l = P_{m_l} - P_{e_l}, \quad l \in S \tag{3.6}$$

The center of inertia (COI) for each generator group is defined as:

$$\delta_{COI,K} = \frac{1}{M_{TK}} \sum_{k \epsilon K} M_k \delta_k , \quad M_{TK} = \sum_{k \epsilon K} M_k \tag{3.7}$$

$$\delta_{COI,S} = \frac{1}{M_{TS}} \sum_{l \epsilon S} M_l \delta_l , \quad M_{TS} = \sum_{l \epsilon S} M_l \tag{3.8}$$

Summing the swing equations for each group, we obtain:

$$M_{TK} \ddot{\delta}_{COI,K} = \sum_{k \epsilon K} P_{m_k} - \sum_{k \epsilon K} P_{e_k} \tag{3.9}$$

$$M_{TS} \ddot{\delta}_{COI,S} = \sum_{l \epsilon S} P_{m_l} - \sum_{l \epsilon S} P_{e_l} \tag{3.10}$$

Equations (3.9) and (3.10) can be combined to yield the swing equation for an equivalent SMIB system:

$$M_{eq} \ddot{\delta}_{eq} = P_{m_{eq}} - P_{e_{eq}} \tag{3.11}$$

where:

$$\delta_{eq} = \delta_{COI,K} - \delta_{COI,S} \tag{3.12}$$

$$M_{eq} = \frac{M_{TK} M_{TS}}{M_{TK} + M_{TS}} \tag{3.13}$$

$$P_{m_{eq}} = (M_{TS} \sum_{k \epsilon K} P_{m_k} - M_{TK} \sum_{l \epsilon S} P_{m_l}) / (M_{TK} + M_{TS}) \tag{3.14}$$

$$P_{e_{eq}} = (M_{TS} \sum_{k \epsilon K} P_{e_k} - M_{TK} \sum_{l \epsilon S} P_{e_l}) / (M_{TK} + M_{TS}) \tag{3.15}$$

At each time step of a time domain simulation, the quantities associated with the equivalent machine (δ_{eq}, Pm_{eq}, Pe_{eq}) can be computed based on the quantities associated with each individual machine using equations (3.12) to (3.15). Using the approach as described in section 2.3.2, a transient energy

function for the equivalent SMIB system can be defined, with the machine representing the critical generator group:

$$V^{grp} = V_{ke}^{grp} + V_{pe}^{grp} \tag{3.16}$$

Between any two time instants t_1 and t_2 along a system trajectory, the potential and kinetic energy components of the critical generator group (i.e, the equivalent machine) are given below:

$$V_{pe}^{grp} = \int_{\delta_{eq}^{t_1}}^{\delta_{eq}^{t_2}} (P_{e_{eq}} - P_{m_{eq}}) \, d\delta_{eq} \tag{3.17}$$

$$V_{ke}^{grp} = \frac{1}{2} M_{eq} (\omega_{eq}^{t_2} - \omega_{eq}^{t_1})^2 \tag{3.18}$$

where:

$$\omega_{eq} = \omega_{COI,K} - \omega_{COI,S} \tag{3.19}$$

$$\omega_{COI,K} = \sum_{k \in K} \frac{M_k \omega_k}{M_{TK}}, \quad \omega_{COI,S} = \sum_{l \in S} \frac{M_l \omega_l}{M_{TS}} \tag{3.20}$$

To evaluate the potential energy of the critical generator group along a system trajectory, the terms Pe_{eq} and δ_{eq} can be computed using equations (3.15) and (3.12) respectively at each time step. Note that Pe_{eq} must be computed using the post-fault admittance matrix.

3.5 ENERGY MARGIN CALCULATION

Energy margin (ΔV) provides a quantitative measure of how stable or unstable the system is for a given disturbance. If the system is stable, ΔV indicates how far the system is from being unstable. If the system is unstable, ΔV indicates how far the system is from being stable. This section first presents the procedure of energy margin calculation for a classical model of a single-machine-infinite-bus (SMIB) system. Such a model neglects saliency. This procedure is then extended to compute energy margin for detailed generator representation. Finally, a procedure for computing energy margins for multi-machine systems is provided.

3.5.1 THE SMIB SYSTEM - CLASSICAL GENERATOR MODEL

Figure 3.4 shows the post-fault power-angle curve for a SMIB system whose generator is represented by a constant voltage E' behind the transient reactance. In this figure, it is assumed that the generator electrical power output is zero while the fault is on. The initial rotor angle is δ^o and the mechanical power input is P_m. A fault is applied at time t^o causing the rotor to accelerate. The fault is cleared at time t^{cl}, and the corresponding rotor angle is δ^{cl}. If the fault clearing time t^{cl} is less than the critical clearing time (cct), the rotor will advance to a peak angle of δ^p and then retreat. The longer the fault clearing time, the larger the peak angle.

In figure 3.4, the post-fault power-angle curve intersects with the horizontal line $P_e=P_m$ at two locations, δ^s and δ^u, which represent the SEP and UEP of the post-fault system respectively. The post-fault SEP represents the state into which the system will eventually settle, provided there is enough damping on

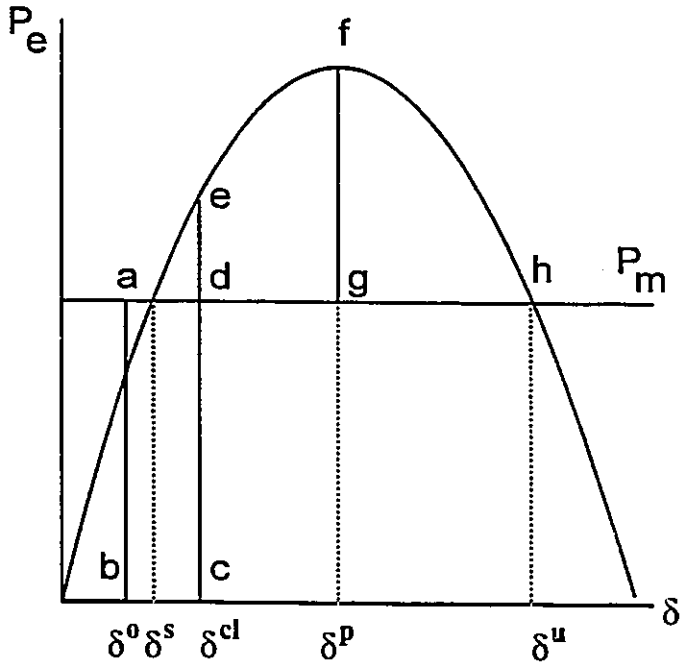

Figure 3.4: Power-Angle Curve for a Classical SMIB System

the system. The UEP represents the maximum rotor angle the machine can take in the forward swing without losing stability. Once the rotor angle swings past δ^u, the machine will lose stability. The system potential energy is minimum at δ^s and maximum at δ^u.

Let us now consider how the energy margins for stable cases can be computed for the SMIB system by the RFT method. The generator power-angle trajectory a-b-c-d-e-f in figure 3.4 is provided from the time domain simulation of the first swing transient during stage 1. Point f corresponds to the time instant of t_{kemin} when the transient kinetic energy of the machine reaches a minimum of zero. Area abcd represents the transient kinetic energy injected into the machine by the fault, which is then converted into potential energy represented by area defg after fault removal. For the classical generator model, these two areas are

equal and the total energy of the post-fault system ($V_{pe}+V_{ke}$) is constant. The energy margin for this case is represented by area fgh, which can be evaluated by simulating a fault-on trajectory in stage 2, starting with the system conditions at point f. Along this fault-on trajectory, the rotor angle will advance from δ^p to δ^u, thus providing the trajectory f-h for energy margin calculation as given by equation 3.21 below:

$$\Delta V = \Delta V_{pe} \Big|_{\delta^p}^{\delta^u} = -\int_{\delta^p}^{\delta^u} (P_m - P_e) d\delta \qquad 3.21$$

Note that in equation 3.21, P_e must be computed using the post-fault admittance matrix.

3.5.2 THE SMIB SYSTEM - DETAILED GENERATOR MODEL

In modern power systems, generators are equipped with effective excitation controls for transient stability enhancement. For these machines, the classical generator model is no longer adequate and detailed representations for generators and excitation systems are required. The energy margin calculation procedure described in the previous section for the classical SMIB system can be easily extended to accommodate these representations. With the effects of field forcing included, the generator internal voltage becomes a variable. Similarly, the mechanical power input (P_m) will also become a variable if a turbine/speed governor model is represented. For transient stability analysis, however, the speed governor control can usually be neglected because of its relatively large time constants.

For a classical generator, the generator electrical power is a function of

the rotor angle only, $P_e = P_e(\delta)$, so that different fault clearing times still result in the same post-fault power-angle curve (figure 3.5). When the generator and its excitation control are represented in detail, the generator electrical power is a function of the rotor angle as well as other state variables, $P_e = P_e(\delta, x)$. As a result, different fault clearing times will result in different post-fault power-angle trajectories (figure 3.6), even for the same pre-fault conditions. It implies that the potential energy between two rotor angle positions is now trajectory dependent.

To calculate the energy margin for a fault clearing time of t^{cl}, which has a clearing angle of δ^{cl} as shown in figure 3.5, one needs to compute the potential energy along the trajectory e-f. For a classical generator, the rotor angle at point f represents the UEP (δ^u). However, the concept of UEP for a detailed generator model with excitation control represented is not yet well understood. In developing the RFT method, the author has proposed to compute area efg by simulating a sustained fault based on an equivalent classical generator model, which has worked well for the Hybrid method. The conversion of a detailed generator model into its equivalent classical representation is given by equation 3.22:

$$\bar{E}' = \bar{E}_t + \frac{\bar{S}_g^*}{\bar{E}_t^*} (r_a + j\, x'') \qquad (3.22)$$

where: $\bar{E}_t$ = terminal voltage of the detailed generator

$\bar{S}_g$ = complex power output of the detailed generator

$\bar{E}'$ = internal voltage of the equivalent classical model

Along the fault-on trajectory from point e to point f, the potential energy of the generator reaches a peak at point f.

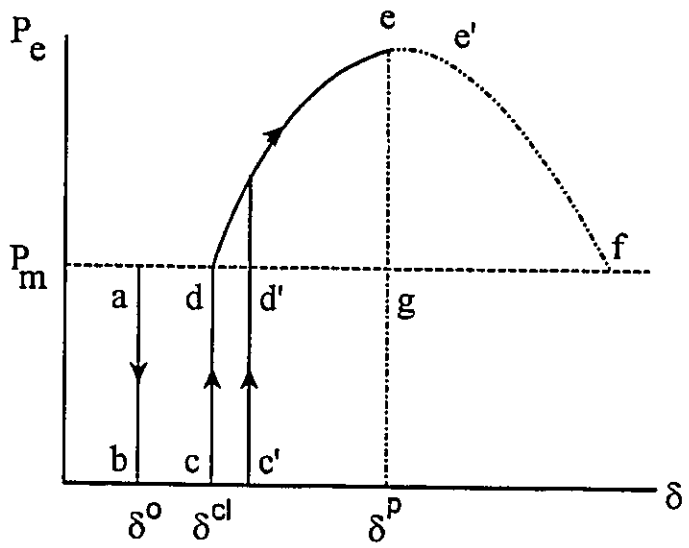

Figure 3.5: Power-Angle Trajectories for a Classical SMIB System

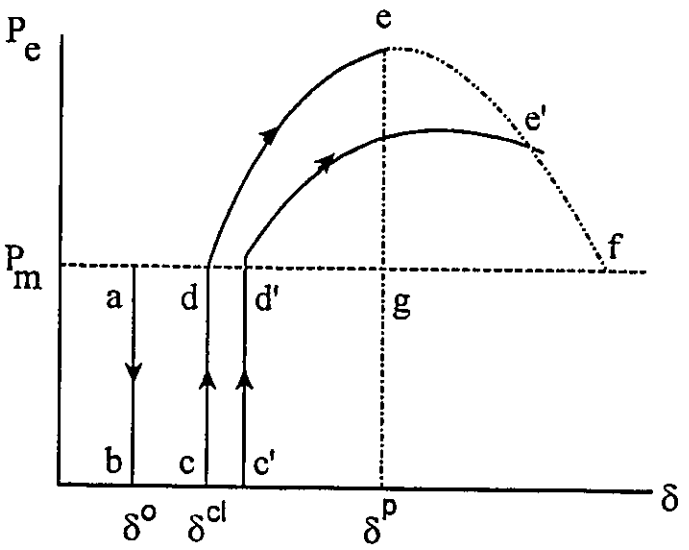

Figure 3.6: Power Angle Trajectories for a Detailed SMIB System

3.5.3 EXTENSION TO MULTI-MACHINE SYSTEMS

A realistic power system consists of a large number of generators and loads connected through a transmission network. The behaviour of one machine can influence some others through the transmission system. Depending on the fault locations, many different modes of instability exist, representing different system separation patterns. This sub-section describes how the two-stage RFT method computes energy margins for multi-machine systems.

For a given disturbance, a conventional time domain simulation of the first swing transient is first performed in stage 1 to determine whether the system is stable or unstable. Within the same run, the transient kinetic energy of the critical generator group (V_{ke}^{grp}) is computed at each time step. If the system is stable, V_{ke}^{grp} will reach zero some time after the fault is cleared, indicating that the transient kinetic energy directly responsible for system separation is fully absorbed. This time instant is designated as t^{kemin}. To calculate the energy margin for a stable case, stage 2 is initiated which simulates a fault-on trajectory starting with the system conditions at time t^{kemin}. If detailed generators are present, they will be converted into their equivalent classical models using equation (3.24) based on the generator conditions at time t^{kemin}. Along this fault-on trajectory, the potential energy of the critical generator group increases until it reaches a peak at time t^{p}. The energy margin is defined as the potential energy gained by the critical generator group between t^{kemin} and t^{p}, which can be evaluated using equation (3.17).

3.6 BENCHMARK ENERGY MARGINS

In order to assess the accuracy of the RFT method, it is required to establish benchmarks against which the energy margins produced by the RFT method can be compared. The energy margin produced by the RFT method for an unstable case represents the portion of the transient kinetic energy, injected into the critical generator group by the disturbance, that fails to be absorbed in the post-fault period. This energy margin is considered very accurate. It is the energy margins for stable cases that need to be assessed in order to determine the accuracy of the RFT method. Benchmark energy margins for stable cases can be conveniently established using transient kinetic energies associated with critical fault clearing times, as described below.

For a given disturbance cleared at time t^{cl}, let $V_{ke}^{grp}(t^{cl})$ represent the transient kinetic energy injected into the critical generator group by the disturbance. Furthermore, let $V_{ke}^{grp}(cct)$ represent the transient kinetic energy injected into the critical group by the disturbance which is critically cleared. The difference between these two kinetic energy quantities provide a benchmark energy margin (ΔV^{BM}) for the disturbance under consideration:

$$\Delta V^{BM} = V_{ke}^{grp}(cct) - V_{ke}^{grp}(t^{cl}) \tag{3.23}$$

Figure 3.7 illustrates the benchmark energy margin for a single-machine-infinite-bus system with the machine represented in full detail. The transient kinetic energy injected into the machine by the disturbance cleared at time t^{cl} is represented by area abcd. When the disturbance is critically cleared, the injected transient kinetic energy is given by area abc'd'. Therefore, the benchmark energy margin is represented by the area cc'd'd. Alternatively, the benchmark

energy margin is represented by the quantity (area d'e'f' -area def) from the potential energy viewpoint.

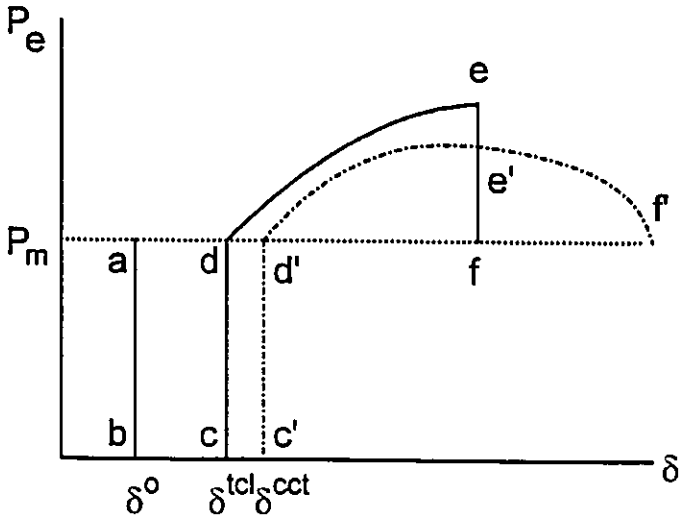

Figure 3.7: Benchmark Energy Margin

3.7 PROPOSED ALGORITHM

This section briefly summarizes the implementation of the two-stage RFT method for energy margin calculation. The first stage is identical to a conventional time domain simulation, with the addition of transient kinetic energy calculation. The second stage is the simulation of a relevant fault-on trajectory, along which potential energy of the critical generator group is evaluated. The algorithm for the RFT method is given below:

(a) First Stage: Time Domain Simulation of the First Swing Transient

1. Simulate the disturbance by performing a conventional time domain simulation with the switching events specified. A simulation period of 2 to 5 seconds is usually required to cover the first swing transient. At each time step, compute the transient kinetic energy of the critical generator group (V_{ke}^{grp}).

2. Along the post-fault system trajectory, determine the time (t^{kcmin}) when V_{ke}^{grp} reaches a global minimum. Save the system conditions at time t^{kcmin}.

3. If the system is unstable, one or more rotor angles will become infinitely large. The time domain simulation is terminated as soon as one of the rotor angles exceeds 360°. The energy margin is defined as the negative of the minimum V_{ke}^{grp} along the post-fault trajectory.

4. If the system is stable, initiate stage 2 for energy margin calculation.

(b) Second Stage: Simulation of the Fault-on Trajectory

1. Restore the system conditions at time t^{kcmin}, and convert all detailed generators into their equivalent classical models. Initialize the energy margin as zero and compute $\delta_{eq}(t)$, $Pm_{eq}(t)$, and $Pe_{eq}(t)$, using equations (3.12), (3.14) and (3.15).

2. Apply a 3ϕ fault at one (or more) location for one time step. The fault location(s) is chosen in such a way that the fault-on trajectory will have the same system separation pattern as that of the critically unstable system trajectory

3. Compute $\delta_{eq}(t+\Delta t)$ by numerical integration. Compute $Pe_{eq}(t+\Delta t)$ using the post-fault Y-matrix.

4. Compute ΔV_{pe}^{grp} between t and $t+\Delta t$ using the trapezoidal rule:

$$(t, t+\Delta t) = [Pe_{eq}(t)-Pm_{eq}(t)+Pe_{eq}(t+\Delta t)-Pm_{eq}(t+\Delta t)] \times [\delta_{eq}(t+\Delta t)-\delta_{eq}(t)]/2 \qquad (3.24)$$

5. Increment the energy margin by $\Delta V_{pe}^{grp}(t, t+\Delta t)$.

6. Repeat steps 2 to 5 until the energy margin reaches a peak. This condition is detected by $\Delta V_{pe}(t, t+\Delta t)$ being less than or equal to zero, which terminates the second stage.

Figures 3.8 and 3.9 illustrate respectively the simplified flow charts for stages 1 and 2 of the RFT method.

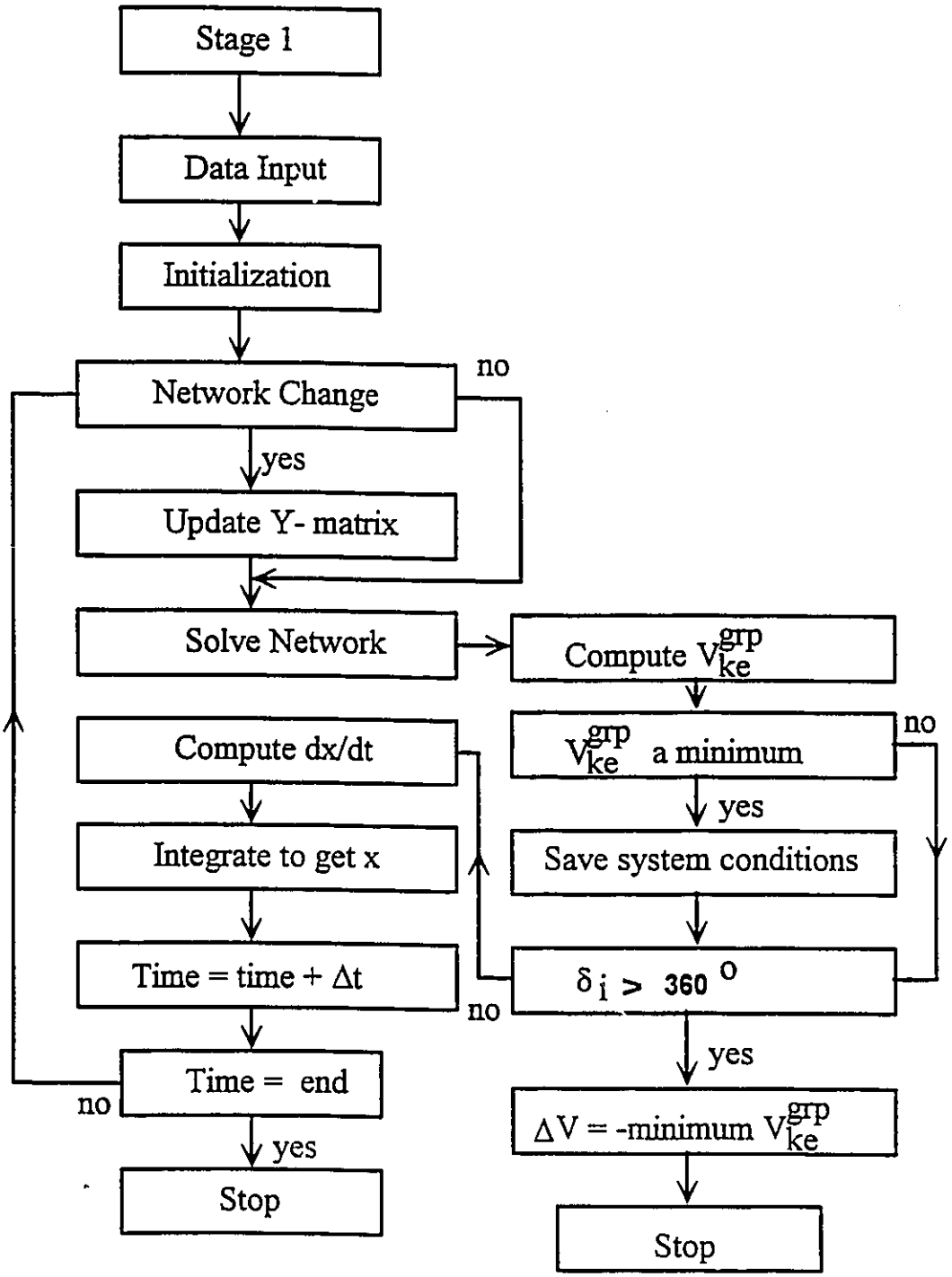

Figure 3.8: Stage 1 of the RFT Method

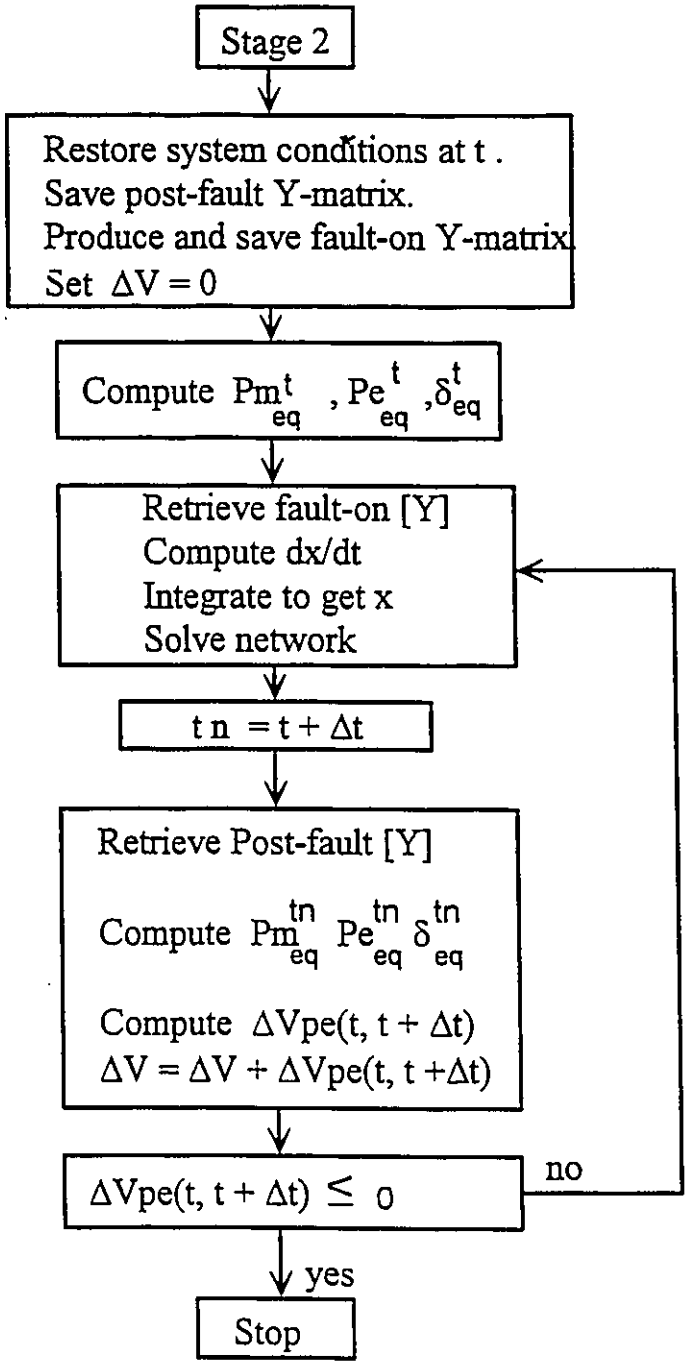

Figure 3.9: Stage 2 of the RFT Method

3.8 TEST RESULTS

Three Ontario Hydro test systems have been used to demonstrate the accuracy and practicality of the RFT method: the 27-generator, and the 89-generator, and the 144-generator system. These test systems were chosen to assess the capability of the RFT method in analysing power systems of different modelling details and of different modes of instability. The 27-generator system exhibits plant mode instability phenomenon, while the 144-generator system exhibits simple area mode instability. The 89-generator system displays complex area mode instability.

For each RFT simulation, stage 1 was performed using the production tool of Ontario Hydro for transient stability analysis, with the incorporation of transient kinetic energy calculation. A prototype program has been developed to perform stage 2, which is essentially another time domain simulation but involving classical generator models only. This prototype program uses the modified Euler method to perform numerical integration. The simulation of the fault-on trajectory in stage 2 requires both the faulted and the post-fault admittance matrices, with the latter required for potential energy calculation.

3.8.1 The 27-Generator System

3.8.1(a) System Description

The 27-generator system was developed to analyze the Bruce system of Ontario Hydro, which was presented in [64]. The Bruce generating station has eight nuclear units with a total capacity of approximately 6500 MW. Its generation is delivered to remote load centers via four 500 kV lines and six 230

kV lines as shown in figure 3.10. These ten circuits constitute a stability interface, known as FABC (Flow Away From Bruce), for which transient stability limits are derived.

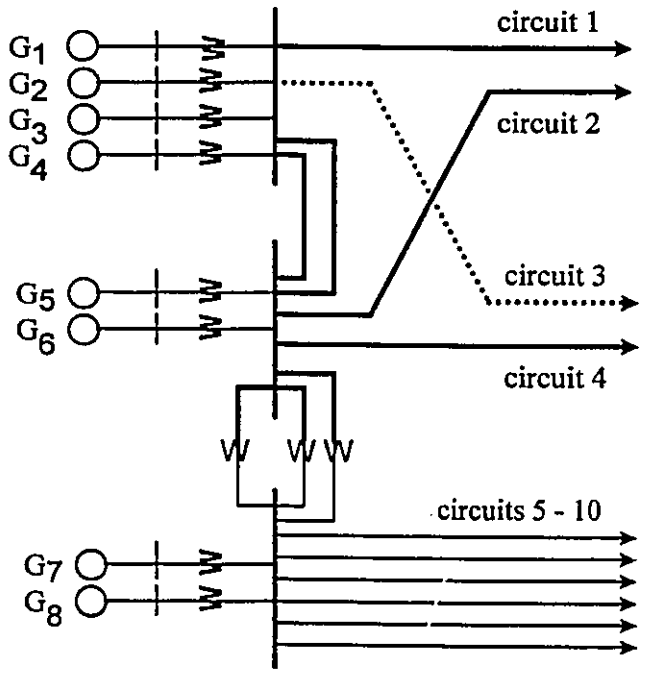

Figure 3.10: The Bruce System

In this study, all Bruce machines were in service and one of the 500 kV circuits (circuit 2) was out of service for maintenance. The Bruce machines were modelled as round rotor generators with their excitation systems fully represented as given in Appendix 2. For this test system, fifteen machines were modelled in full detail, while eight machines were modelled as classical generators. The remaining four machines were represented as infinite buses. Loads were represented as constant impedances.

The contingency simulated was the loss of the 500 kV circuits 1 and 3, through simultaneous phase-to-ground faults near Bruce. For this contingency, the Bruce machines constitute the critical generator group. When the system becomes unstable, the eight Bruce machines will separate from the rest of the system. A relevant fault-on trajectory was easily obtained by applying a sustained three-phase 500 kV fault near Bruce.

3.8.1(b) Test Results

A study was performed to derive the transient stability limit for the stability interface as defined earlier. Sixteen test cases were prepared with the interface flow varying from 4500 to 6000 MW. The RFT method was applied to calculate energy margins for these test cases.

The rotor angle plots of the Bruce machines as computed in stage 1 of the RFT simulations are shown in figures 3.11 and 3.12. This illustrates the mode of instability of the Bruce system. Only three of the eight Bruce machines are shown in these figures, since the remaining Bruce machines are of similar behaviour. Figure 3.11 corresponds to the marginally stable case, in which the Bruce machines are severely disturbed but still remain in synchronism with the rest of the system. Figure 3.12 corresponds to the marginally unstable case, in which the Bruce machines separate from the rest of the system.

Figures 3.13 and 3.14 shows the behaviour of the one of the Bruce machines as the interface flow is increasingly stressed. Figure 3.13 shows six stable cases (cases 4 to 9), while figure 3.14 shows six unstable cases (cases 10 to 15). Note that from the rotor angle trajectories, one cannot derive any quantitative measure of the degree of stability.

The internal voltages of three Bruce machines for the marginally unstable case are given in figure 3.15, which shows that as the Bruce machines are pulling away from the rest of the system, during time period from about 0.5 to 2 seconds, the internal voltages of the Bruce machines remain relatively flat. This observation provides a justification for using equivalent classical models when simulating the fault-on trajectory in stage 2 of the RFT method.

The plots of V_{ke}^{grp} as computed in stage 1 of the RFT simulations for six stable cases (cases 4 to 9) and six unstable cases (cases 10 to 15) are shown in figures 3.16 and 3.17 respectively. Figure 3.16 shows that V_{ke}^{grp} continues to increase after the fault is removed, due to the line switching which also injects transient kinetic energy into the critical machines. Note that when the system is stable, V_{ke}^{grp} will reach a minimum of zero some time after the fault is cleared. At this time instant (designated as t^{kemin}), the transient kinetic energy injected by the disturbance is fully absorbed. System conditions at this time instant are saved for energy margin calculation to be done in stage 2. If the system is unstable, V_{ke}^{grp} will not reach zero in the post-fault period as shown in figure 3.17. The RFT method defines the energy margin for an unstable case as the minimum of V_{ke}^{grp} along the post-fault trajectory.

Energy margins obtained by the RFT method (ΔV^{RFT}) are tabulated in table 3.1, along with the benchmark energy margins (ΔV^{BM}) obtained from critical clearing time studies. The derivation of benchmark energy margins has been described in section 3.6. The stability results obtained form conventional time domain simulations (CTDS) are also provided in table 3.1. Note that a conventional time domain simulation can only tell whether the system is stable or unstable, with no information on the degree of stability.

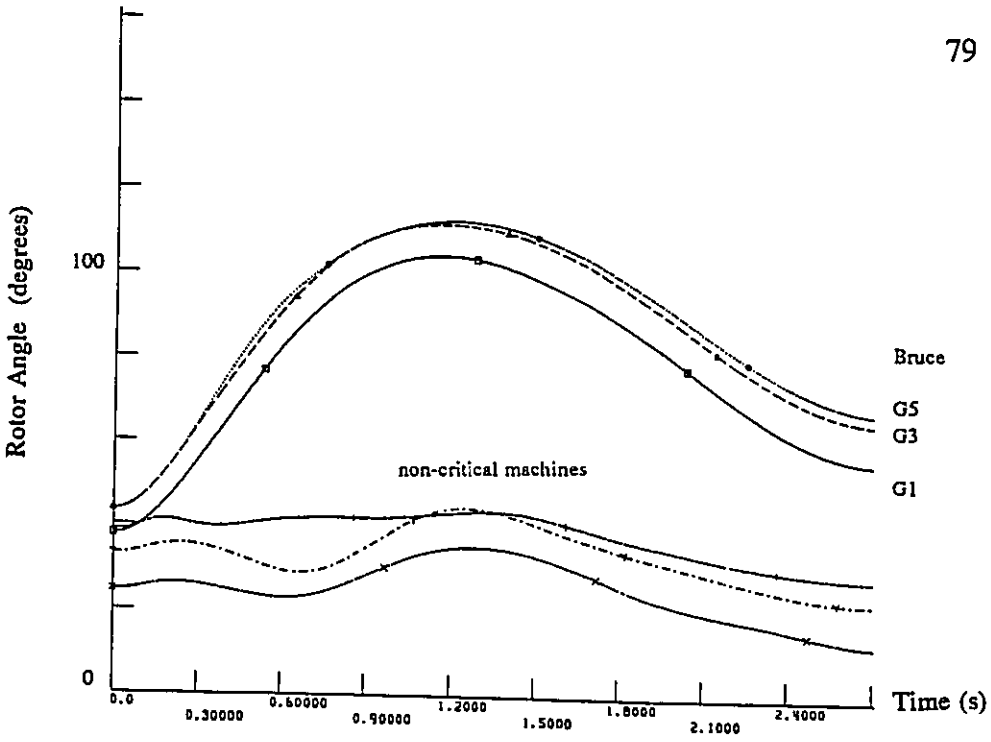

Figure 3.11: Stable Case - Critical and Non-Critical Machines

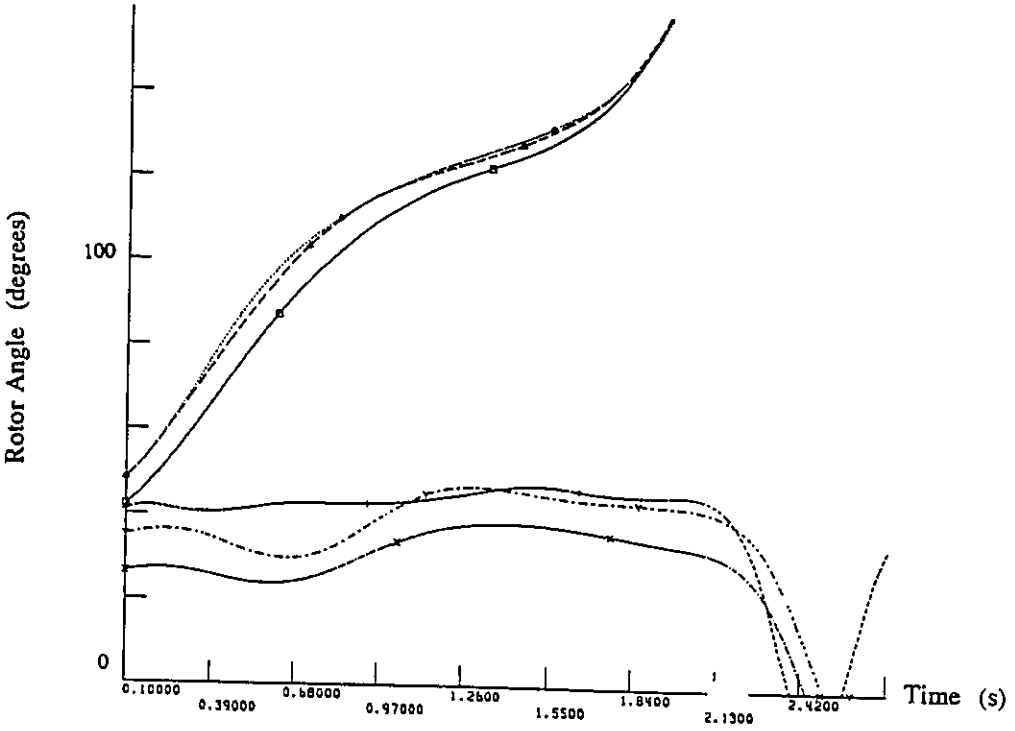

Figure 3.12: Unstable Case - Critical and Non-Critical Machines

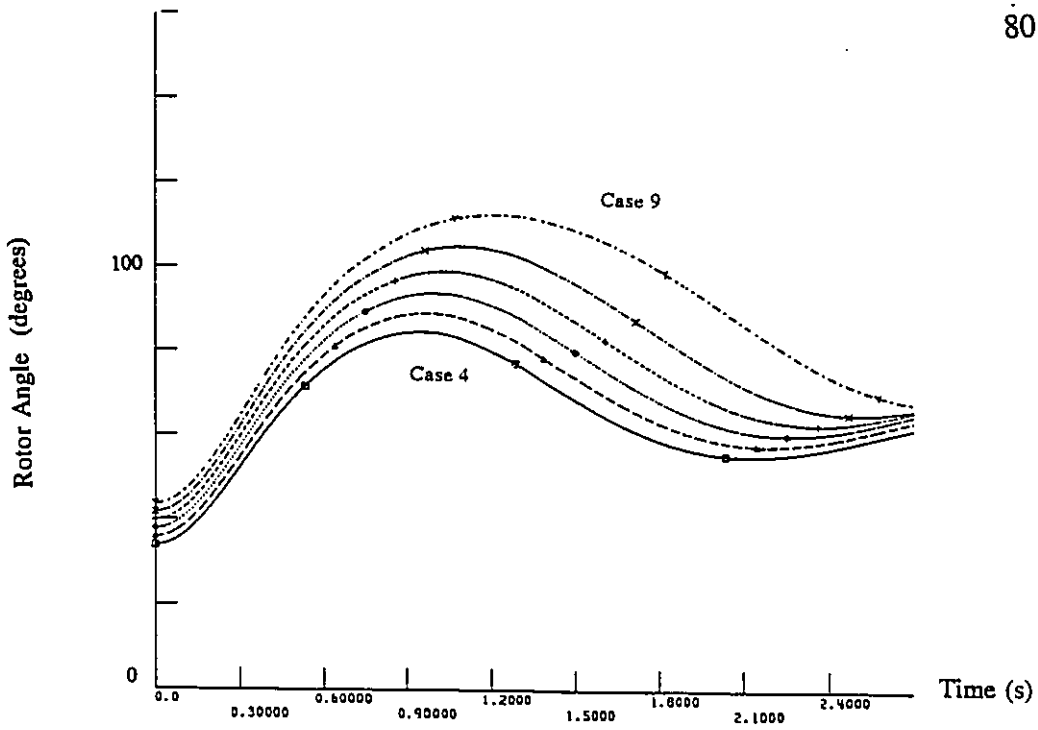

Figure 3.13: Stable Cases - Rotor Angle Plots of Bruce G5

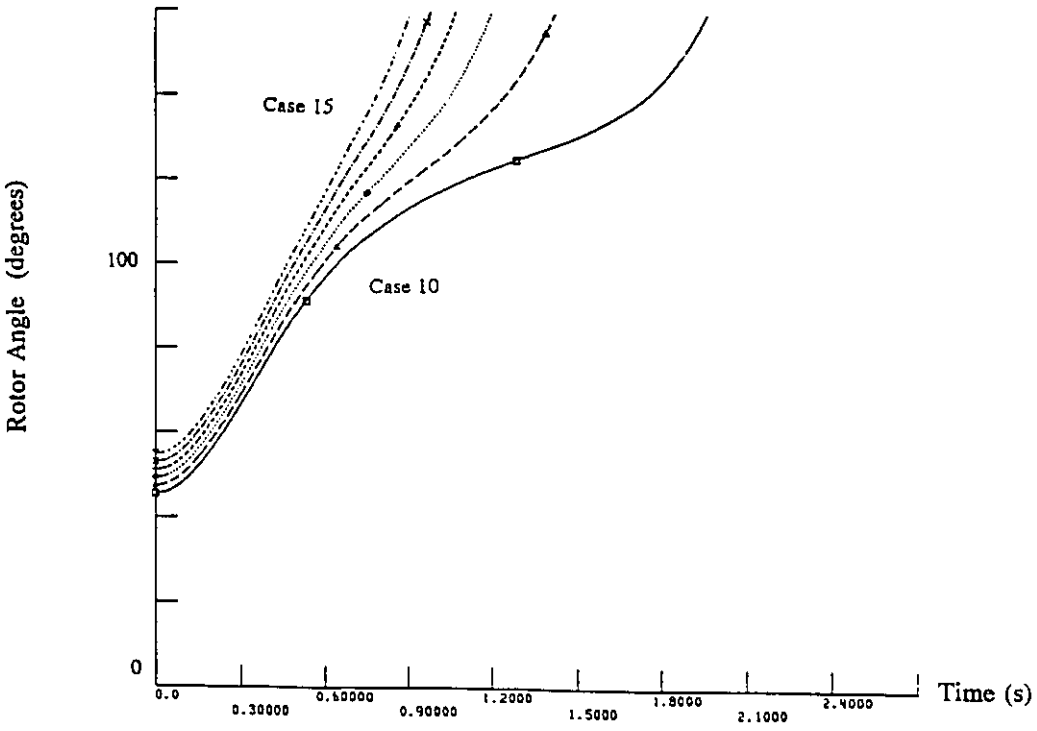

Figure 3.14: Unstable Cases - Rotor Angle Plots of Bruce G5

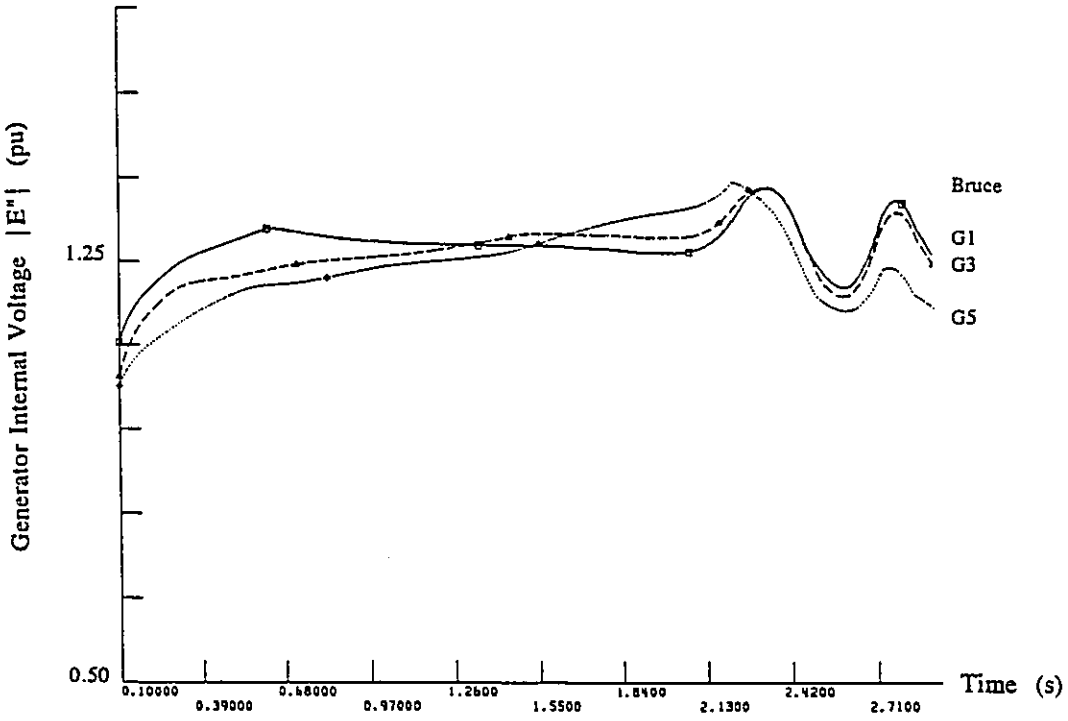

Figure 3.15: Marginally Unstable Case - |E"| of Bruce G1, G3, G5

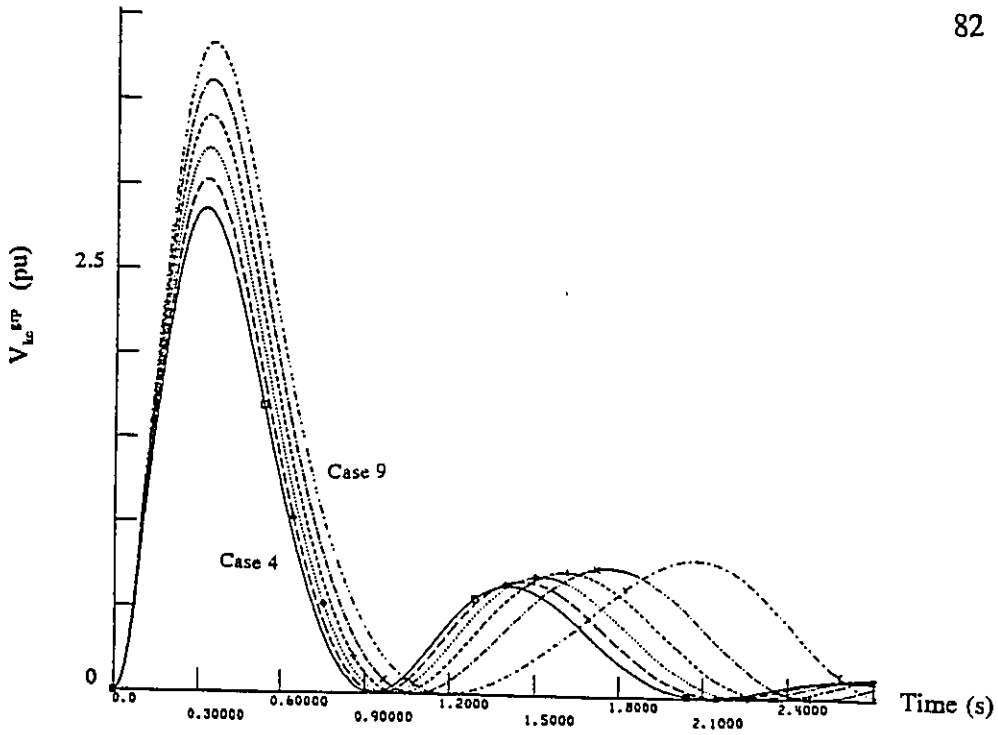

Figure 3.16: V_{ke}^{grp} for Stable Cases

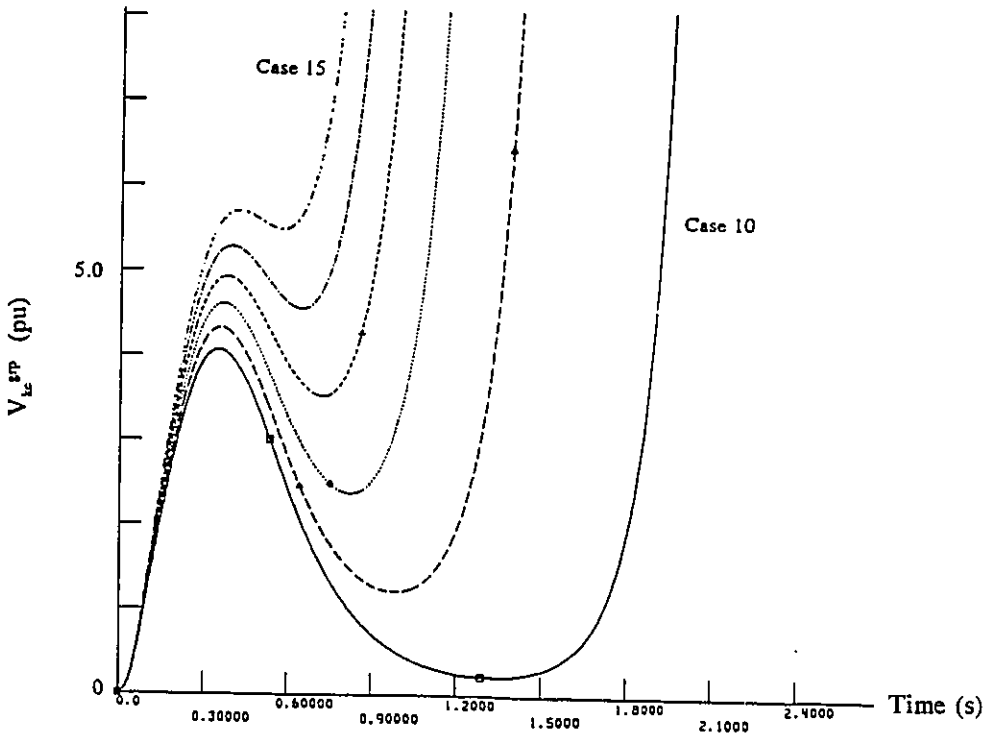

Figure 3.17: V_{ke}^{grp} for Unstable Cases

Table 3.1: Energy Margins for the Bruce System

Case	Flow (MW)	ΔV^{RFT} (pu)	ΔV^{BM} (pu)	CTDS
1	4500	5.311	5.775	stable
2	4600	4.551	5.269	stable
3	4700	3.839	4.706	stable
4	4800	3.189	4.136	stable
5	4900	2.575	3.407	stable
6	5000	2.012	2.815	stable
7	5100	1.481	2.085	stable
8	5200	0.979	1.421	stable
9	5300	0.459	0.447	stable
10	5400	-0.222	-0.222	unstable
11	5500	-1.218	-1.218	unstable
12	5600	-2.376	-2.376	unstable
13	5700	-3.524	-3.524	unstable
14	5800	-4.557	-4.557	unstable
15	5900	-5.497	-5.497	unstable
16	6000	undefined	undefined	unstable

3.8.1(c) Discussion

(i) Accuracy

Let us first consider the accuracy of transient stability limit derivation by the RFT method. As shown in table 3.1, the RFT method yields a transient stability limit of 5300 MW for the stability interface, as would be produced by the conventional time domain simulation method. For each simulation, the RFT method determines the transient stability of the test system in exactly the same way as the conventional time domain simulation method does. Therefore, the two methods would result in the same transient stability limit.

The advantage of the RFT method is its ability to provide energy margins for indicating the degree of stability. These energy margins can be used to speed up transient stability limit derivation by reducing the number of stability runs. The energy margins obtained from the RFT method for the Bruce system are plotted in figure 3.18, which shows that the energy margin decreases monotonically (and almost linearly) as the interface flow increases. Such energy margin vs interface flow relationship is highly desirable, allowing fast transient stability limit derivation through application of sensitivity techniques. More discussion on sensitivity analysis will be provided in chapter 5.

When the interface flow is at or above 6000 MW (case 16), its energy margin is undefined. This is because the system is so stressed that the critical generator group virtually has no energy absorbing capability in the post-fault period. An undefined energy margin can also be useful in speeding up transient stability limit derivation. When the system is so unstable that its energy margin cannot be defined, one can justify to reduce the interface flow by a larger

decrement in submitting the next run, while deriving the transient stability limit.

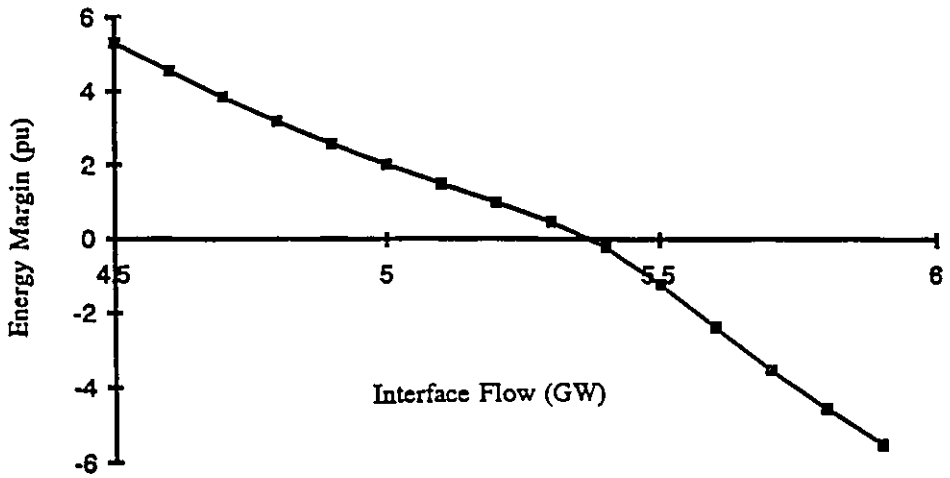

Figure 3.18: Energy Margin vs Interface Flow

Table 3.1 also provides a comparison of the energy margins computed by the RFT method (ΔV^{RFT}) with the benchmark energy margins (ΔV^{BM}). As described in section 3.6, the benchmark energy margin for a given fault is defined as the difference between $V_{ke}^{grp}(cct)$ and $V_{ke}^{grp}(t^{cl})$. The first quantity is the maximum transient kinetic energy associated with the critical generator group when the fault is critically cleared. The second quantity represents the maximum transient kinetic energy gained by the critical generator group, when the fault is normally cleared. Table 3.1 shows that the energy margins obtained from the RFT method are only approximate, when compared to the benchmark energy margins. However, this is not considered as a disadvantage, since the approximate energy margins can also contribute significantly to the speeding up of transient stability limit derivation, as will be discussed in chapter 5.

(ii) Computing Requirements

Similar to the conventional time domain simulation method, the computing requirements of the RFT method are directly proportional to the length of the time domain simulation period, the numerical integration technique chosen, and the integration step size. In comparing the RFT method with the conventional time domain method in terms of computing requirements, it is assumed that both methods employ the same numerical integration technique and the same integration step size.

The RFT method consists of two stages in computing energy margins. The first stage is equivalent to a conventional time domain simulation of the first swing transient, but with transient kinetic energy calculation included. The computing effort for kinetic energy calculation is very small, compared to the simulation of the first swing transient, which requires step by step solution of the differential and algebraic equations describing the power system dynamics. The second stage involves potential energy calculation along a fault-on trajectory. For an unstable case, the RFT method only requires the first stage, and its computing requirements are approximately 0.5% higher than those of the conventional time domain simulation technique, due to the additional kinetic energy calculation.

For a stable case, the RFT method requires both stages 1 and 2 in order to compute an energy margin. Therefore, it actually requires slightly more cpu time than the conventional time domain simulation technique because of the additional energy margin calculation being done in stage 2. For the stable cases of the Bruce system, table 3.2 summarizes the computing requirements of the RFT method in terms of the time domain simulation periods. In table 3.2, T_s^I

Table 3.2: Simulation Periods for Stages 1 and 2

Case	T_s^I(s) RFT	T_s^{II}(s) RFT	T_s^{total}(s) RFT	T_s (s) CTDS
1	3.0	0.305	3.305	3.0
2	3.0	0.285	3.285	3.0
3	3.0	0.270	3.270	3.0
4	3.0	0.250	3.250	3.0
5	3.0	0.235	3.235	3.0
6	3.0	0.215	3.215	3.0
7	3.0	0.195	3.195	3.0
8	3.0	0.170	3.170	3.0
9	3.0	0.135	3.135	3.0

and T_s^{II} represent the time domain simulation periods for stages 1 and 2 respectively. The simulation periods for conventional time domain (CTD) simulations are also provided for comparison. Table 3.2 assumes that the first swing period for the Bruce system is about three seconds, as shown by the rotor angle plot of one of the Bruce machines in figure 3.11. The simulation period for the second stage (T_s^{II}) of the RFT method depends on how stable the system is. The more stable the system is, the longer the fault-on trajectory is required before the potential energy of the critical generator group reaches a maximum. Usually, T_s^{II} is less than 10% of the first swing period as shown in table 3.2.

3.8.2 The 144-Generator System

3.8.2(a) System Description

Containing 144 generators, the second test system was chosen to evaluate the capability of the RFT method in computing energy margins for simple area mode systems involving the stability of a few generating plants located close to each other. This test system was presented in [44] and was used to study the transient stability of five hydraulic stations along the Moose River in Northern Ontario. The Moose River generation is delivered to remote load centers over a long 500 kV transmission path (figure 3.19). The contingency studied was the loss of circuit 2 through a three-phase fault. For this test system, the five hydraulic stations were represented in detail while the rest of the machines were classically represented. All loads were represented as constant impedance loads.

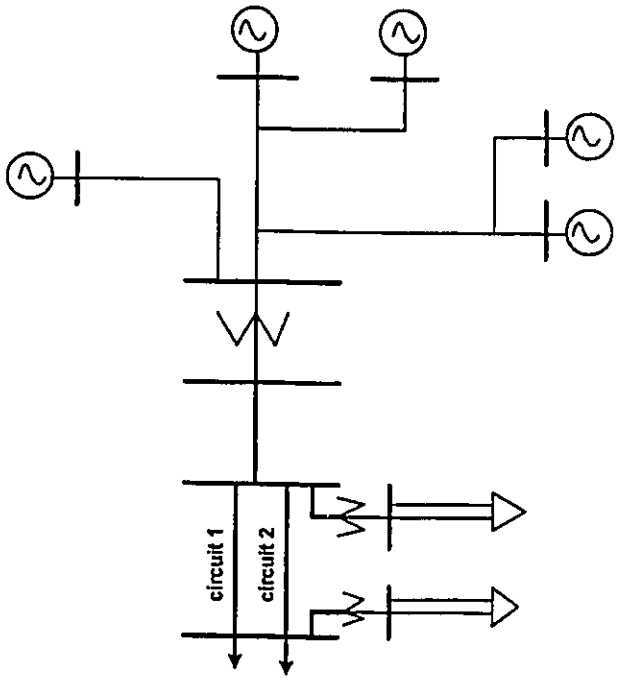

Figure 3.19: The Moose River System

3.8.2(b) Test Results

A study was made to determine the transient stability limit of the Moose River generation for the given contingency. Seven test cases were prepared, with the Moose River generation varying from 500 MW to 850 MW. Energy margins were computed for these test cases using the RFT method.

The rotor angle plots of the generators at the five hydraulic stations for the marginally stable and unstable cases are given in figure 3.20 and 3.21 respectively. When the system goes unstable, the machines at these five hydraulic stations form the critical generator group and separate from the rest of the system as one coherent group, as shown in figure 3.21. This mode of instability is considered as simple area mode, since only several generating plants lose synchronism with the rest of the system. A relevant fault-on trajectory was easily obtained by applying a sustained three-phase fault at the original fault location.

Figures 3.22 and 3.23 show the behaviour of one of the critical generators (Kipling Unit 1) as the Moose River generation increases. Figure 2.22 shows five stable cases (case 1 to 5), while figure 3.23 shows three unstable cases (cases 6 to 8). Although rotor angle plots indicate whether the system is stable or unstable, they do not provide any quantitative measure of the degree of stability.

The internal voltages of the generators at the five Moose River plants are given in figure 3.24 for the marginally unstable case. This figure shows that as the critical generators are pulling away from the rest of the system, during the time period between 0.5 and 1 second, their internal voltages are relatively flat.

The plots of V_{ke}^{ep} for the stable and unstable cases are shown in figure 3.25 and 3.26 respectively. These figures also show that due to the effects of line switching, V_{ke}^{ep} continues to increase for a little longer after the fault is removed. As shown in figure 3.25, V_{ke}^{ep} reaches a minimum of zero some time after the fault is cleared. For unstable cases, V_{ke}^{ep} does not reach zero in the post-fault period, as shown in figure 3.26.

The energy margins are tabulated in table 3.3, together with the benchmark energy margins based on critical clearing time studies. Stability results obtained from conventional time domain simulations are also provided in table 3.3.

Case	Moose River Gen. (MW)	ΔV^{RFT} (pu)	ΔV^{BM} (pu)	CTDS
1	500	3.018	3.578	stable
2	550	2.088	2.843	stable
3	600	1.307	1.975	stable
4	650	0.666	0.963	stable
5	700	0.088	0.132	stable
6	750	-0.641	-0.641	unstable
7	800	-1.049	-1.049	unstable
8	850	Undefined	Undefined	unstable

Table 3.3: Energy Margins for the Moose River System

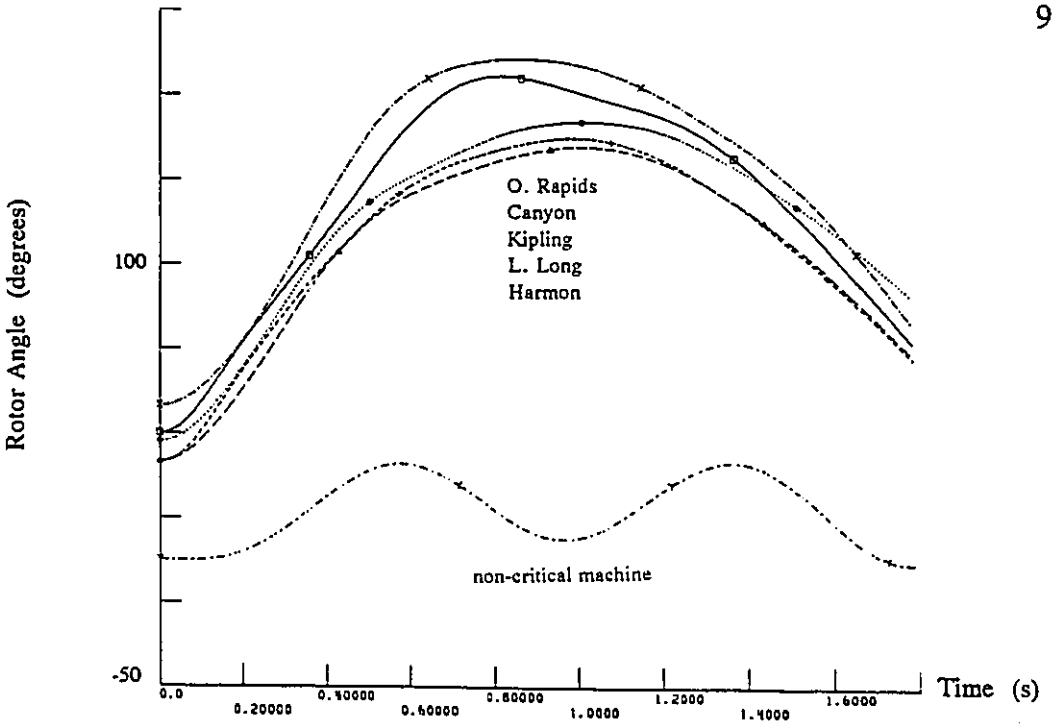

Figure 3.20: Stable Case - Critical and Non-Critical Machines

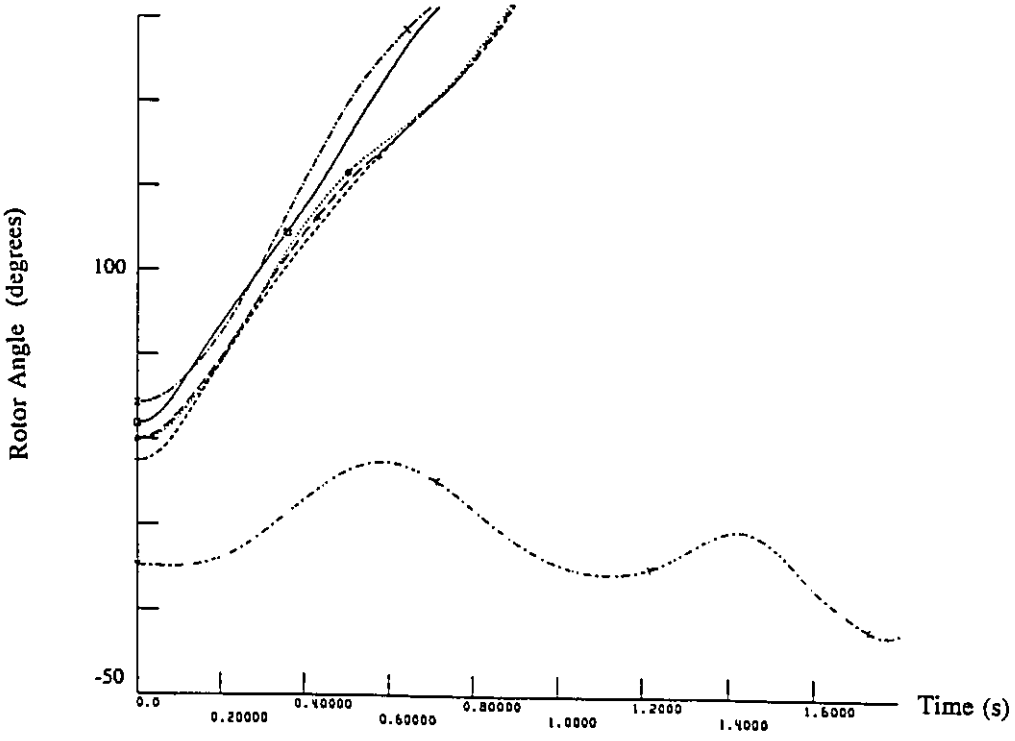

Figure 3.21: Unstable Case - Critical and Non-Critical Machines

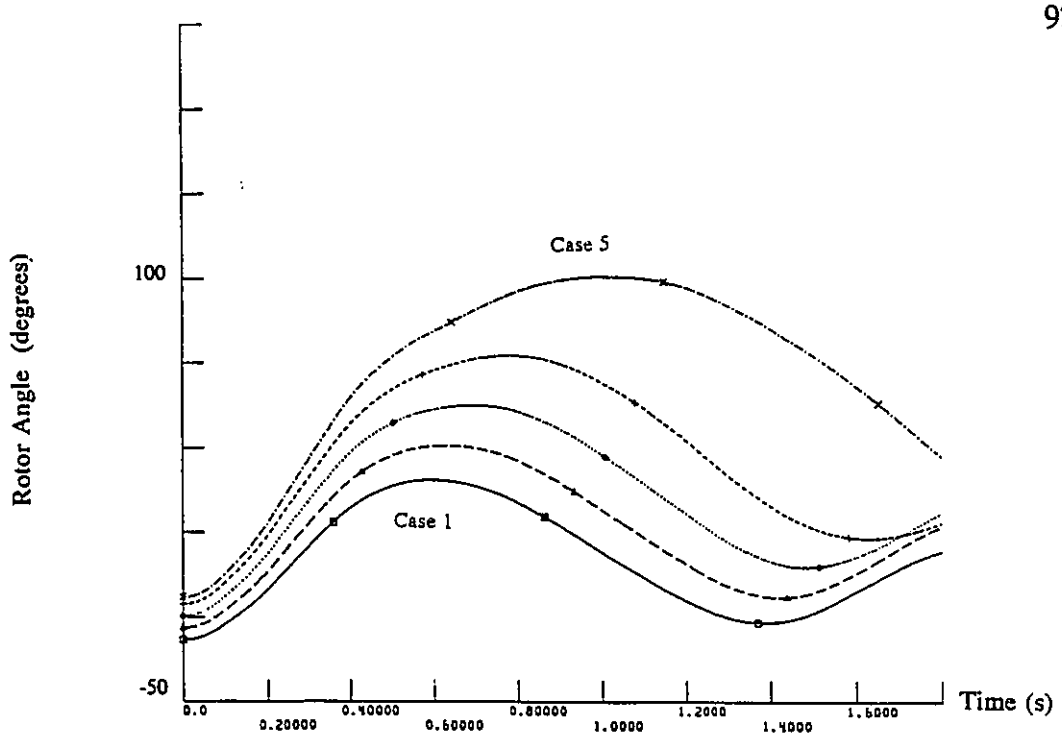

Figure 3.22: Stable Cases - Rotor Angle Plots of Kipling G1

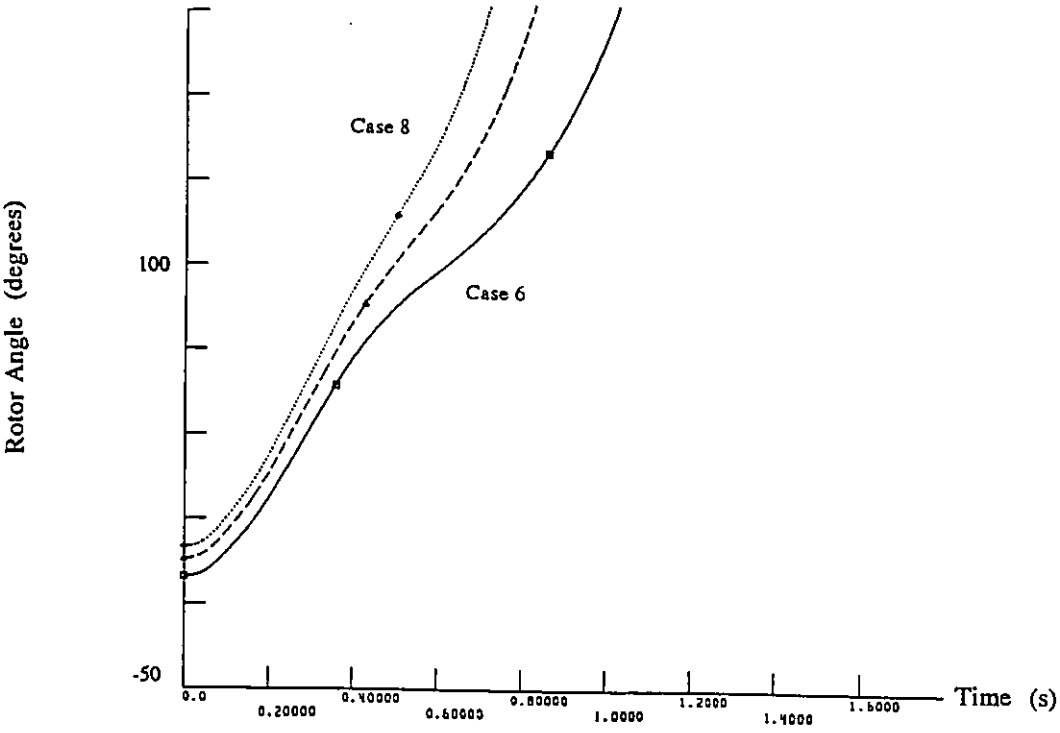

Figure 3.23: Unstable Cases - Rotor Angle Plots of Kipling G1

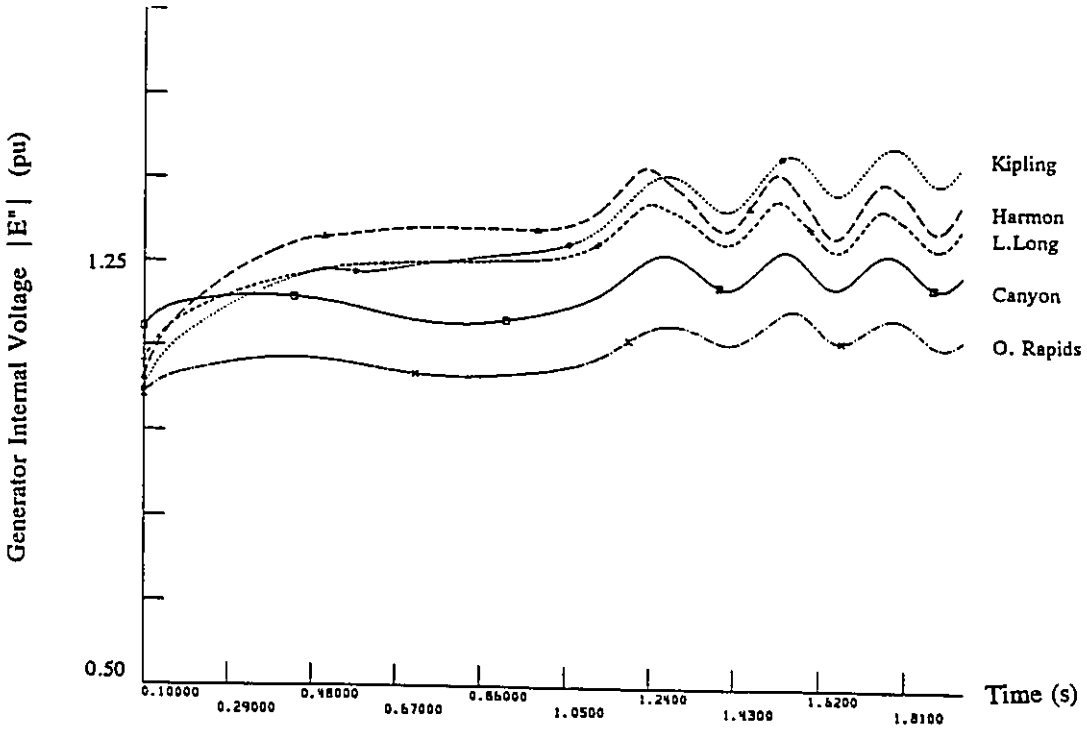

Figure 3.24: Marginally Unstable Case - |E"| of Moose River Machines

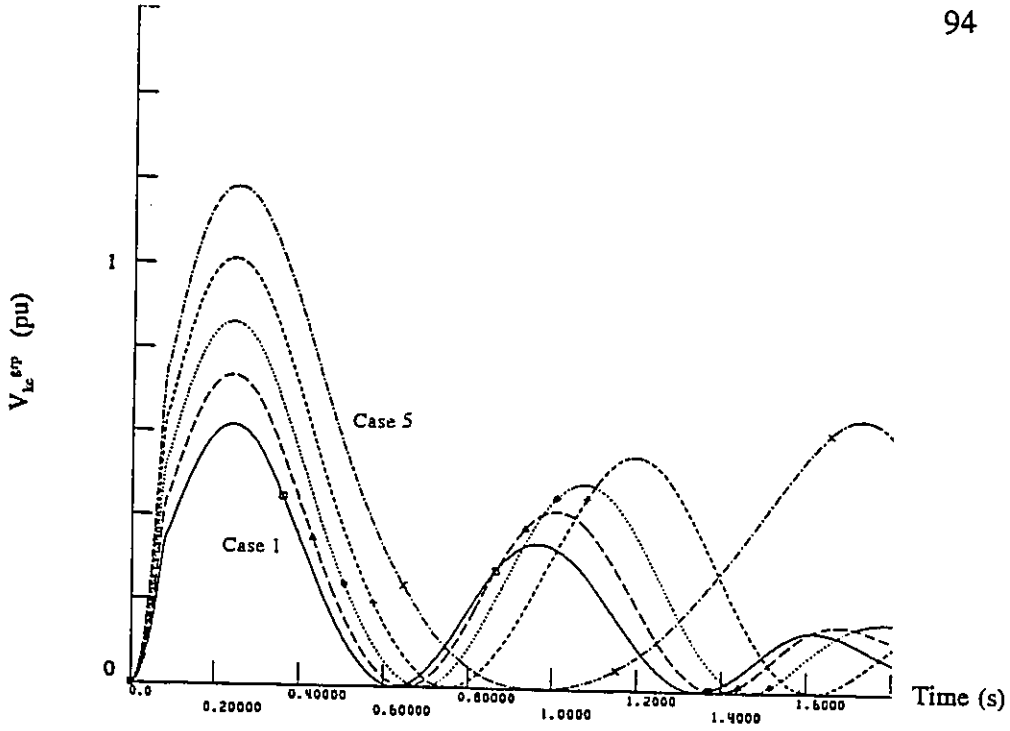

Figure 3.25: V_{ke}^{gFP} for Stable Cases

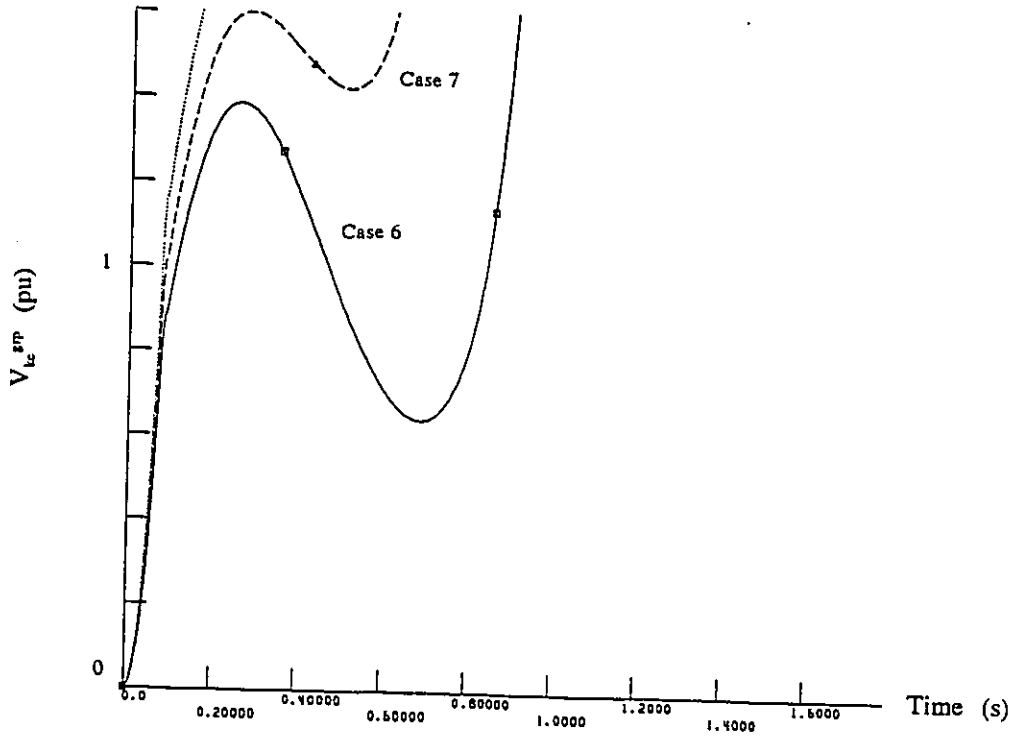

Figure 3.26: V_{ke}^{gFP} for Unstable Cases

3.8.2 (c) Discussion

(i) Accuracy

As shown in table 3.3, the RFT method yields a transient stability limit of 700 MW for the Moose river generation, as would be produced by conventional time domain simulations. Note that in deriving transient stability limits, the RFT method produces the same limits as the conventional time domain simulation method does. Figure 3.27 plots the energy margins vs the Moose River generation, which shows almost a linear relationship. Such energy margin

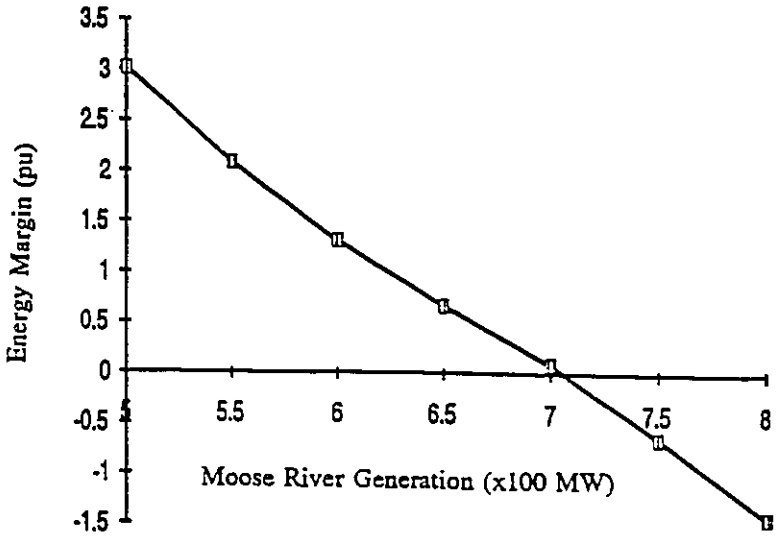

Figure 3.27: Energy Margin vs Moose River Generation

behaviour allows fast transient stability limit derivation through application of numerical sensitivity techniques, as will be discussed in chapter 5. Similar to the Bruce system, table 3.3 shows that when the Moose River generation is increased to or above 850 MW, the RFT method fails to produce an energy margin. Table 3.3 also shows that the energy margins calculated by the RFT method are only approximate, when compared to the benchmark energy margins.

(ii) Computing Requirements

As previously discussed, the computing requirements of the RFT method for unstable cases are almost the same as those of the conventional time domain simulation technique. For stable cases, the computing requirements of the RFT method mainly depend on the time domain simulation period of stage 1. The simulation periods for the two stages of the RFT method are given in table 3.4. The Moose River system requires two seconds of time domain simulation to cover the first swing period, as shown by the rotor angle plot of one of the Moose River machines (figure 3.15). Table 3.4 shows that the energy margin calculation performed in stage 2 of the RFT method requires a relatively small amount of computing effort, when compared to that of stage 1. For a very stable case (case 1), energy margin calculation in stage 2 only requires approximately 0.3 seconds of time domain simulation, compared to the 2 seconds required for the simulation of the first swing period.

Table 3.4: Simulation Periods of the RFT Method

Case	T_s^I(s) RFT	T_s^{II}(s) RFT	T_s^{total}(s) RFT	T_s (s) CTD
1	2.0	0.27	2.27	2.0
2	2.0	0.23	2.23	2.0
3	2.0	0.19	2.29	2.0
4	2.0	0.15	2.25	2.0
5	2.0	0.09	2.09	2.0

3.8.3 The 89-Generator System

3.8.3(a) System Description

The third test system was chosen to evaluate the capability of the RFT method in computing energy margins for the 1987 Southwestern Ontario (SWO) system which exhibited very complex area mode instability. Since 1988, this mode of instability has been virtually eliminated because of the additional 500 kV transmission lines installed in this area. Part of the old Southwestern Ontario system is shown in figure 3.28. This test system has also been reported in [42]. It was obtained through a dynamic reduction of a 4000 bus base case representing the eastern portion of the North American power grid. The test system contains 89 generators, many of which are dynamic equivalents. The mode of instability

for this test system is quite complex, with the critical generator group consisting of 40 machines spread over a large geographic area.

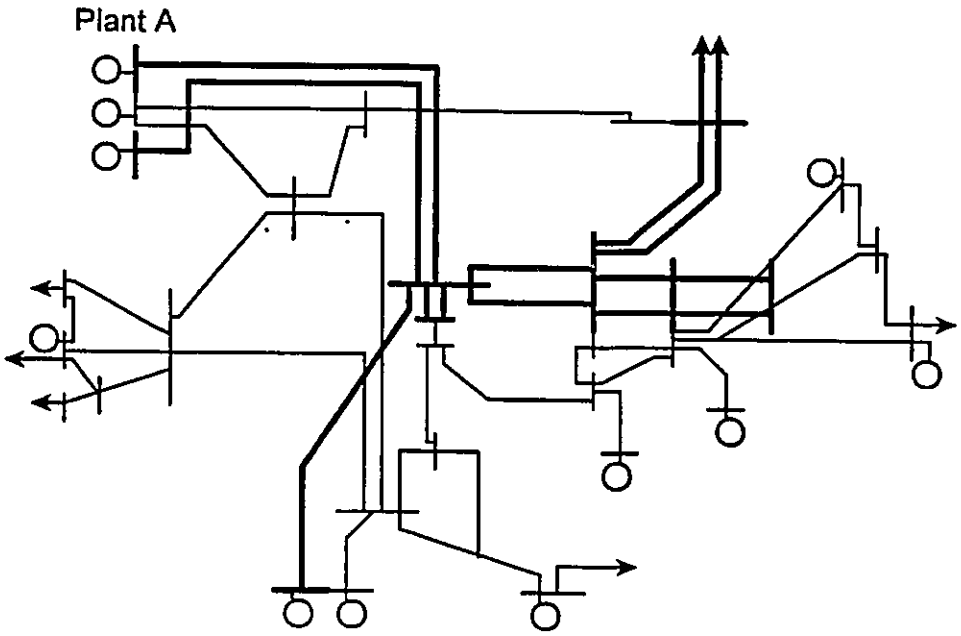

Figure 3.28: The Southwestern Ontario System

3.8.3(b) Test Results

A study was made to determine the transient stability limit of a major generating station (Plant A) within Southwestern Ontario. Eight test cases were created by varying the power output at plant A. The most critical contingency for area mode instability was the loss of one of the two 500 kV lines carrying the generation out of plant A, through a 3-phase fault. The test system was represented by classical generator models and constant impedance loads. The main purpose of this test system is to investigate the effects of complex mode of instability on energy margin calculation by the RFT method.

The rotor angle plots of some of the critical and non-critical machines are given in figures 3.29 and 3.30. The mode of instability of this test system is quite complex, with the critical generator group consisting of 40 machines. Figures 3.29 and 3.30 shows that there is a significant amount of inter-machine oscillations among the critical generators.

In calculating energy margins for this test system by the RFT method, the most difficult step was to obtain a relevant fault-on trajectory due to the large number of critical machines spread over a large geographical area. Applying a sustained fault at the original fault location caused a few machines near the fault to go unstable very rapidly, before other critical machines which are far away from the fault got a chance to accelerate. After some investigation, the best results were obtained by applying simultaneous faults at two major transmission interfaces that separate the critical machines from their neighbouring areas. When the system goes unstable, the bus voltages at these two interfaces collapse, as shown in figure 3.31.

The plot of V_{ke}^{gp} for the stable and unstable cases are shown in figures 3.32 and 3.33 respectively. Figure 3.32 illustrates that when the system is stable, V_{ke}^{gp} reaches a minimum of zero some time after the fault is cleared. If the system is unstable, V_{ke}^{gp} will not reach zero in the post-fault period, as shown in figure 3.33.

The energy margins calculated by the RFT method are given in table 3.5, along with the benchmark energy margins. Stability results obtained from conventional time domain simulations are also provided in table 3.5.

Table 3.5: Energy Margins for the SWO System

Case	Plant A (MW)	ΔV^{RFT} (pu)	ΔV^{BM} (pu)	CTDS
1	3800	1.213	1.791	stable
2	3900	1.010	1.316	stable
3	4000	0.711	0.817	stable
4	4100	0.000	0.281	stable
5	4200	-0.100	-0.100	unstable
6	4300	-0.542	-0.542	unstable
7	4400	-2.027	-2.027	unstable
8	4500	-4.540	-4.540	unstable
9	4600	Undefined	Undefined	unstable

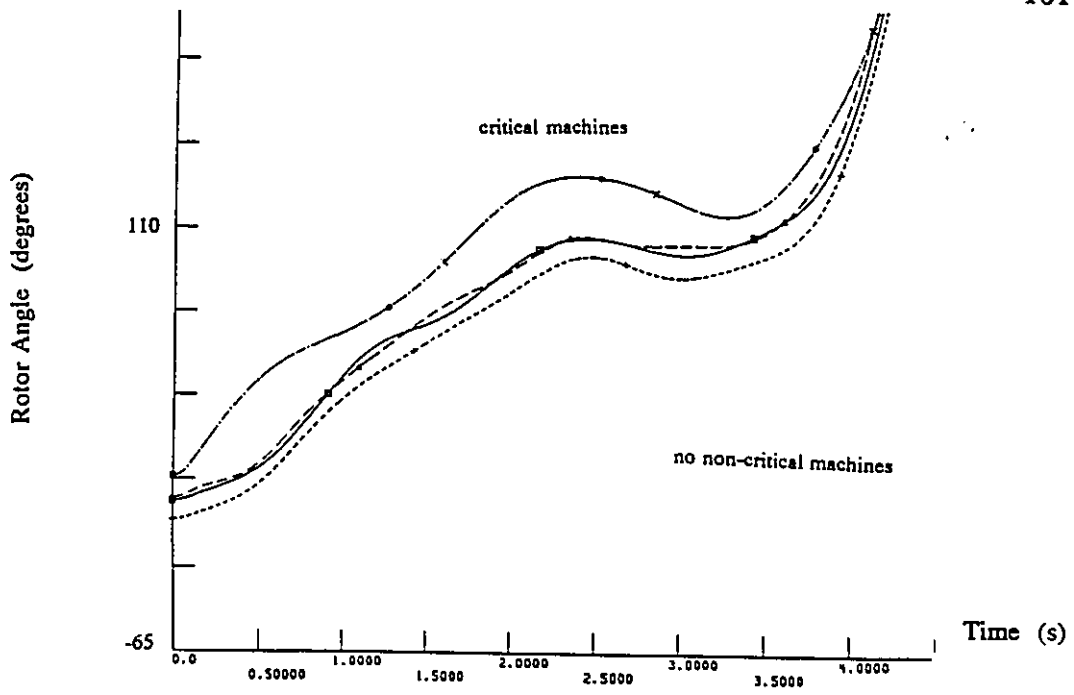

Figure 3.29: Unstable Case - Critical and Non-Critical Machines

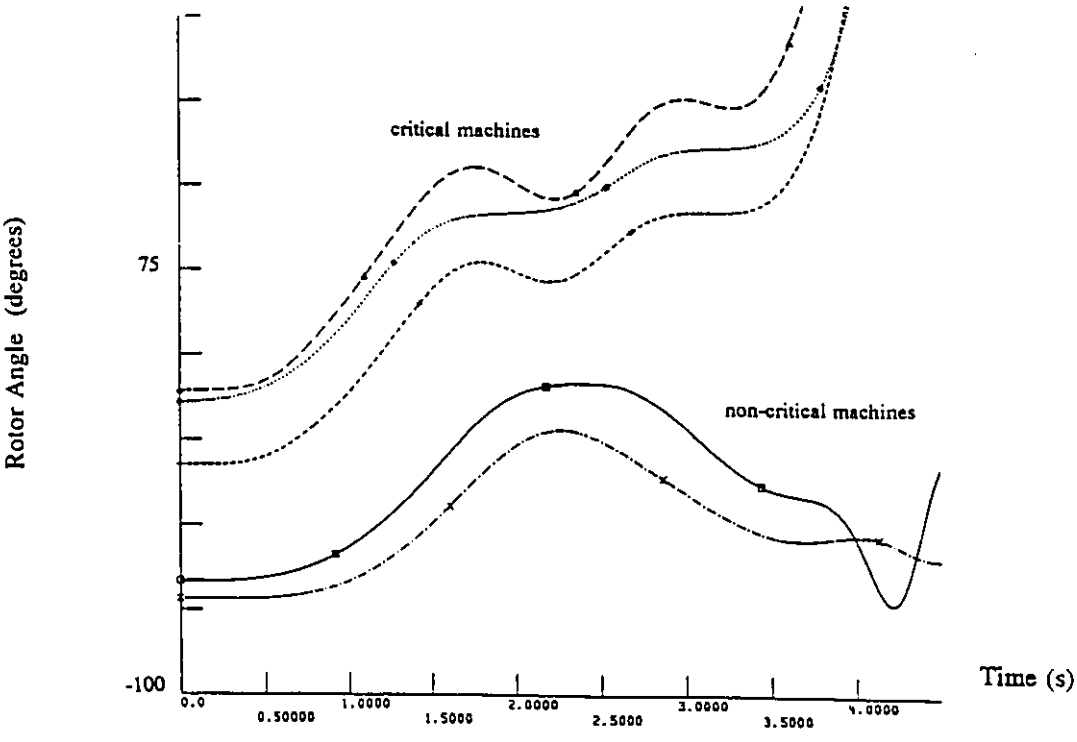

Figure 3.30: Unstable Case - Critical and Non-Critical Machines (cont'd)

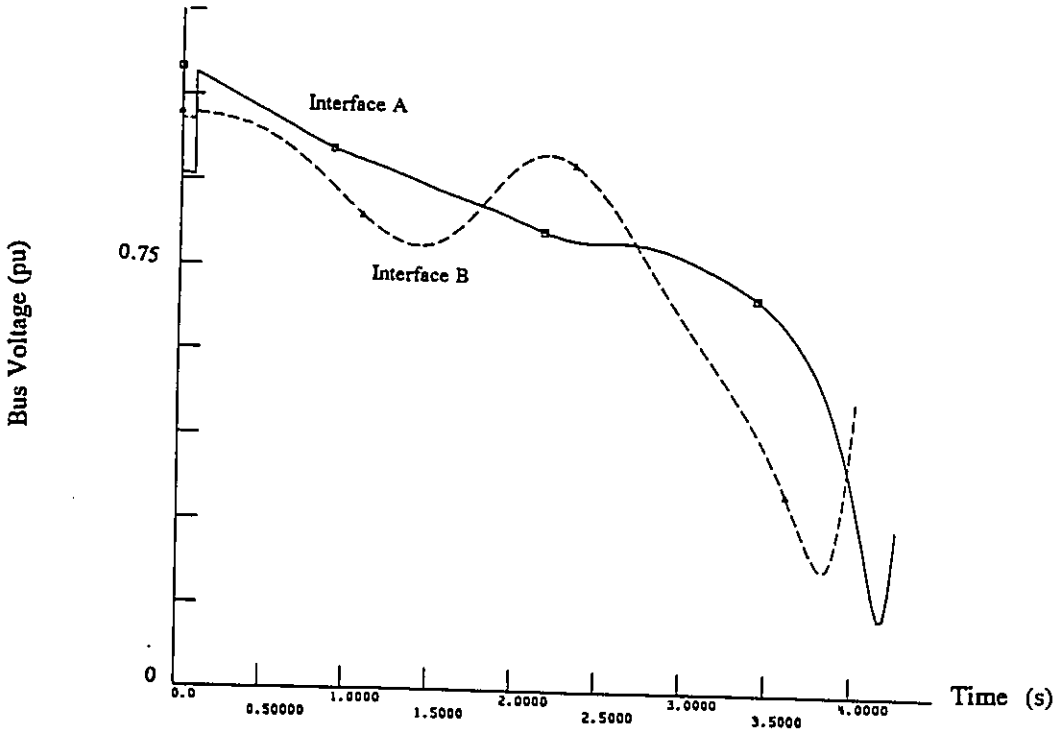

Figure 3.31: Unstable Case - Bus Voltages at Key Interfaces

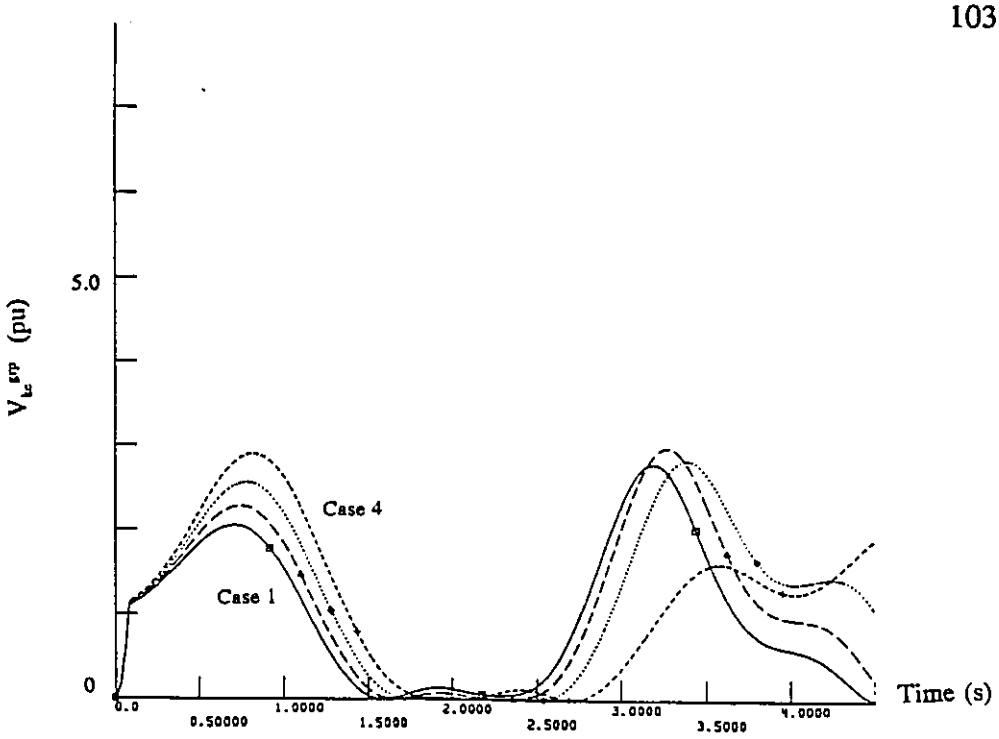

Figure 3.32: V_{ke}^{EFP} for Stable Cases

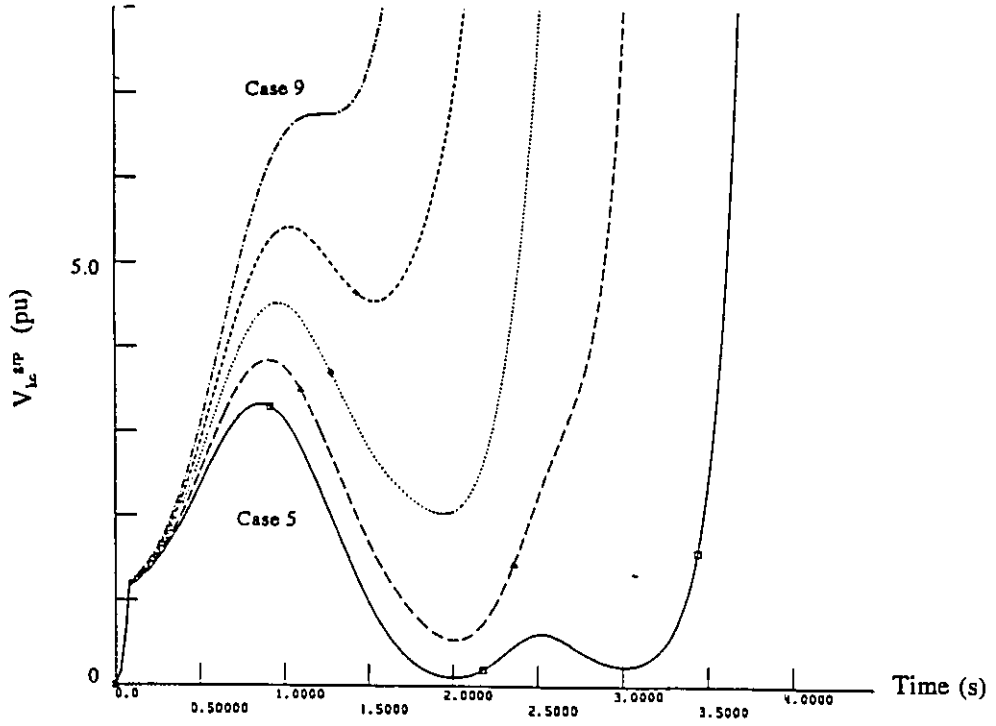

Figure 3.33: V_{ke}^{EFP} for Unstable Cases

3.8.3(c) Discussion

(i) Accuracy

As shown in table 3.5, the RFT method produced a transient stability limit of 4100 MW for the plant A output. Figure 3.34 plots the energy margins as a function of the plant A output, which displays a high degree of non-linearity. In deriving transient stability limits based on energy margins and their sensitivities, a highly non-linear energy margin behaviour would make this task more difficult. Under this circumstance, energy margins may not be useful in speeding up transient stability limit derivation. Table 3.5 also indicates that the energy margins produced by the RFT method are only approximate, when compared to the benchmark energy margins.

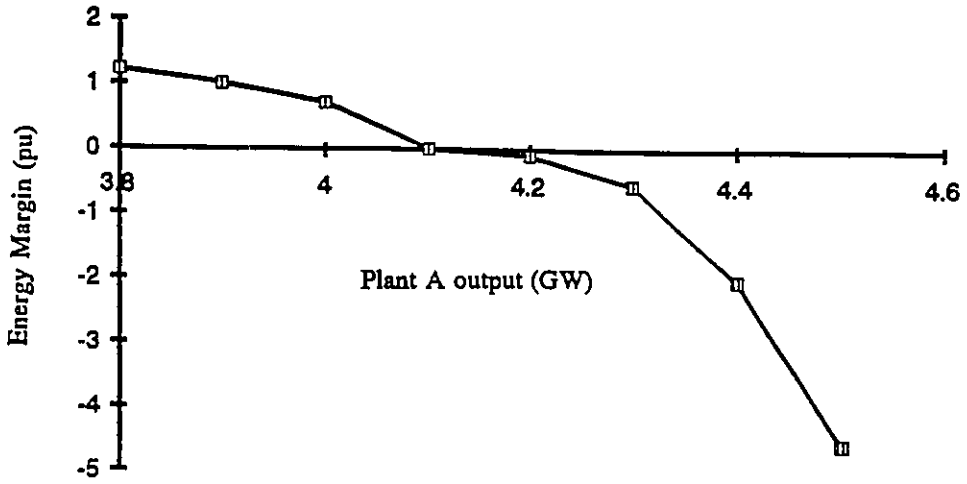

Figure 3.34: Energy Margin vs Plant A Output

(ii) Computing Requirements

For this test system, the first swing period requires about 5 seconds to simulate, as shown by the rotor angle plot of one of the plant A machines (figure 3.35). The entire first swing period has to be simulated in stage 1 of the RFT method. Table 3.8 presents the simulation periods for stages 1 and 2 of the RFT runs. The simulation periods for conventional time domain simulations are also provided for comparison. Table 3.6 shows that for this test system, the additional computing effort for energy margin calculation performed in stage 2 of the RFT method is relatively small, less than 5% of that required for simulating the first swing period.

Table 3.6: Simulation Periods of the RFT Method

Case	T_s^I(s) RFT	T_s^{II}(s) RFT	T_s^{total}(s) RFT	T_s (s) CTD
1	5.0	0.235	5.235	5.0
2	5.0	0.223	5.223	5.0
3	5.0	0.220	5.220	5.0
4	5.0	0.000	5.000	5.0

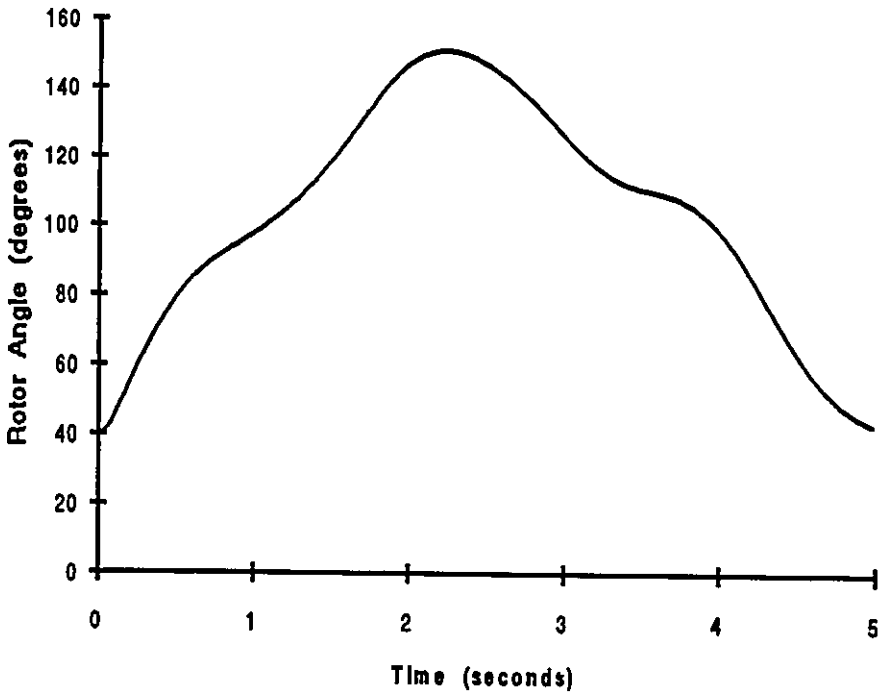

Figure 3.35: The 89-Generator System: Rotor Angle Plot

3.9 CONCLUSIONS

The conventional time domain simulation technique is the principal tool for power system transient stability analysis. This technique is accurate, flexible, and reliable, and has superb power system modelling capability. Its major shortcoming is its inability to produce any information on the degree of stability. To overcome this shortcoming, a new analytical method, referred to as the Relevant Fault-on Trajectory (RFT) method, has been developed to incorporate energy margin calculations into conventional time domain simulations. Energy margins produced by the RFT method have the capability to speed up transient stability limit derivation by reducing the number of stability runs.

The development of the RFT method is essentially based on a combination of the Hybrid method, the PEBS method, and the analysis of the transient energy of the critical generator group. The RFT method adopts a two-stage approach for computing energy margins. The first stage is basically equivalent to a conventional time domain simulation, with the incorporation of transient kinetic energy calculation. The main purpose of stage 1 is to determine whether the system is stable or unstable, and to identify the time instant (t^{kcmin}) when the transient kinetic energy of the critical generator group reaches a minimum in the post-fault period.

If the system is unstable, the RFT method defines the energy margin as the minimum transient kinetic energy of the critical generator group along the post-fault trajectory simulated in stage 1. For a stable case, the RFT method requires simulation of a relevant fault-on trajectory in stage 2, starting with the system conditions at time t^{kcmin}. The maximum potential energy gained by the critical generator group along the relevant fault-on trajectory is then used to

define the energy margin.

The RFT method is reliable and has the same modelling capability as the conventional time domain simulation technique. It can be used to compute energy margins for both plant mode and area mode systems. Its practicality and usefulness has been successfully demonstrated on three Ontario Hydro test systems: the 27-generator Bruce system, and the 144-generator Moose River system, and the 89-generator Southwestern Ontario system. In terms of determining whether the system is stable or unstable, the RFT method has the same accuracy as the conventional time domain simulation technique. Hence the two methods will yield the same results in deriving transient stability limits. Test results indicate that the energy margins obtained by the RFT method are only approximate when compared to the benchmark energy margins derived based on critical clearing time studies. However, this is not viewed as a disadvantage, since approximate energy margins also have the capability to speed up transient stability limit derivation by reducing the number of stability runs.

The RFT method is computationally efficient. For computing energy margins for unstable cases, the RFT method essentially requires the same computational effort as that of the conventional time domain simulation method. For stable cases, the RFT method requires slightly higher computational effort than the conventional time domain simulation technique. The amount of the additional computing effort is usually less than 10% of that required for the simulation of the first swing period.

CHAPTER 4
APPROXIMATE GROUP ENERGY FUNCTIONS

4.1 INTRODUCTION

The RFT method adopts a two-stage approach to compute energy margins for stable cases. The first stage is to perform a conventional time domain simulation of the first swing transient to determine the stability of the system, and to identify the system conditions at which the transient kinetic energy of the critical generator group (V_{ke}^{gp}) reaches a minimum of zero after fault removal. Starting with these conditions, a relevant fault-on trajectory is simulated in the second stage. Energy margin is defined as the potential energy gained by the critical generator group along this relevant fault-on trajectory. As described in section 3.4.2, the transient energy of the critical generator group is represented by the transient energy associated with an equivalent SMIB system in the previous chapter, with the equivalent machine representing the critical generator group. This transient energy is associated with the motion of the COI of the critical generator group, swinging against the COI of the rest of the machines. The equivalent SMIB representation has the desirable effect of filtering out the inter-machine oscillations among the critical generators. This chapter investigates an alternative way of computing the transient energy of the critical generator group.

In [68], Vittal proposed the application of individual machine energy functions and group energy functions for direct transient stability assessment. This is based on the observation that when a system becomes unstable, one or more machines separate from the rest of the system. Hence direct transient

stability assessment can be made by determining the transient energy of a machine (or group of machines) injected by the disturbance, and the post-fault energy absorbing capability of this machine (or group of machines). As a result of Vittal's work, and the work of Fouad [17], the RFT method presented in the previous chapter computes energy margins based on the transient energy of the critical generator group. However, the accounting of the transient energy for the critical group in the previous chapter is different from that presented in [68].

In [68], the group energy function for a critical generator group has two components, the transient kinetic energy and potential energy. The transient kinetic energy component is based on the formation of an equivalent SMIB system, hence identical to that used in the previous chapter. The potential energy component of the group energy function, however, is defined as the sum of the potential energies of the critical machines, minus the potential energy due to the power flows among the critical machines (ΔPE). The physical assumption is that there is no transfer of energy among the critical machines.

The purpose of this chapter is to investigate the accuracy and effectiveness of energy margin calculation by the RFT method, using approximate group energy functions (AGEF) which have the ΔPE term retained, for a reason to be explained in the next section. The three test systems presented in the previous chapter are also used in this investigation. The mathematical formulation of approximate group energy functions is given in section 4.2, and a modified RFT algorithm for energy margin calculation using AGEF is provided in section 4.3. Test results are presented in section 4.4, while section 4.5 provides a brief summary of the conclusions.

4.2 MATHEMATICAL FORMULATION

Let us consider an n-generator system represented by classical generator models and constant impedance loads. After reducing the Y-matrix to the generator internal nodes, the swing equation for machine i is given below:

$$M_i\dot{\omega}_i = P_i - P_{ei} - \frac{M_i}{M_T}P_{COI} \tag{4.1}$$

where:

$$\dot{\theta}_i = \omega_i \tag{4.2}$$

$$P_{ei} = \sum_{\substack{j=1 \\ j\neq i}}^{n} [C_{ij}\sin\theta_{ij} + D_{ij}\cos\theta_{ij})] \ , \quad \theta_{ij} = \theta_i - \theta_j \tag{4.3}$$

$$P_i = P_{mi} - E_i^2 G_{ii} \tag{4.4}$$

$$P_{COI} = \sum_{i=1}^{n} (P_i - P_{ei}) \tag{4.5}$$

$$C_{ij} = E_iE_jB_{ij}, \quad D_{ij} = E_iE_jG_{ij} \tag{4.6}$$

P_{mi}, P_{ei} = mechanical power input and electrical power output of machine i

E_i = internal voltage of machine i

M_i = moment of inertia of machine i

θ_i,ω_i = rotor angle and speed of machine i in the COI frame of reference

G_{ii} = driving point conductance

G_{ij} = transfer conductance in the reduced Y-matrix

B_{ij} = transfer susceptance in the reduced Y-matrix

In [68], the individual machine energy function for machine i is given as:

$$V_i = \frac{1}{2}m_i\varpi_i^2 - P_i(\theta_i - \theta_i^s) + \sum_{\substack{j=1 \\ j\neq i}} C_{ij}\int_{\theta_i^s}^{\theta_i} \sin\theta_{ij}\, d\theta_i + \sum_{\substack{j=1 \\ j\neq i}} D_{ij}\int_{\theta_i^s}^{\theta_i} \cos\theta_{ij}\, d\theta_i + \frac{m_i}{m_T}\int_{\theta_i^s}^{\theta_i} P_{COI}\, d\theta_i \tag{4.7}$$

Let K represent the index set of the critical machines and S represent the index set of the remaining machines. The group energy function for the critical generator group is defined below [68]:

$$V^{GEF} = V_{ke}^{GEF} + V_{pe}^{GEF} \tag{4.8}$$

The kinetic energy component (V_{ke}^{GEF}) in equation (4.8) is the same as that associated with an equivalent SMIB system as described by equation (2.57). The potential energy component (V_{pe}^{GEF}) is defined based on individual machine energy functions as shown below:

$$V_{pe}^{GEF} = -\sum_{i\in K} P_i(\theta_i - \theta_i^s) + \sum_{i\in K}\sum_{j\in S}\left[C_{ij}\int_{\theta_i^s}^{\theta_i} \sin\theta_{ij}\, d\theta_i + D_{ij}\int_{\theta_i^s}^{\theta_i} \cos\theta_{ij}\, d\theta_i\right] + \frac{1}{M_T}\sum_{i\in K} M_i \int_{\theta_i^s}^{\theta_i} P_{COI}\, d\theta_i \tag{4.9}$$

The potential energy of the critical generator group described above is the sum of the potential energies of the critical machines, minus a component (ΔPE) due to the power flows among the critical machines:

$$V_{pe}^{GEF} = \sum_{i\in K} V_{pe,i} - \Delta PE \tag{4.10}$$

The reduced Y-matrix formulation is only computationally efficient for transient stability analysis of relatively small systems with constant impedance

loads. For most practical systems, a structure preserving model for network representation is preferred which is based on a sparse Y-matrix. For such network representation, the calculation of ΔPE in equation 4.10 poses a problem, since it requires the reduced Y-matrix. In this chapter, an approximate group energy function is formulated and tested, assuming the effect of ΔPE is small and negligible. This assumption is reasonable when the critical machines swing coherently during the first swing period. The approximate group energy function is defined below:

$$V^{AGEF} = V_{ke}^{AGEF} + V_{pe}^{AGEF} \tag{4.11}$$

$$V_{ke}^{AGEF} = V_{ke}^{GEF} \tag{4.12}$$

$$V_{pe}^{AGEF} = \sum_{i \in K} \int_{\theta_i^s}^{\theta_i} (P_{mi} - P_{ei} - \frac{M_i}{M_T} P_{COI})\, d\theta_i \tag{4.13}$$

Note that equation (4.13) can accommodate any generator and exciter models.

4.3 ENERGY MARGIN CALCULATION

The two-stage RFT method presented in the previous chapter can be easily modified to accommodate the use of V_{pe}^{AGEF} for energy margin calculation. The modified algorithm is briefly described below:

(a) First Stage: Time Domain Simulation of the First Swing Transient

1. Simulate the disturbance by performing a conventional time domain simulation with the switching events specified. At each time step, compute V_{ke}^{sumK} and V_{ke}^{AGEF}. The former is used to identify the time instant at which the potential energy V_{pe}^{AGEF} reaches a peak along the post-fault trajectory, while the latter is used to define the energy margin in case the system is unstable.

$$V_{ke}^{sumK} = \frac{1}{2} \sum_{i \in K} M_i \omega_i^2 \qquad (4.14)$$

2. Along the post-fault system trajectory, determine the global minimum of V_{ke}^{sumK} and of V_{ke}^{AGEF}. Save the system conditions at the time V_{ke}^{sumK} reaches its global minimum.

3. If the system is unstable, the energy margin is represented by the global minimum of V_{ke}^{AGEF}

$$\Delta V = - \text{ minimum } V_{ke}^{AGEF} \qquad (4.15)$$

5. If the system is stable, initiate stage 2 for energy margin calculation.

(b) Second Stage: Simulation of the Fault-on Trajectory

1. Restore system conditions at the time V_{ke}^{sumK} reaches a global minimum. Convert all detailed machines into their equivalent classical models. Initialize energy margin as zero.

2. Apply a 3-phase fault at one (or more) location for one time step. Compute $\theta^{t+\Delta t}$ by performing numerical integration.

3. Compute generator electrical powers ($P_{ei}^{t+\Delta t}$) using the post-fault admittance matrix. Compute the change in V_{pe}^{AGEF} over this time step using equations 4.16 and 4.17. Increment energy margin by this amount.

$$f_i = P_{mi} - P_{ei} - \frac{M_i}{M_T} P_{COI} \qquad (4.16)$$

$$\Delta V_{pe}^{AGEF} = \sum_{i \epsilon K} \frac{1}{2} (f_i^{t+\Delta t} + f_i^t)(\theta_i^t - \theta_i^{t+\Delta t}) \qquad (4.17)$$

5. Repeat steps 2 and 3 until the energy margin reaches a peak along the fault-on trajectory. This condition is detected by $\Delta V_{pe}^{AGEF} = 0$, which terminates the second stage.

4.4 TEST RESULTS

Energy margins have been re-calculated for the three test systems presented in chapter 3 using approximate group energy functions (Δ^{AGEF}). This section compares the results to those obtained based on the formation of equivalent SMIB system (ΔV^{smib}).

4.4.1 The 27-Generator System

The Bruce system is a typical plant mode stability systems, with the eight machines within the generating complex swinging coherently. The energy margins were re-calculated for the nine stable cases using approximate group energy functions, and are tabulated in table 4.1.

Table 4.1: Energy Margins for the 27-Generator System

Case	Flow (MW)	ΔV^{AGEF} (pu)	ΔV^{SMIB} (pu)	ΔV^{BM} (pu)
1	4500	5.998	5.311	5.775
2	4600	5.122	4.551	5.269
3	4700	4.303	3.839	4.706
4	4800	3.558	3.189	4.136
5	4900	2.861	2.575	3.407
6	5000	2.224	2.012	2.815
7	5100	1.630	1.481	2.085
8	5200	1.074	0.979	1.421
9	5300	0.489	0.459	0.447

Table 4.1 shows that the two sets of energy margins (ΔV^{AGEF} and ΔV^{SMIB}) are similar, with ΔV^{AGEF} being slightly higher. This is expected as the approximate group energy function contains a small portion of potential energy due to the power flows among the critical machines.

The duration of the fault-on trajectory (T_s) as simulated in the second stage of the RFT method provides a good indication of the computing effort for energy margin calculation. In this regard, both ΔV^{AGEF} and ΔV^{SMIB} require approximately the same amount of cpu time to compute, as shown in table 4.2.

Case	Flow (MW)	T_s^{AGEF} (s)	T_s^{SMIB} (s)
1	4500	0.315	0.305
2	4600	0.295	0.285
3	4700	0.280	0.270
4	4800	0.260	0.250
5	4900	0.240	0.235
6	5000	0.220	0.215
7	5100	0.200	0.195
8	5200	0.175	0.170
9	5300	0.135	0.135

Table 4.2: Duration of Fault-on Simulation

4.4.2 The 144-Generator System

In this test system, the critical machines are from the Moose River generating plants which swing as a coherent group. Energy margins were re-calculated for the five stable cases and presented in table 5.3, which also indicates that the two sets of energy margins (ΔV^{AGEF} and ΔV^{SMIB}) are similar, with ΔV^{AGEF} being slightly higher. Table 4.4 shows that both ΔV^{AGEF} and ΔV^{smib} require approximately the same amount of cpu time to compute.

Table 4.1: Energy Margins for the 144-Generator System

Case	Flow(MW)	ΔV^{AGEF}(pu)	ΔV^{SMIB} (pu)	ΔV^{BM}(pu)
1	500	3.161	3.018	3.578
2	550	2.262	2.088	2.843
3	600	1.502	1.307	1.975
4	650	0.825	0.666	0.963
5	700	0.140	0.088	0.132

Table 4.2: Duration of Fault-on Simulation

Case	Flow (MW)	T_s^{AGEF} (s)	T_s^{SMIB} (s)
1	500	3.161	3.018
2	550	2.262	2.088
3	600	1.502	1.307
4	650	0.825	0.666
5	700	0.140	0.088

4.4.3 The 89-Generator System

The third test system is the 89-generator system as presented in section 3.8.3, which displays a very complex mode of instability. When the system loses stability, there are 40 machines separating from the rest of the system. However, the 40 critical machines are spread over a large geographical area and do not swing as one coherent group, resulting in a substantial amount of power flowing among them.

Figure 4.1 shows two potential energy trajectories during the first swing transient. The first one represents the potential energy of the critical generator

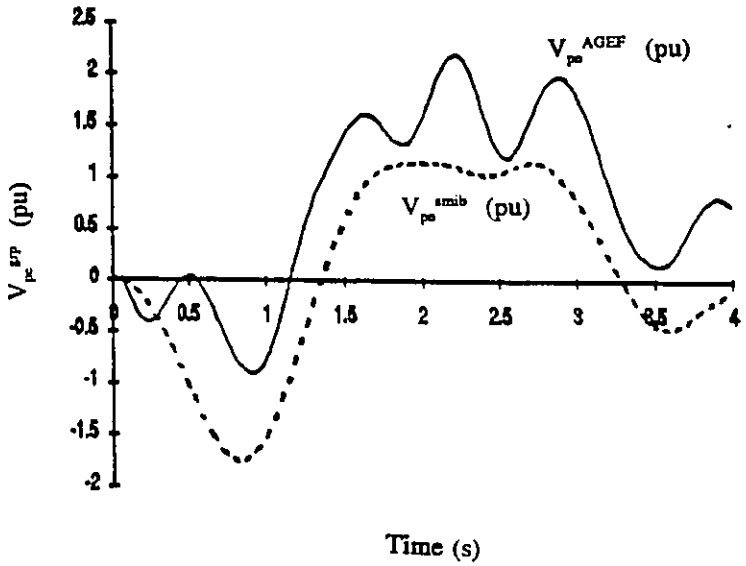

Figure 4.1: Potential Energy Behaviour of the Critical Generator Group

group calculated based on an approximate group energy function (V_{pe}^{AGEF}). For the sake of comparison, the potential energy of the critical generator group computed based on the formation of an equivalent SMIB system is also shown (V_{pe}^{SMIB}). As indicated by figure 4.1, the V_{pe}^{AGEF} trajectory contains a substantial amount of inter-machine oscillation, which is undesirable. The marginally stable case (case 4) is simulated again, with the potential energy of the critical generator group obtained from an approximate group energy function. For this marginally stable system, the energy margin based on V_{pe}^{AGEF} is about 2.8 p.u., much greater than the benchmark value of 0.281 p.u. as given in table 3.3.

4.5 CONCLUSIONS

The RFT method computes energy margins for stable cases based on the energy absorbing capability of the critical generator group, along a relevant fault-on trajectory. In the previous chapter, the transient energy of the critical generator group was obtained by forming an equivalent SMIB system. In this chapter, an alternative way of obtaining potential energy for the critical generator group has been investigated, by using individual machine energy functions.

Based on the work of Vittal [68], the potential energy of the critical generator group can be defined as the sum of the potential energies of the individual machines, minus a component (ΔPE) due to the power flows among the internal nodes of the critical machines. The physical assumption is that there is no energy transfer among the critical machines. This ΔPE component can be easily obtained when the test system is represented by a reduced Y-matrix. For most practical systems which require sparse matrix representation, this ΔPE component is not available.

Therefore, in this chapter, an approximate group energy function is formulated, by summing the individual machine energy functions of the critical machines while retaining the ΔPE component. Energy margins have been computed for two test systems both exhibiting group instability. It is concluded that when the critical machines are coherent, having little or no inter-machine oscillation, the energy margins obtained based on approximate group energy functions are very close to those obtained using the transient energy associated with an equivalent SMIB system. However, when the inter-machine oscillation among the critical generators is significant, the use of approxmiate group energy functions could result in significant errors in energy margin calculation.

In terms of CPU time, the computing requirements of the second stage are solely dominated by the time domain simulation of the fault-on trajectory, and are not affected by how the potential energy of critical generated group is computed. Therefore, except for systems whose critical machines belong to one coherent group, it is recommended to compute the potential energy of the critical generator group based on the formation of an equivalent SMIB system.

CHAPTER 5
ENERGY MARGIN SENSITIVITY AND TRANSIENT STABILITY LIMIT DERIVATION

5.1 INTRODUCTION

The RFT method for incorporating energy margin calculation into the conventional time domain simulation technique has been presented in chapter 3. The most important application of energy margin is to speed up transient stability limit derivation. Power system operators ensure transient stability by making sure that the power flows on all stability interfaces are below their pre-determined limits. These transient stability limits are usually derived off-line by performing conventional time domain simulations.

Transient stability limit derivation by the conventional time domain simulation technique is accomplished through a trial and error approach. To derive the transient stability limit for a given interface, an engineer usually starts with an initial estimate of the limit. The flow level is then perturbed by equal increments, with a transient stability run submitted for each flow level until a marginally stable case is obtained. Deriving limits in this manner usually results in a large number of stability runs, hence requiring a significant amount of computing resources.

Power engineers will benefit significantly from a faster transient stability limit derivation process in a number of ways. First, they can analyze more operating scenarios than they would have with a slower process, thus

resulting in less conservative limits being produced, which in turn lead to reduced system operating costs. Secondly, they can respond faster to sudden system changes such as forced outages or during system restoration from a major blackout, hence improving the level of system security. Finally, it will make on-line transient stability limit derivation closer to reality, which has the capability of providing accurate limits very quickly for all system conditions.

Research efforts have been made to speed up transient stability limit derivation by making use of energy margins. In [15] and [69], fast transient stability limit derivation for classically represented systems using linearized energy margin vs interface flow relationship. In these attempts, the sensitivities of energy margin w.r.t. a change in system parameter were obtained numerically through small perturbations. Analytical derivation of first order energy margin sensitivities for classical systems were proposed in [71]. This chapter presents fast derivation of approximate transient stability limits by applying first order energy margin sensitivities, which are obtained numerically based on the RFT method. Test results are based on the 27-generator and the 89-generator system.

5.2 TRANSIENT STABILITY LIMITS BY FIRST ORDER ΔV SENSITIVITIES

For a given interface, let us assume that the energy margin (ΔV) is a function of the interface flow (F):

$$\Delta V = f(F) \tag{5.1}$$

Let us further assume that for a given interface flow F°, the corresponding energy margin is ΔV°. By perturbing the interface from F° to F^1, a new energy margin is ΔV^1 is obtained. The first order sensitivity of ΔV with respect to F (ΔV/ΔF) is given below:

$$S = \frac{\Delta(\Delta V)}{\Delta F} = \frac{\Delta V^1 - \Delta V^\circ}{F^1 - F^\circ} \tag{5.2}$$

An estimate of the transient stability limit (F^{lim}) for the interface can be derived by assuming linear energy margin vs interface flow relationship as shown in figure 5.1. Hence,

$$F^{lim} = F^\circ - \frac{\Delta V^\circ}{S} \tag{5.3}$$

or alternatively,

$$F^{lim} = F^1 - \frac{(\Delta V^1)}{S} \tag{5.4}$$

For a radial system, the interface flow (F) usually represents the output of a generating plant. In this case, the sensitivity factor (S) is equivalent to

$\Delta(\Delta V)/\Delta G$, where ΔG represents the change in the plant output. While the interface flow is being increased or decreased by a small perturbation, generation at a remote machine with large inertia is usually adjusted to maintain the generator-load balance.

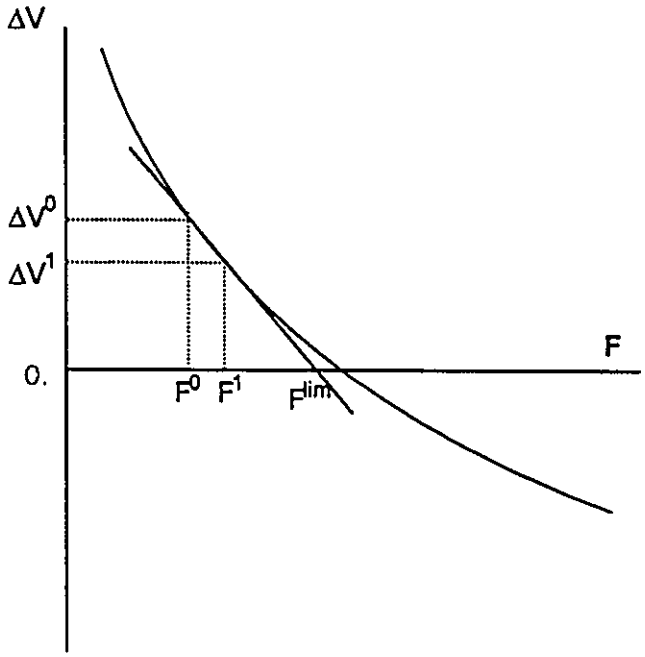

Figure 5.1: Stability Limit by Sensitivity Analysis

5.3 TEST RESULTS

The 27-generator and the 89-generator systems are used to demonstrate fast derivation of approximate transient stability limits by applying first order ΔV sensitivities. Calculation results are summarized in table 5.1. The 27-generator system shows simple plant mode stability phenomenon, while the 89-generator system displays complex area mode stability phenomenon. All energy margins presented in this section are derived from the RFT method.

5.3.1 The 27-Generator System

For this test system, the stability interface carries the power output from the Bruce generating station to remote load centers. The most critical contingency is the loss of circuits 1 and 2 through simultaneous phase to ground faults. Energy margins for fifteen different interface flow levels have been presented in table 3.2. The transient stability limit has been fine-tuned to 5350 MW, at a tolerance of 50 MW. Two scenarios have been considered with different initial flow levels.

5.3.1(a) Scenario 1

The initial interface flow was 4700 MW, and the system was stable at this flow level with an energy margin of 3.839 pu. The interface flow was then perturbed by an increment of 100 MW, causing the energy margin to decrease to 3.189 pu. The first order senstivity of the energy margin w.r.t the interface flow was -0.65 pu/100 MW. Note that two energy margin calculations were required to produce this numerical sensitivity factor, meaning two transient stability runs are required. Applying this sensitivity at the flow level of 4700 MW produced

a transient stability limit of 5290 MW, resulting in an error of approximately 60 MW on the conservative side. Using the conventional trial and error approach and assuming the initial flow is raised at equal increments of 100 MW, one would require eight transient stability runs to obtain the limit. Hence for this scenario, applying first order ΔV sensitivities can save six transient stability runs, speeding up the limit derivation by a factor of 4.

5.3.1(b) Scenario 2

In this scenario, the initial interface flow was 5900 MW and the system was unstable with an energy margin of -5.497 pu. Perturbing the interface flow by 100 MW produced an energy margin sensitivity of -0.94 pu/100 MW. Based on this sensitivity, the transient stability limit was found to be 5315 MW, with an error of 35 MW on the conservative side. The conventional trial and error approach would require seven transient stability runs to obtain the limit, starting with an initial flow of 5900 MW and assuming the flow is decreased by equal decrements of 100 MW. Hence for this scenario, applying ΔV sensitivities can save five transient stability runs and speed up the limit derivation by a factor of 3.5.

5.3.2 The 89-Generator System

For this test system, the transient stability limit of a major generating station has been derived previously based on the conventional trial and error approach. The results have been presented in table 3.7 of chapter 3. The transient stability limit was found to be 4100 MW, at a tolerance of 50 MW. Again, two scenarios are considered for the investigation of fast transient stability limit derivation by applying first order ΔV sensitivities.

5.3.2(a) Scenario 1

The initial plant output was 3800 MW, and the system was stable with an energy margin of 1.213 pu. The plant output was then increased by 100 MW, resulting in an energy margin of 1.010 pu. Therefore the first order sensitivity of energy margin w.r.t. a change in the plant output was -0.2 pu/100 MW. Applying this sensitivity factor at the flow level of 3900 MW produced an approximate limit of 4398 MW, which has an error of 298 MW. Note that derivation of this approximate limit only requires two stability runs, compared to five required by the conventional trial and error approach.

5.3.2(b) Scenario 2

In this scenario, the initial plant output was 4500 MW and the system was unstable with an energy margin of -4.54pu. Reducing the plant output by 100 MW increases the energy margin to -2.027 pu, yielding a sensitivity factor of -0.25 pu/100 MW. Based on this sensitivity, an approximate limit of 4319 MW was obtained, which has an error of 219 MW. Again, only two stability runs are required to derive an approximate limit while five runs are required based on the conventional trial and error approach.

Table 5.1: Transient Stability Limits by Sensitivity Analysis

	27-Gen System		89-Gen System	
	Study 1	Study 2	Study 1	Study 2
F° (MW)	4700	5900	3800	4500
ΔV° (pu)	3.839	-5.497	1.213	-4.540
F^{1} (MW)	4800	5800	3900	4400
ΔV_1 (MW)	3.189	-4.557	1.010	-2.027
S (pu)	-0.0065	-0.0094	-0.0020	-0.0025
F^{lim} (MW)	5290	5315	4398	4319
Error(MW)	60	35	298	219

5.4 CONCLUSIONS

Derivation of transient stability limits by conventional time domain simulations has been considered as a tedious and time consuming process. This is partly due to the fact that the conventional time domain simulation technique only yields a yes-or-no answer, providing no information on the degree of stability. Using this tool, power engineers have to rely on a trial and error approach in deriving transient stability limits, resulting in many stability runs. The limit derivation process can be significantly improved by incorporating energy margin calculation into time domain simulations. In this chapter, it has been demonstrated that energy margins obtained from the RFT method, together with their first order numerical sensitivities, can potentially speed up transient

stability limit derivation by a factor of two or more.

Test results indicate that deriving limits by applying first order sensitivities obtained from just two stability runs may not always yield reasonably accurate results. For practical applications, an efficient scheme for transient stability limit derivation needs to be developed, taking advantage of the nature of the test system, the knowledge that has been already gained on the system, and the energy margin information obtained from the RFT method. The advantage of the RFT method is that it retains the same accuracy of the conventional time domain simulation technique, while at the same time reduces the number of stability runs required for transient stability limit derivation.

An efficient transient stability limit derivation process enables more operating scenarios to be analyzed, hence resulting in less conservative limits. It also enables power engineers to respond more quickly to sudden changes in the power system. Finally, it makes on-line transient stability limit derivation closer to reality, which has the benefit of providing limits under all operating conditions.

CHAPTER 6
DYNAMIC CONTINGENCY RANKING

6.1 INTRODUCTION

Dynamic contingency ranking is a major aspect of power system transient stability assessment. For a given stability interface, there could be many credible contingencies for which the power system must be able to withstand. Fast and accurate transient stability limit derivation is only meaningful if the most critical contingency can be correctly and efficiently identified.

Dynamic contingency ranking from conventional time domain simulations is very difficult due to the lack of information on the degree of stability. An engineer may resort to studying several potentially harmful contingencies, in order to ensure that he or she has not missed the most critical one. This approach often leads to a large number of transient stability runs being submitted.

A major application of energy margin is in dynamic contingency ranking. In [57], dynamic contingency ranking was achieved using normalized energy margins. In [7], approximate transient stability limits were derived from energy margins and their senstivities, which were then used to perform contingency ranking. The purpose of this chapter is to demonstrate the usefulness of energy margins obtained from the RFT method in dynamic contingency ranking.

6.2 SYSTEM DESCRIPTION

Let us consider the 27-generator test system again (figure 6.1), which was presented in section 3.8.2. In this test system, the output from the Bruce generating station is delivered to remote load centers through four 500 kV lines and six 230 kV lines, which comprise the stability interface. In this test, all transmission lines are in service. Of the large number of credible contingencies for this test system, a total of five 500 kV contingencies have been identified as potentially harmful. A study was made to rank these five contingencies based on the energy margins obtained from the RFT method. The five potentially harmful contingencies are given in table 6.1.

Cont. #	Description
1	Simultaneous phase-to-ground faults, loss of circuits 1 and 2
2	Simultaneous phase-to-ground faults, loss of circuits 3 and 4
3	Simultaneous phase-to-ground faults, loss of circuits 1 and 3
4	three-phase fault, loss of circuit 1
5	three-phase fault, loss of circuit 3

Table 6.1: Description of Potentially Harmful Contingencies

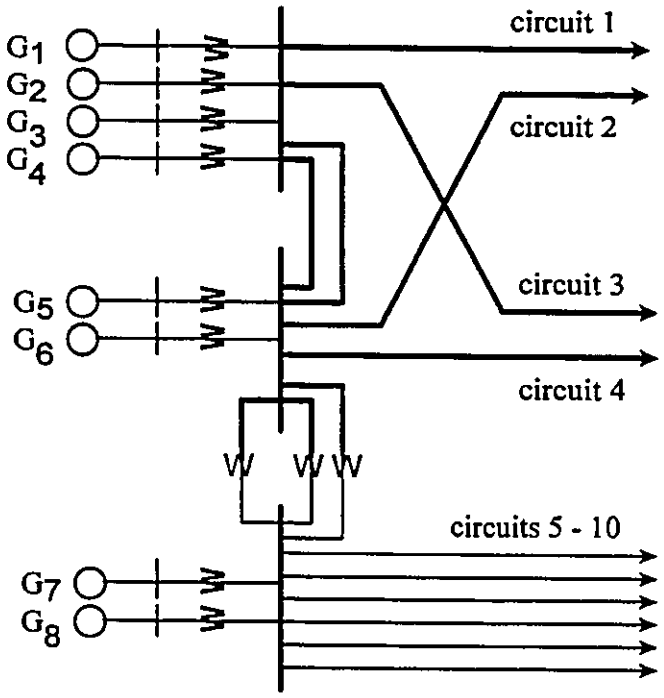

Figure 6.1: Critical Lines of the 27-Generator System

6.3 TEST RESULTS

Two load flow base cases were created to evaluate the effectiveness of energy margins obtained from the RFT method in dynamic contingency ranking. The stability interface flows in these two cases were set to 5500 MW and 6000 MW respectively. For each load flow base case, energy margins were calculated for the five contingencies, using the RFT method. Table 6.2 presents the energy margins calculated at these two flow levels.

Table 6.2: Dynamic Contingency Ranking

Cont #	ΔV(pu) at 5500 MW	ΔV(pu) at 6000 MW	Rank
1	5.105	2.387	1
2	14.49	9.93	2
3	15.77	11.45	3
4	23.50	18.12	4
5	31.83	24.94	5

Let us first examine the energy margins corresponding to 5500 MW flow level. Using energy margin as the index for indicating the severity of transient stability, contingency 1 (loss of circuits 1 & 2) was found to be most critical, followed by contingencies 2 and 3 which are about the same in terms of severity. Contingency 5 (loss of circuit 3) was least critical. The ranking of the five contingencies is given in the last column of table 6.2. The contingency

ranking based on energy margins agrees well with the transient stability limits derived by running conventional time domain simulations. In these simulations, contingency 1 produced the lowest transient stability limit for the stability interface, while contingency 5 gave the highest limit. Table 6.2 indicates that the energy margins calculated at the 6000 MW flow level also result in the same ranking.

6.4 CONCLUSIONS

Although being accurate, the conventional time domain simulation technique is an inefficient tool for dynamic contingency ranking, due to the lack of information on the degree of stability. This shortcoming can be remedied by the incorporation of energy margin calculation. This chapter has demonstrated the capability of energy margins, obtained from the RFT method, in performing dynamic contingency ranking. Accurate contingency ranking allows engineers to ignore many less critical contingencies and to just analyze the critical ones in deriving transient stability limits. Hence a significant number of transient stability runs can be saved.

CHAPTER 7
CONCLUSIONS

7.1 SUMMARY

Transient stability analysis is an important aspect of power system planning and operation, which requires adherence to a set of stringent operating security guidelines. This task is becoming increasingly difficult due to the increased complexity and size of interconnected power systems. There is now a greater need for better analytical tools for fast and accurate transient stability assessment. The conventional time domain simulation technique is considered inadequate to meet all user needs, and new tools like the so-called direct methods are emerging.

The mode of power system operation is constantly changing. The electricity market is now getting more competitive, moving towards a new trend in favour of providing open transmission access to all customers and producers. This new trend requires power system operation to be much more flexible and accommodating, hence imposing additional requirements on power system security analysis. The effectiveness of the conventional trial and error approach of deriving off-line transient stability limits needs to be improved. Power utilities require system operating security limits to be more adaptive to system changes, and this can be achieved by providing fast transient stability derivation capability.

The main objective of this thesis is to enhance the capability of the conventional time domain simulation technique, by the incorporation of energy

margin calculation. Energy margin provides additional insight into the stability problem being studied, and has important applications in fast transient stability limit derivation and dynamic contingency ranking. Both of these applications are essential to on-line transient stability assessment.

To achieve the objective of the thesis, both the conventional time domain simulation method and the so-called direct methods of transient stability analysis have been reviewed, and their strengths and weaknesses compared. The literature on direct methods provides a rich collection of tools for producing transient stability indices. In this research, various techniques for computing energy margins have been studied and analyzed. A new analytical technique, named the **Relevant Fault-on Trajectory (RFT) method**, has been developed for incorporating energy margin calculation into the conventional time domain simulation method.

The RFT method is essentially a variation of the Potential Energy Boundary Surface (PEBS) method, based on a two-stage approach. To compute an energy margin for a stable case, the first stage is to identify along the post-fault trajectory the time instant when the transient kinetic energy of the critical generator is fully absorbed. This transient kinetic energy is injected by the disturbance. The second stage is to determine at this time instant, the additional energy absorbing capability of the critical generator group along a relevant fault-on trajectory. For an unstable case, the RFT method computes an energy margin by determining how much transient kinetic energy of the critical generator group fails to be absorbed in the post-fault period.

During the development of the RFT method, two methods of computing the transient energy of a critical generator group have been investigated. The

first method is based on the transient energy associated with an equivalent single-machine-infinite-bus system. The second method is based on approximate group energy functions which are obtained from individual machine energy functions. Test results have indicated that the first method can be applied to all systems, while the second method is only recommended for systems in which the critical machines belong to the same coherent group.

The RFT method has been successfully applied to realistic utility systems containing up to 1153 buses and 144 generators. Its capability of analysing systems of different modes of instability and of different levels of modelling details has been demonstrated. The RFT method is computationally efficient. For computing energy margins for unstable cases, the RFT method essentially requires the same computing effort as that of the conventional time domain simulation technique. For stable cases, the RFT method requires slightly more computing effort than the conventional time domain simulation technique. The amount of the additional computing effort is usually less than 10% of that required for the simulation of the first swing period.

In terms of determining whether the system is stable or unstable, the RFT method has the same accuracy as the conventional time domain simulation technique. Hence the two methods will yield the same results in deriving transient stability limits. Test results indicate that energy margins obtained by the RFT method are only approximate when compared to the benchmark energy margins derived based on critical clearing time studies. However, this is not viewed as a disadvantage, since approximate energy margins also have the capability to speed up transient stability limit derivation by reducing the number of stability runs.

The conventional time domain simulation technique is an inefficient tool for dynamic contingency ranking, and this shortcoming can be remedied by the incorporation of energy margin calculation. This thesis has successfully demonstrated the effectiveness of dynamic contingency ranking using energy margins obtained from the RFT method.

The following are the main contributions of the thesis:

- A new analytical technique, the Relevant Fault-On Trajectory (RFT) method, has been developed to incorporate energy margin calculation into the conventional time domain simulation technique for power system transient stability analysis. This method computes approximate energy margins efficiently and reliably for power systems of different modes of instability and of different levels of modelling details.

- The RFT method retains the accuracy, flexibility, and reliability of the conventional time domain simulation technique, and at the same time extends its capability and usefulness by providing approximate energy margins as additional output quantities.

- The effectiveness of the RFT method has been demonstrated on realistic power system models containing over a thousand buses and a hundred generators.

- The RFT algorithm is simple, and can be easily incorporated into any production grade time domain simulation program for practical applications.

- The RFT method speeds up the conventional trial and error approach of transient stability limit derivation, by reducing the number of stability runs. It

has been demonstrated that energy margins and their sensitivities can speed up transient stability limit derivation by a factor of two or more.

■ A faster transient stability limit derivation process enables power engineers and system operators to respond more quickly to sudden system changes with preventive or corrective actions. In addition, it paves the way for the derivation of on-line transient stability limits. This would make power system operation more secure and more flexible at reduced operating costs.

■ The RFT method enables the conventional time domain simulation technique to become more efficient in ranking contingencies for transient stability studies. Energy margins obtained from the RFT method indicate the relative degree of stability and provide a means to rank the severity of contingencies.

■ The RFT method provides new practical applications for transient energy analysis, which up to now has drawn the attention of mainly power system researchers. Its combination of the conventional time domain simulation technique and transient energy analysis is capable of setting a new trend in the power industry. With the RFT method, power engineers will start examining the transient energy behaviour of their systems.

7.2 SUGGESTIONS FOR FUTURE WORK

To enhance the steady state and dynamic system performance, modern power systems contain complex elements such as HVDC and flexible AC transmission devices. Their impacts on the critical energies of post-fault systems are yet to be explored, in order to produce meaningful energy margins. Further testing of the RFT method on a variety of utility systems with complex devices

is recommended, so that a better understanding of the method itself and the transient energy behaviour of such systems can be obtained.

For a given power system, correct identification of the mode of instability is essential to the success of the RFT method. The current implementation relies on the user to supply, as part of the input data, the mode of instability and the fault location(s) for the simulation of the relevant fault-on trajectory. This information requires the user to be knowledgeable about the system under study. For more general use and especially for on-line applications, an efficient methodology needs to be developed for providing this information. Pursuit of previous research efforts in this area [5,47,76] can be of help.

Power systems are complex and highly non-linear systems. Applying first order energy margin sensitivities may not always result in the fastest way of deriving transient stability limits. An efficient methodology for fast transient stability limit derivation can be developed, based on expert system techniques, energy margins and their sensitivities. The power industry in North America is being de-regulated and open transmission access is likely to be the mode of operation in the near future. A fast, efficient, and highly accurate transient stability limit derivation process will enable power system operators to cope with the ever changing operating environment in a secure and cost effective manner.

APPENDIX 1: PER UNIT SYSTEM FOR SYNCHRONOUS MACHINE MODELLING

The synchronous generator equations given in Chapter 2 are expressed in the d-q frame of reference. A three-phase synchronous generator has three stator windings and a number of rotor windings. The rotor windings are symmetrical with respect to the magnetic axis of the rotor. For expressing the rotor quantities, a d-q frame of reference can be conveniently defined with the d-axis (direct axis) aligned with the magnetic axis of the rotor and the q-axis (quadrature axis) lagging the d-axis by 90 degrees. Furthermore, to simplify the calculation of generator performance, the phase quantities are transformed into the d-q frame of reference by using Park's transformation. This is analogous to referring the secondary side quantities of a transformer to the primary side.

In expressing and solving synchronous generator equations, a per unit system is devised to normalize system variables, in order to minimize computational efforts. The base values are chosen in such a way that the principle variables are equal to 1 pu under rated conditions. This appendix provides the base values of the per unit system.

Stator Base Quantities:

3-phase VA_{base} = rating of machine(VA)

$e_{s,base}$ = peak phase-neutral rated voltage(V)

f_{base} = rated frequency (Hz)

$$i_{s,base} = \text{peak line current} = \frac{3\text{-phase } VA_{base}}{\frac{3}{2}e_{s,base}} \text{ (A)}$$

$$Z_{s,base} = \frac{e_{s,base}}{i_{s,base}} \ (\Omega)$$

$$\omega_{base} = 2\pi f_{base} \text{ (elect. rad/s)}$$

$$\omega_{m,base} = \omega_{base} \frac{2}{N_p} \text{ (mech. rad/s)}$$

$$L_{s,base} = \frac{Z_{s,base}}{\omega_{base}} \text{ (H)}$$

$$\psi_{base} = L_{s,base} i_{s,base} \text{ (Wb-turns)}$$

Rotor Base Quantities:

$$i_{fdbase} = \frac{L_{ad}}{L_{afd}} i_{sbase} \text{ (A)}$$

$$i_{kd,base} = \frac{L_{ad}}{L_{akd}} i_{s,base} \text{ (A)}$$

$$i_{kq,base} = \frac{L_{aq}}{L_{akq}} i_{s,base} \text{ (A)}$$

$$e_{fd,base} = \frac{3\text{-phase } VA_{base}}{i_{fd,base}} \text{ (V)}$$

$$Z_{fd,base} = \frac{e_{fd,base}}{i_{fd,base}} = \frac{3\text{-phase } VA_{base}}{i_{fd,base}^2} \text{ (A)}$$

$$Z_{kd,base} = \frac{3\text{-phae } VA_{base}}{i_{kd,base}^2} (\Omega)$$

$$Z_{kq,base} = \frac{3\text{-phae } VA_{base}}{i_{kq,base}^2} (\Omega)$$

$$L_{fd,base} = \frac{Z_{fd,base}}{\omega_{base}} (H)$$

$$L_{kd,base} = \frac{Z_{kd,base}}{\omega_{base}} (H)$$

$$L_{kq,base} = \frac{Z_{kq,base}}{\omega_{base}} \text{ (H)}$$

$$T_{base} = \frac{3\text{-phase } VA_{base}}{\omega_{m,base}} \text{ (N-m)}$$

APPENDIX 2: DYNAMIC DATA FOR BRUCE G1-G8

Bruce G1 to G4

Generator Data:

MVA base	= 889.
H	= 6.47 pu
x_l	= 0.22 pu
x_d	= 1.75 pu
x_q	= 1.72 pu
x'_d	= 0.427 pu
x'_q	= 0.65 pu
x''_d	= 0.265 pu
x''_q	= 0.265 pu
T'_{do}	= 8.5 s
T''_{do}	= 0.037 s
T'_{qo}	= 1.24 s
T''_{qo}	= 0.074 s
A_{sat}	= 0.02015
B_{sat}	= 11.7747

Exciter Data (Figure A2.1):

K_A	= 185.
T_A	= 0.
T_C	= 1.0
T_B	= 1.0
K_F	= 0.
T_F	= 0.
T_{F1}	= 0.
T_{F2}	= 0.
V_{RMAX}	= 8.86
V_{RMIN}	= -7.0
E_{TV}	= 1.0
K_C	= 0.077
E_{TMIN}	= 0.25

K_{IFL}	= 4.54
I_{FLMT}	= 4.40
T_R	= 0.015
R_C	= 0.
X_C	= 0.
K_{ETL}	= 17.0
T_{L1}	= 0.025
T_{L2}	= 1.2125
E_{TLMT}	= 1.0750
LIMOUT	= 0.
V_{IMAX}	= 0.
V_{IMIN}	= 0.
V_{TMAX}	= 1.1
V_{TMIN}	= 1.09
V_{OMX}	= 0.8
V_{OMN}	= -0.308
ACON	= 5000.
BCON	= 5.0
V_{SMAX}	= 0.2
V_{SMIN}	= -0.066

Stabilizer Data (Figure A2.1):

KS	= 20.
TS	= 10.
T1	= 1.013
T2	= 1.013
T3	= 0.113
T4	= 0.013

Bruce G5 to G8

Generator Data:

MVA base	= 1025.
H	= 5.32 pu
x_l	= 0.2135 pu
x_d	= 1.943 pu
x_q	= 1.815 pu
x'_d	= 0.368 pu
x'_q	= 0.587 pu
x''_d	= 0.277 pu
x''_q	= 0.277 pu
T'_{do}	= 10.04 s
T''_{do}	= 0.033 s
T'_{qo}	= 0.431 s
T''_{qo}	= 0.0582 s
A_{sat}	= 0.01443
B_{sat}	= 9.6276

Exciter Data (Figure A2.2):

K_A	= 200.
T_A	= 0.
T_C	= 1.0
T_B	= 1.0
K_F	= 0.
T_F	= 0.
T_{F1}	= 0.
T_{F2}	= 0.
V_{RMAX}	= 8.86
V_{RMIN}	= -7.0
E_{TV}	= 1.0
K_C	= 0.077
E_{TMIN}	= 0.25
K_{IFL}	= 4.54
I_{FLMT}	= 4.40
T_R	= 0.015

R_C	= 0.
X_C	= 0.
K_{ETL}	= 17.0
T_{L1}	= 0.025
T_{L2}	= 1.2125
E_{TLMT}	= 1.0750
LIMOUT	= 0.
V_{IMAX}	= 0.
V_{IMIN}	= 0.
V_{TMAX}	= 1.1
V_{TMIN}	= 1.09
V_{OMX}	= 0.8
V_{OMN}	= -0.308
ACON	= 5000.
BCON	= 5.0
V_{SMAX}	= 0.2
V_{SMIN}	= -0.066

Stabilizer Data (Figure A2.1):

KS	= 20.
TS	= 10.
T1	= 0.08
T2	= 0.029
T3	= 0.08
T4	= 0.029

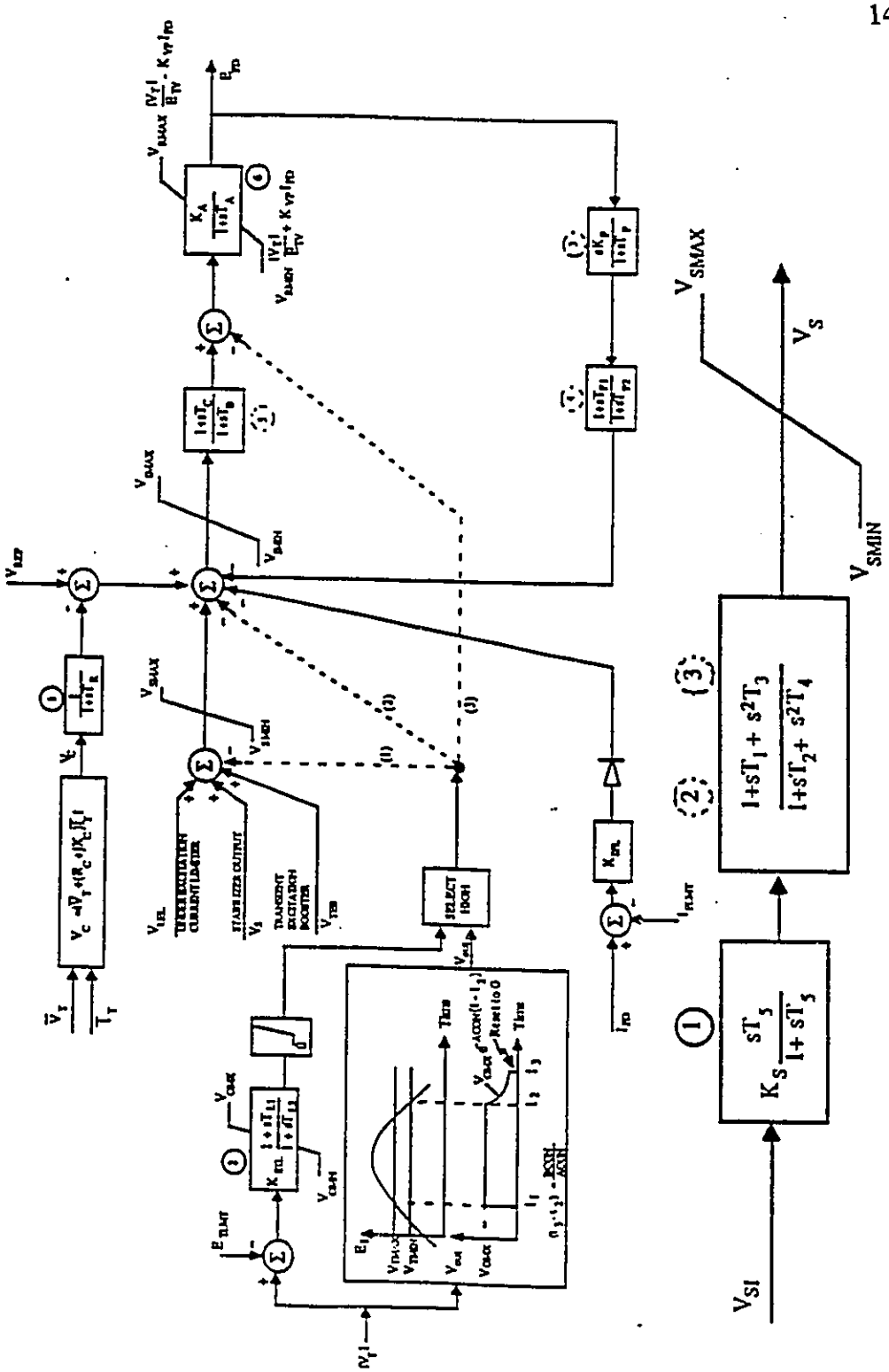

Figure A2.1: Excitation System - Bruce G1 to G4

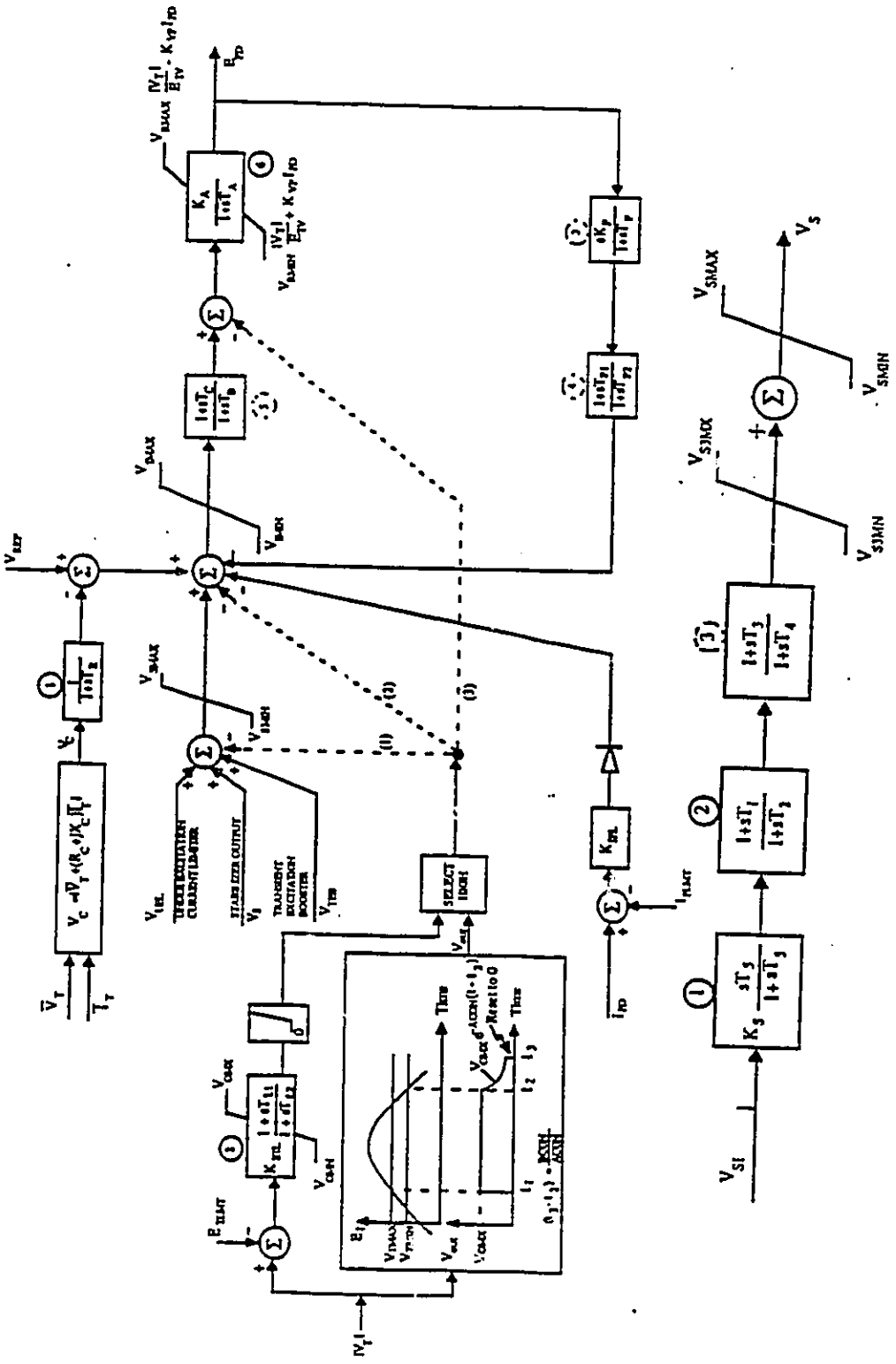

Figure A2.2: Excitation System - Bruce G5 to G8

REFERENCES

1. M.M. Abu-Elnaga, M.A. El-Kady, R.D. Findlay, "Sparse Formulation of the Transient Energy Function Method for Applications to Large-Scale Power Systems," IEEE Trans. on Power Systems, Vol. 3, No. 4, November 1988, pp. 1648-1654

2. M.M. Abu-Elnaga, M.A. El-Kady, R.D. Findlay, "Stability Assessment of Highly Stressed Power Systems Using the Sparse Formulation of the Direct Method," IEEE Trans. on Power Systems, Vol. 3, No. 4, November 1988, pp. 1655-1661.

3. T. Athay, R. Podmore, S. Virmani, "A Practical Method for Direct Analysis of Transient Stability," IEEE Trans., Vol. PAS-98, 1979, pp. 573-580.

4. T. Athay, V.R. Sherket, R. Podmore, S. Virmani, C. Puech, "Transient Energy Analysis," U.S. Department of Energy Publication No. CONF-790904-PL, 1980.

5. P.D. Aylett, "The Energy Integral-Criterion of Transient Stability Limits of Power Systems," Proc. IEE, Vol. 105c, No. 8, September 1958, pp. 527-536.

6. A. Bose, "Application of Direct Methods to Transient Stability Analysis of Power Systems," IEEE Trans., Vol. PAS-103, No. 7, July 1984, pp. 1624-1636.

7. V.F. Carvalho, M.A. El-Kady, E. Vaheedi, P. Kundur, C.K. Tang, G. Rogers, J. Liabaque, D. Wong, A.A. Fouad, V. Vittal, S. Rajagopal, "Direct Analysis of Transient Stability Analysis for Large Power Systems," Report EL-4980 Project RP2206-1, EPRI, Palo Alto, December 1986.

8. Y. Chen, A. Bose, "Direct Ranking for Voltage Contingency Selection," IEEE Trans., Vol. 4, No. 4, November 1989, pp. 1335-1344.

9. H.D. Chiang, M. Hirsch, F.F. Wu, "Foundation of PEBS Method for

Power System Transient Stability Analysis," IEEE Trans., Vol. CAS-35, June 1988, pp. 712-728.

10. H.D. Chiang, F.F. Wu, P.P. Varaiya, "A BCU Method for Direct Analysis of Power System Transient Stability," IEEE Trans. on Power Systems, Vol. 9, August, 1994, pp. 1194-1208.

11. P.L. Dandeno, P. Kundur, "A Non-iterative Transient Stability Program Including the Effects of Variable Load-Voltage Characteristics," IEEE Trans., Vol. PAS-92, September 1973, pp. 1478-1484.

12. A. Debs, J. Kim, G. Maria, F. Rahimi, C. Tang, "On-Line Dynamic Security Assessment Using Stability Transient Energy Function Analysis," EPRI Seminar Notes, EPRI Project 2206-7, September, 1991.

13. G.C. Ejebe, H.P. Van Meeteren, B.F. Wollenberg, "Fast Contingency Screening and Evaluation for Voltage Security Analysis," IEEE Trans., Vol. 3, No. 4, November 1988, pp. 1582-1588.

14. A.H. El-Abiad, K. Nagappan, "Transient Stability Regions of Multimachine Power Systems," IEEE Trans, Vol. PAS-85, No. 2, February 1966, pp. 169-178.

15. M.A. El-Kady, C.K. Tang, V.F. Carvalho, A.A. Fouad, V. Vittal, "Dynamic Security Assessment Utilizing the Transient Energy Function Method," IEEE Trans., Vol. PWRS1, No. 3, August 1986, pp. 284-291.

16. L. Elden, L. Wittmeyer-Koch, "Numerical Analysis-An Introduction," Academic Press Inc., 1990.

17. A.A. Fouad, S.E. Stanton, "Transient Stability of Multimachine Power Systems, Parts I and II," IEEE Trans., Vol. PAS-100, July 1981, pp. 3408-3424.

18. A.A. Fouad, S.E. Stanton, K.R.C. Mamandur, K.C. Kruempel, "Contingency Analysis Using Transient Energy Margin Technique," IEEE Trans., Vol. PAS-101, No. 4, April 1982, pp. 757-766.

19. A.A. Fouad, V. Vittal, "Power System Response to a Large Disturbance: Energy Associated With System Separation," IEEE Trans., Vol. 102, November 1983, pp. 3534-3540.

20. A.A. Fouad, V. Vittal, and Taekyoo Oh, "Critical Energy for Transient Stability Assessment of a Multimachine Power System," IEEE Trans., Vol. PAS-103, 1984, pp. 2199-2206.

21. A.A. Fouad, K.C. Krumpel, V. Vittal, A. Ghafurian, K. Nodehi, J.V. Mitsche, "Transient Stability Program Output Analysis," IEEE Trans., Vol. PWRS-1, No. 1, February 1986, pp. 2-9.

22. A.A. Fouad, V. Vittal, S. Rajagopal, V.F. Carvalho, M.A. El-Kady, C.K. Tang, J.V. Mitsche, M.V. Pereira, "Direct Transient Stability Analysis Using Energy Functions: Application to Large Power Networks," IEEE Trans., Vol. PWRS-2, Februray 1987, pp. 37-44.

23. A.A. Fouad, V. Vittal, Y-X. Ni, H.M. Zein El-din, E. Vaahedi, H.R. Pota, K. Nodehi, J. Kim, "Direct Transient Stability Assessment With Excitation Control," IEEE Trans. on Power Systems, Vol. 4, No. 1, February, 1989, pp. 75-82.

24. A.A. Fouad, "Dynamic Security Assessment Practices in North America," Committee Report, IEEE Trans. on Power Systems, Vol. 3, No. 3, August 1988, pp. 1310-1321.

25. B. Gao, "Assessment of Power System Transient Stability Using Energy Functions," M.A.Sc. Thesis, University of Toronto, 1986.

26. G.E. Gless, "Direct Method of Lyapunvo Applied to Transient Power System Stability," IEEE Trans., Vol PAS-85, February 1966, pp. 164-179.

27. A. Ipakchi, V. Brandwajn, R. Kumar, et al, "Power System Dynamic Security Analysis Using Artificial Intelligence Systems - Phase 1 - Feasibility Evaluation," EPRI Project 3102-02, Final Report, March 1993.

28. W. Janischewskyj, P. Kundur, "Simulation of the Non-Linear Dynamic Response of Interconnected Synchronous Machines, Parts I and II" IEEE Trans., Vol. PAS-91, September/October 1972, pp. 2064-2076.

29. Kakimoto, N., Y. Ohsawa, M. Hayashi, "Transient Stability Analysis of Electric Power System Via Lure' Type Lyapunov Functions, Parts I and II," Trans. IEE of Japan, Vol 98, No. 516, May/June 1978, pp. 63-79.

30. N. Kakimoto, Y. Ohsawa, M. Hayashi, "Transient Stability Analysis of Multimachine Power Systems With Field Flux Decay Via Lyapunov's Direct Method," IEEE Trans., Vol. PAS-99, No 5, September/October 1980, pp. 1819-1827.

31. N. Kakimoto, Y. Ohnogi, H. Matsuda, H. Shibuya, "Transient Stability Analysis of Large Scale Power Systems by Lyapunov's Direct Method," IEEE Trans., Vol. PAS-103, January 1986, pp. 160-167.

32. J. Kim, G. Maria, V. Wong, "Contingency Ranking and Simulation for On-line Use," IEEE Trans., Vol. PAS-104, No. 9, September 1985, pp. 2401-2407.

33. J. Kim, C.K. Tang, G.A. Maria, "Online Transient Stability Calculation for Ontario Hydro Energy Management System," Paper presented at the 1990 CEA Conference, Montreal, Quebec, Canada.

34. P. Kundur, "Digital Simulation and Analysis of Power System Dynamic Performance," Ph.D. Thesis, University of Toronto, 1967.

35. P. Kundur, P.L. Dandeno, "Implementation of Advanced Generator Models into Power System Stability Programs," IEEE Trans., Vol. PAS-102, July 1983, pp. 2047-2052.

36. P. Kundur, G.J. Rogers, D.Y. Wong, "Extended Transient Mid-term Stability Program," Final Report, EPRI Project 1208-9, December, 1992.

37. P. Kundur, D.Y. Wong, G.J. Rogers, S. Arabi, L. Wang, P. Hirsch, "Extended Transient/Midterm Stability Program, User's Manual", Version 3.1, EPEI Project 1208-9, October, 1993.

38. P. Kundur, L. Wang, R.S. Dhillon, T. McGuire, "Feasibility Assessment of Transient Stability Solutions in Real Time," CEA Report No. 347T868, February, 1994.

39. D.C. Lee, P. Kundur, "Advanced Excitation Controls for Power System Stability Enhancement," CIGRE Paper 38-01, 1986.

40. W. Lemmon, K.C. Mamandur and W.R. Barcelo, "Transient Stability Prediction and Control in Real Time by QUEP," IEEE Trans. on Power Systems, Vol. 4, No. 2, May 1989, pp. 627-642.

41. P.C. Magnusson, "Transient Energy Method of Calculating Stability," AIEE Trans., Vol. 66, 1947, pp. 747-755.

42. Y. Mansour, E. Vaahedi, A.Y. Chang, B.R. Corns, B.W. Garrett, K. Demaree, T. Athay, K. Cheung, "B.C. Hydro's On-Line Transient Stability Assessment (TSA) Model Development, Analysis, and Post-Processing," Trans. on Power Systems, Vol. 10, No. 1, February 1995, pp. 241-253.

43. G.A. Maria, C.K. Tang, J. Kim, "Hybrid Transient Stability Analysis," IEEE Trans., Vol. PWRS-5, No. 2, May 1990, pp. 384-393.

44. G.A. Maria, C.K. Tang, J. Kim, A.A. Fouad, V. Vittal, M.A. El-Kady, "On-Line Transient Stability Calculator," EPRI Project RP2206-1, Final Report, January 1994.

45. A.N. Michel, A.A. Fouad, V. Vittal,"Power System Transient Stability Using Individual Machine Energy Functions," IEEE Trans., Vol. CAS-30, No. 5, May 1983, pp. 266-276.

46. T.A. Mikolinnas, B.F. Wollenberg, "An Advanced Contingency Selection Algorithm," IEEE Trans., Vol. PAS-100, No. 2, February 1981, pp. 608-617.

47. Y.X. Ni, A.A. Fouad, "A Simplified Two Terminal HVDC Model and Its Direct Transient Stability Assessment," IEEE Trans., Vol. PWRS-2, No 4, November 1987, pp. 1006-1013.

48. R.H. Park, "Two-Reaction Theory of Synchronous Machines," AIEE Trans., Part I, Vol. 48, 1929, pp. 716-730; Part II, VOl. 52, 1933, pp. 352-355.

49. M.A. Pai, "Power System Stability," North Holland Publishing Co., New York, 1981.

50. M.A. Pai, "Energy Function Analysis for Power System Stability," Kluwer Academic Press, 1989.

51. A. Rahimi, G. Schaffer, "Power System Transient Stability Indices for Online Analysis of Worst Case Dynamic Contingencies," IEEE Trans., Vol. PWRS, No. 2, August 1987, pp. 660-668.

52. F.A. Rahimi, "Evaluation of Transient Energy Function Method Software for Dynamic Security Analysis," EPRI Project RP4000-18, Final Report, December 1990.

53. F.A. Rahimi, M.G. Lauby, J.N. Wrubel, K.L. Lee, "Evaluation of the Transient Energy Function Method for On-Line Dynamic Security Analysis," IEEE Trans., Vol. 8, No. 2, May 1993, pp. 497-507.

54. M. Ribbens-Pavella, L. Gruije, J. Sabatel, A. Bouffioux, "Direct Methods for Stability Analysis of Large Scale Power Systems," Proc. of IFAC Symposium on "Computer Applications in Large Scale Power Systems," Vol II, August 1979, New Delhi, India, pp. 168-175,.

55. M. Ribbens-Pavella, P.G. Murthy, J.L. Howard, "The Acceleration Approach to Practical Stability Domain Estimation in Power Systems," Proc. of 20th IEEE Conference on Decision and Control, San Diego, December 1981, Vol. I, pp. 471-476.

56. H. Sasaki, "An Approximate Incorporation of Field Flux Decay Into Transient Stability Analysis of Multi-machine Power Systems by the Second Method of Lyapunov," IEEE Trans., Vol. PAS-98, No. 2, March/April 1979, pp. 473-483.

57. P.W. Sauer, K.D. Demaree, M.A. Pai, "Stability Limited Load Supply and Interchange Capability," IEEE Trans., Vol. PAS-102, November 1983, pp. 3637-3643.

58. P.W. Sauer, A.K. Behera, M.A. Pai, J.R. Winkelman, J.H. Chow, "Trajectory Approximations for Direct Energy Methods That Use Sustained Faults With Detailed Power System Models," IEEE Trans. on Power Systems, Vol. 4, No. 2, May 1989, pp. 499-506.

59. M.W. Siddiqee, "Transient Stability of an AC Generator by Lyapunov's Direct Method," Int. Journal of Control, Vol. 8, No. 2, 1968, pp. 131-144.

60. M.W. Siddiqee, J. Peschon, "Application of Equal-Area Criterion to Multimachine Power System Stability Problems," Paper 69 CP 120-PWR, IEEE Winter Meeting, New York, January 26-31, 1969.

61. S.E. Stanton, "Transient Stability Monitoring for Electric Power Systems

Using a Partial Energy Function," IEEE Trans., Vol. 4, No. 4, October 1989, pp. 1389-1395.

62. B. Stott, "Power System Dynamic Response Calculations," Proc. IEEE, Vol. 67, February 1979, pp. 219-241.

63. C.K. Tang, "Evaluation of the Direct Method for Power System Transient Stability Analysis," M. Eng. Thesis, University of Toronto, August 1984.

64. C.K. Tang, C.E. Graham, M.A. El-Kady, R.T.H. Alden, "Transient Stability Index from Conventional Time Domain Simulation," IEEE Trans., Vol. 9, No. 3, August 1994, pp. 1524-1530.

65. C.K. Tang, M.A. El-kady, R.T.H. Alden, "Energy Margin from Time Simulation Using Partial Energy Function," Proc. of the 1994 Canadian Conference on Electrical and Computer Engineering, Halifax, Nova Scotia, Canada.

66. J. Tong, H.D. Chiang, T.P. Conneen, "A Sensitivity-Based BCU Method for Fast Derivation of Stability Limits in Electric Power Systems," IEEE Trans., Vol. 8, No. 4, November 1993, pp. 1418-1428.

67. B. Toumi, R. Dhifaoui, Th. Van Cutsem, M. Ribbens-Pavella, "Fast Transient Stability Assessment Revisited," IEEE Trans., Vol. PWRS-1, No. 2, May 1986, pp. 211-220.

68. V. Vittal, "Power System Stability Analysis Using Critical Energy of Individual Machines," Ph.D. Thesis, Iowa State University, Ames, Iowa, 1982.

69. V. Vittal, A.A. Fouad, P.Kundur, "Determination of Transient Stability - Constrained Plant Generation Limits," Proceedings of the IFAC Symposium on Automation & Instrumentation for Power Plants, Bangalore, India, December 1986, pp. A8-1 to A8-5.

70. V. Vittal, S. Rajagopal, A.A. Fouad, M.A. El-kady, E. Vaahedi, V.F. Carvalho, "Transient Stability Analysis of Stressed Power Systems Using Energy Function Method," IEEE TPS, Vol. 3, No. 1, February 1988, pp. 239-244.

71. V. Vittal, E.Z. Zhou, C. Hwang, A.A. Fouad, "Derivation of Stability

Limits Using Analytical Sensitivity of the Energy Margin," IEEE Trans. on Power Systems, Vol. 4, No. 1, February 1989, pp. 44-52.

72. V. Vittal, N. Bhatia, A.A. Fouad, G.A. Maria, H.M. Zein-Eldin, "Incorporation of Nonlinear Load Models in the Transient Energy Function Method," IEEE Trans., Vol. PWRS-4, No. 3, Aug 1989, pp. 1031-1036.

73. J. Willems, "Direct Methods for Transient Stability Studies in Power Analysis," IEEE Trans., Vol. AC-16, No. 4, July/Aug 1971, pp. 1469-1481.

74. Y. Xue, Th. Van Cutsem, M. Ribbens-Pavella, "A Simple Direct Method for Transient Stability Assessment of Large Power Systems," IEEE Trans., Vol. 3, No. 1, May 1988, pp. 400-412.

75. Y. Xue, Th. Van Cutsem, M. Bibbens-Pavella, "Extended Equal Area Criterion: Justifications, Generalizations and Applications," IEEE Trans. on Power Systems, Vol. 4, No. 1, February 1989, pp. 44-52.

76. Y. Xue, Th. Van Cutsem and M. Ribbens-Pavella, "Real-Time Analytic Sensitivity Method for Transient Security Assessment and Preventive Control," Proc. IEE, Vol. 135, No. 2, March 1988, pp. 107-117.

77. E.Z. Zhou, A.A. Fouad, "Second Order Correction to the Energy Margin Sensitivity in the TEF Method," paper presented at the North American Power Symposium, Purdue University, West Layfette, IN, September, 1988.

78. "Excitation System Models for Power System Stability Studies," IEEE Committee Report, IEEE Trans., Vol. PAS-100, February, 1981, pp. 494-504.

79. "Development of Dynamic Equivalents for Transient Stability Studies," EPRI Report EL-456, May, 1977.